

Mathematical Approaches to Seed Germination

Anthony Hampstead, MMath

Thesis submitted to the University of Nottingham
for the degree of Doctor of Philosophy

July 2014

ABSTRACT

Plant seeds progress through specific stages during germination, from quiescence in the dry state through water uptake, testa rupture and finally endosperm rupture. The stages of seed germination are fairly well classified but the underlying biochemical and mechanical processes are unknown. The ability to control a seeds progression through the stages of germination has implications on farming efficiency and so the following thesis explores *Arabidopsis thaliana* and *Lepidium sativum* seeds during the germination process.

A systematic approach to analysing the shape of cells within the radicle (embryonic root tissue) is developed, using confocal imaging, in order to characterise the shape of cells in the different tissues of the radicle. The cell shape approximations are not refined enough to characterise the different cell tissues. With more data, this approach would hope to find the region in which cells alter through the germination process.

Change in the activity of cell wall modifying enzymes within the endosperm, that surrounds the emerging embryo, is a key part of the germination process and temporally and spatially defined high resolution transcriptomics data-sets are available to inform models. Through the course of this thesis, biochemical networks are developed, with ordinary and partial differential equation models being constructed and analysed. The models highlight elements for further investigation as well as differences between the two species considered. The mathemat-

ical models, along with data from biomechanical experiments on the endosperm, inform discussion on how the cell wall biochemistry of a cell wall alters the cell wall properties. These discussions focus on cell wall permeability, extensibility and the final cell separation event associated with germination. From the considered proteins, polygalacturonase and pectin lyase arise as the only viable candidates to cause the cell separation event with the model framework.

CONTENTS

1. <i>Introduction</i>	8
1.1 Seed Physiology and the Germination Process	8
1.1.1 Seed Physiology	8
1.1.2 Stages of Germination	10
1.2 Plant Cell Wall Physiology	13
1.2.1 Polysaccharides	13
1.2.2 Proteins influencing cell wall structure	15
1.3 Data from the ERA-NET vSEED consortium	19
1.4 Enzyme Kinetics	21
1.5 Thesis Outline	23
2. <i>Cell Shape Analysis</i>	24
2.1 Introduction	24
2.2 Digitalising the Cells	26
2.3 Shape Simplification	26
2.4 Analysis	28
2.5 Cell Orientation	35
2.5.1 Curve of best fit	35
2.5.2 Relabelling The Eigenvalues	38
2.6 Separation of Cell Types	41
2.7 Conclusion	43

3. <i>Ordinary differential equation model of PME</i>	45
3.1 Biological Network	46
3.2 Mathematical model	47
3.3 Cross-species house keeping genes	52
3.4 Results	54
3.5 Parameter Sensitivity Analysis	56
3.6 Parameter fitting	61
3.7 Model Simplification	71
3.8 Conclusion	74
4. <i>Ordinary differential equation model of Cell Walls</i>	76
4.1 Introduction	76
4.2 Homogalacturonan Network	77
4.2.1 Parameter Sensitivity	87
4.3 Arabinan Network	93
4.3.1 Parameter Sensitivity	96
4.4 Xyloglucan Network	98
4.4.1 Parameter Sensitivity	100
4.5 Cell Wall Properties	103
4.5.1 Cell Separation	103
4.5.2 Cell Wall Permeability	107
4.5.3 Cell Wall extensibility	108
4.6 Conclusion	110
5. <i>Partial Differential Equation Model of Cell Wall Behaviour During Germination</i>	114
5.1 Introduction	114
5.2 Biological Network	115
5.2.1 Homogalacturonan network	117

5.2.2	Xyloglucan network	118
5.2.3	Arabinan network	119
5.3	Mathematical Model	120
5.3.1	Rate constants	123
5.3.2	Diffusion constants	124
5.3.3	Boundary conditions	125
5.3.4	Initial Conditions	128
5.4	Non-dimensionalised model	129
5.5	Results	130
5.6	Model Implications on Cell Wall Properties	138
5.6.1	Cell Separation	138
5.6.2	Cell Wall Permeability	141
5.6.3	Cell Wall extensibility	142
5.7	Conclusion	143
6.	<i>Conclusions and Further Work</i>	144
6.1	Cell Shape Analysis	144
6.2	Plant Cell walls	145

1. INTRODUCTION

Little is known about the biochemical or mechanical process of seed germination and even less is known about how a seed knows when to germinate. With the ever increasing population and spatial constraints becoming more of a problem, it is essential to make farming as efficient and prosperous as possible. Understanding when, why and how seeds germinate can go a long way to improving agricultural consistency, efficiency and productivity, thus motivating us to study this area fully.

This thesis will focus on the *Brassicaceae* family, specifically *Arabidopsis thaliana* and *Lepidium sativum*; beginning with the seed physiology and highlighting some differences between the seeds of the two species, we will then define germination. Cell walls and their major components are highlighted.

1.1 *Seed Physiology and the Germination Process*

1.1.1 *Seed Physiology*

A mature seed is made up of three components, Testa, Endosperm and Embryo, and this is illustrated in Figure 1.1.

The Testa is the outer shell surrounding the seed. In the *Brassicaceae* family, the cells which form this layer die during seed maturation, leaving a biologically inactive layer [4], [20]. Developed by the maternal plant, it is thought to have a purely protective function during quiescence of the

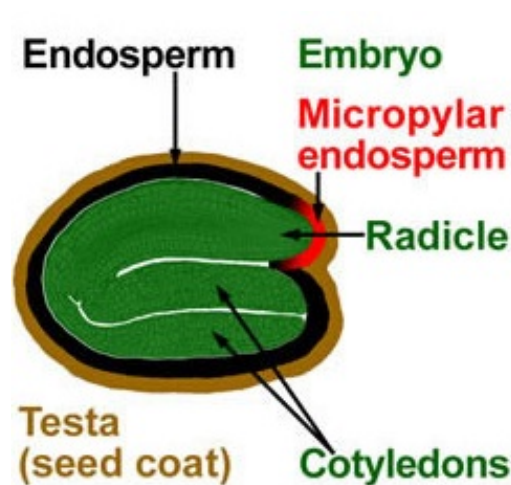


Fig. 1.1: The components of an *Arabidopsis* seed [56]

dry seed, dormancy of the imbibed seed and the germination process, through its waxy composition and the mucilage excreted [4]. There is evidence that it contributes to seed dormancy (as discussed in section 1.1.2) although the majority of this evidence does not distinguish between the endosperm and testa layers, referring to the combination of these layers as the seed coat. This is the case for recent work which has shown the seed coat to be essential for controlling dormancy; by attempting to germinate seeds with their coat removed and set on a bed of excised seed coats, the different conditions explored show a dramatic change in germination rates and thus indicate that the seed coat is required for dormancy although not its exact role [42].

The purpose of endosperm cells can vary from species to species but in general they are said to take part in storage, protection of the embryo and germination control; from dormancy to environmental monitoring and enzymatic activity during the germination process [4]. With the focus of the work discussed below being on the Brassicaceae family, so too is the endosperm's description here. In *Arabidopsis*, the endosperm is a layer of living cells, one cell thick, encapsulating the embryo; this cell layer is

important for controlling germination [35]. The section of the endosperm which covers the radicle is known as the micropylar endosperm, or cap, and the opposite end is known as the chalasal endosperm. Development of the endosperm tissue is well understood and described by Ohad [62] and Brown [9]. The endosperm is thought to have a role in monitoring the environment for favourable germination conditions. Exactly how the seed monitors the external environment and how this translates into starting the germination process is unknown, although water uptake, light [29] and storage [58] are important and will be discussed further in section 1.1.2.

Embryos represent future plants, made up of cotyledons, soon to become the first leaves of the seedling, and the axis, that includes the hypocotyl and radicle. The radicle will become the root of the seedling. The radicle is covered by the root cap, from the end of the root cap progressing towards the cotyledons a short way, there is a region known as the collet and between the collet and cotyledons lies the hypocotyl, which will become the seedling's stem.

While undergoing germination, seeds produce a viscous substance known as mucilage. This mucilage is thought to help protect the seed while securing moisture and nutrients from the soil near by to aid in the germination process. It is comprised of broken down cell wall components and released upon contact with water from the testa [34] [80].

1.1.2 Stages of Germination

Germination is defined as the time at which the radicle emerges through the endosperm, however there are many steps that the seed takes before reaching this moment, and this is referred to as the germination process. Figure 1.2 summarises the events of germination, although most of the

events will not be discussed here, further information can be found in Bewley [6] and Nonogaki [61] and books by Bradbeer [8] and Bewley [4].

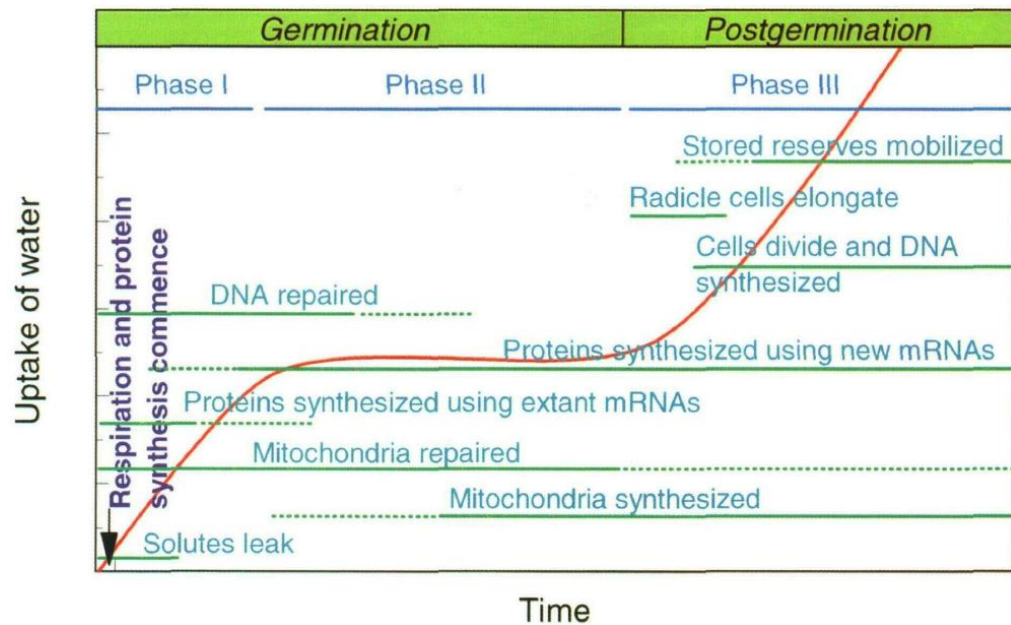


Fig. 1.2: the processes undergone during and post germination [6]

Seeds can survive for many years in a dry, yet viable quiescent state until exposed to water. Water uptake can be used to segment the germination process into two phases; seeds start in what is referred to as a dry state and in phase one begins taking up water rapidly, the imbibition phase. Then the water level within the seed remains constant for the plateau phase. Post germination, water uptake rapidly rises again in a third phase, not explored in this work, although these phases are explained by Bewley [6]. During phase one, a seed can double in size while producing mucilage, for *Arabidopsis* this lasts approximately three hours while phase two continues for a further twenty to forty hours, depending on the environment and previous history of seed storage. The first two phases, with respect to water, occur in all seeds whether they are viable or non-viable, dormant or germinating.

A dormant seed is defined by Finch-Savage as “a block to the comple-

tion of germination of an intact viable seed under favourable conditions” [25]. During seed maturation dormancy is acquired by each seed independently of its siblings in order for the seeds to germinate at different times, increasing the chances of survival for that line of plants [4]. Whether a seed will be dormant or germinate is attributed to the balance of two hormones, namely gibberellin (GA), the promoter of germination [27] and abscisic acid (ABA), the promoter of dormancy [25] [3]. Some of the explored elements which control this balance are light [29], temperature [52], growth potential of the radicle and resistance to it from the endosperm [41] and seed storage times [58]; this list is not exhaustive but it is also not clear to what extent each controller contributes to dormancy release.

During phase two, the dormant and germinating seed’s processes diverge, the exact point at which these two seed types differentiate is unknown but GA and ABA are thought to be responsible. The germinating seed expands further to split the testa and then the radicle extends and germination occurs when the radicle breaks through the endosperm. In order for this germination to take place the force exerted on the endosperm, by the radicle, has to exceed the structural strength of the endosperm cell walls. It is believed that there are two parts to this process; the first is the expanding radicle pushing at the endosperm, and the second is the enzyme activity within the endosperm weakening the cell wall and making it easier for the radicle to emerge; cell wall proteins and enzymes are introduced in section 1.2 and explored in sections 3.2, 4 and 5. Schopfer discusses some early seed modelling and highlights the challenges that the endosperm’s size creates to traditional models [72].

1.2 Plant Cell Wall Physiology

The cell wall is a complex structure, Carpita [13] states that in *Arabidopsis* 15% of the genome is dedicated to maintaining the cell wall. The cell wall is generally considered to be made up of three main groups of polysaccharides: cellulose, hemicellulose and pectin. These polysaccharides account for roughly ninety percent of a cell's dry weight [70] and their structure and function is discussed by Caffall [11].

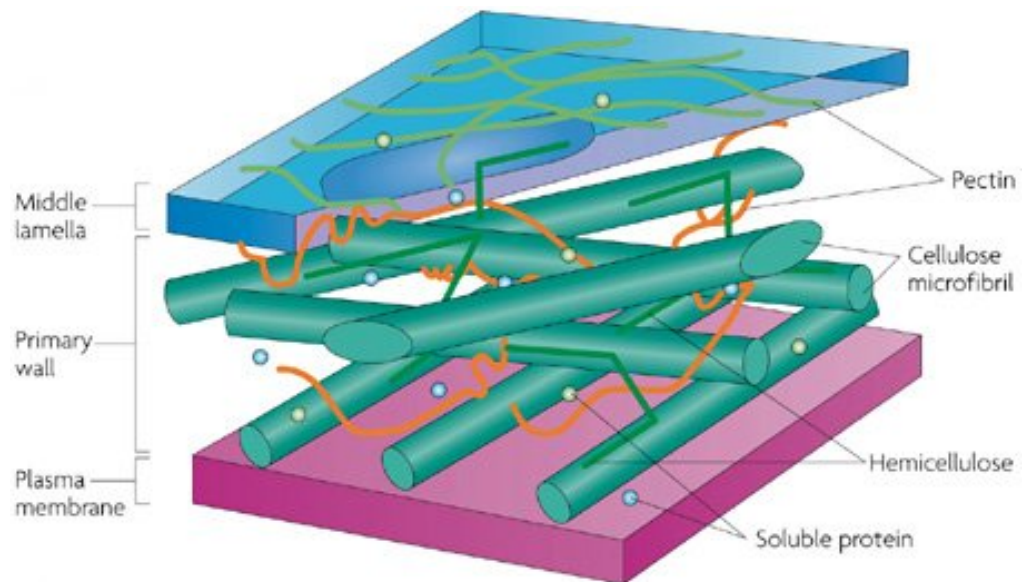


Fig. 1.3: The structure of a plant cell wall[76]

Plant cells are connected to their neighbours by pectin, the area between two cells is known as the intercellular matrix (or middle lamella). Cloetens [15] highlights the importance of the intercellular matrix in seed, as a possible explanation for fast water uptake and gas exchange during germination.

1.2.1 Polysaccharides

Cellulose contributes to the strength of the plant's cell wall more than any other substance considered and is found in microfibril rods with evidence

to suggest the rods are predominantly arranged perpendicular to the direction of elongation. In a laboratory, cellulose is broken down using strong acids and high temperatures, suggesting that it is an extremely stable compound and unlikely to be degraded by enzymes present in the cell wall [70].

The rods of cellulose are tethered together by strands of hemicellulose. The term hemicellulose groups together several polysaccharides, the predominant of these is xyloglucan [68] but glucuronoxylan and mannans, among others, are also included in this umbrella term. Hemicellulose contributes considerably to the tensile strength of the cell wall. The cellulose/hemicellulose structure is accepted to be the main load-bearing element of the cell wall [22].

Pectin is the most abundant substance in the cell wall and fills all the empty space within the primary cell wall. Pectin is split into three major polysaccharides: homogalacturonan, rhamnogalacturonans I and rhamnogalacturonans II. The permeability of pectin can increase as the polysaccharides are broken down, allowing enzymes to affect the hemicellulose and cellulose [1] or at least diffuse more quickly through the cell wall. The homogalacturonan (HG) group is the most abundant of the three [53] and as such is explored more thoroughly here: Biosynthesis of HG polysaccharide occurs within the cell and the chains are transported to the walls at high levels of methylesterification [53] [55]. These methyl groups are built as side chains to the main HG polysaccharide backbone and alter the cell wall properties and binding ability of the chain [53]. Where there are gaps in the methyl side chains, bonds between the HG and other components are possible, such as, calcium [59], each other and other cell wall polymers [53]. Pectin is also thought to be the sole component of the intercellular matrix, homogalacturonan in particular is

shown to be present in high levels using immunohistochemical analysis [10].

Arabinan is part of the Rhamnogalacturonan I group of pectins and is abundant in the cell wall of the endosperm; the high levels of arabinan is one of the major differences between the endosperm's cell walls and cell walls elsewhere in the plant. This arabinan form of pectin is highly flexible, especially when compared to homogalacturonan [36] and its presence may help the endosperm cope with the repeated swelling and shrinking caused by water uptake.

These polysaccharides are remodelled by so called cell wall remodelling enzymes and an introduction to these can be found in articles by Showalter ([73], [74]).

1.2.2 *Proteins influencing cell wall structure*

Xyloglucan endotransglucosylase/hydrolase

Xyloglucan endotransglucosylase/hydrolase (XTH) enzymes are considered to be an important part of cell wall remodelling and it is understood that this remodelling is performed on the hemicellulose, specifically xyloglucan. XTH activity has been shown to be optimum at a pH of around 5.5 pointing towards auxin-induced cell wall growth since acid growth occurs at a pH of less than 4.5 [70]. XTH enzymes can be subdivided into two distinct groups defined by their action.

The first group, xyloglucan endotransglucosylase (XET) are enzymes which cut the xyloglucan and create a temporary covalent bond with the cut section [70]. The XET then reattaches the xyloglucan to a new available site (cellulose or another free xyloglucan). Vissenburg supports this by showing the colocalization of XET with xyloglucan remodelling

activity; this activity is used to integrate new cellulose microfibrils and strengthen the primary cell wall as well as promote cell elongation as discussed by Campbell [12]. It is important to note that XET activity alone does not result in cell wall loosening [16].

XTH's other sub-group performs xyloglucan Hydrolase (XEH) and these enzymes catalyse hydrolysis of the xyloglucan polysaccharides. This leaves unattached xyloglucan and it is suggested that this reduces the tensile strength of the cell wall and allows the cell's internal pressure to extend the cell. If this activity is irreversible and a dominant reaction, intuition implies it could lead to the cell wall breaking down entirely [12] [70].

Expansin

The expansin family of genes is very large and it is suggested that this could be to help the plant control its growth [18] but the intricacies of the network which controls the expansin family are unknown.

It has been shown that reintroducing expansins to a heat-inactivated cell wall can initialise the cell wall's ability to extend [17], this implies that expansins are essential for cell expansion. There are however no known sites of action for expansins, although expansins do not hydrolase the main polysaccharides. It is suggested that expansins are involved in weakening the bond between hemicellulose and cellulose but at pH levels (pH 4.5 to 6 [17]) which indicate acid growth, also referred to as cell wall loosening [16] or an 'unzipping' of the cellulose/hemicellulose bond, aimed at relieving tension in the cell wall structure. This means that expansins are unlikely to work closely with the previously discussed XTH enzymes [70].

Endo- β -mannanase

It has been shown that endo- β -mannanase is expressed in the endosperm of many species during germination, including tomato and it is suggested that this enzyme limits the rate of cell wall weakening [84]. The activity of endo- β -mannanase has been shown to promote germination [5], through interaction with mannans, although it is not capable of achieving germination alone and it appears to have a similar level of activity without the presence of gibberellin or abscisic acid.

There is evidence from the vSEED data [21], section 1.3, that endo- β -mannanase mRNA is present during germination although immunocytochemistry work has as yet been unable to find evidence of its known target, mannans [43], in the endosperm at this time and so this will not be included in later work; Lee [45] and Marcus [47] point to the presence of homogalacturonan in the endosperm being a block to detecting mannans when using immunocytochemistry.

Arabinase

Arabinases have been shown to act on the arabinan, pectin, polysaccharides early in the germination process by Lee [44] although the purpose of this activity is unknown but is assumed to be a cleaving of arabinans. Minic has shown that reducing the amount of arabinase results in later germination and smaller seed size [51].

Pectin Methylesterase

The function of this group of proteins is to strip side chains from the methylesterified HG polysaccharides. Ralet distinguishes between fungal pectin methylesterases (PMEs) which 'randomly' remove methylesters

where as plant PME's remove methyl groups in blocks leaving sections of the polysaccharides backbone exposed [67]. The exposed backbone allows for interaction with calcium and other enzymes.

Pectin methylesterase has a family of known inhibitors, pectin methylesterase inhibitors (PMEI).

Polygalacturonase

The activity of polygalacturonase (PG) is extensively studied in different cell wall weakening or cell separation events, such as fruit ripening [14][28] and senescence [69]. PG is thought to cleave pectin polysaccharides although methylesters seem to interfere with this process. It has been postulated that PG is active along the pectin polysaccharide backbone [28].

A group of inhibitors know as polygalacturonase inhibitor proteins (PGIP) have been documented. Protsenko describes PGIP involvement in pathogen response and suggests that it may bind with pectin in a protective manner although far more work has been done on the binding of PGIP to PG in order to stop PG from interacting with pectin [66]. Kemp [38] suggests that the relationship between PG and PGI is far more complicated and suggests that, depending on the pH of the cell wall PGI may also act as an activator for PG activity; this relationship was however only found with two PG proteins and one PGI protein.

Pectin Lyase

Pectin lyases (PL) are thought to cleave the de-methylesterified pectin polysaccharides in a similar way to the polygalacturonase proteins; they are attributed with fruit ripening and have been found in pollen and germinating seeds [48]. Mallen compares a variety of PL proteins from

different fruits although all experiments are performed *in vitro* and above room temperature [46]. Papers by Gummadi and Ortega find that the optimal temperature for PL activity is 50 °C [33], [63] and a pH of between 4.5-5.5 is optimal [33] for activity, which may point to acid growth.

1.3 Data from the ERA-NET vSEED consortium

The vSEED project, funded by ERA-net, produced detailed transcriptomics data for both *Arabidopsis thaliana* and *Lepidium sativum*, using Affymetrix GeneChip ATH1 microarrays; these micro-arrays contain eleven 25-oligomer probes allocated into probesets. The data for *Arabidopsis* was collected by Bas Dekkers and Merieke van Bolderen-Veldcamp (Wageningen Seed Lab) and published by Bas Dekkers [21], the *Lepidium* data was collected by Karin Weitbrecht (University of Freiburg) and is unpublished and all the data was normalised by Simon Pearce (University of Nottingham).

Microarrays simultaneously measure the mRNA levels of all genes present on the chip within the hybridised biological sample. Active mRNA produces the related protein and so in the following thesis, mRNA levels are used as a proxy for production levels. It is important to note that this is an approximation, as transcriptomic analysis measures only mRNA levels, whether the mRNA is active or not, and does not distinguish between actively translated or inactive RNA.

For *Arabidopsis*, the ecotype Columbia-0 (Col-0) was used to analyse twenty-nine temporal and spatial conditions, with four replicates each. Firstly, a whole dry seed sample was taken (before imbibition was started), then for all further measures four individual compartments were used; the micropylar endosperm, the radicle, the cotyledons and

the remainder of the endosperm (peripheral endosperm).

The *Arabidopsis* radicle and micropylar endosperm samples were taken at times 1, 3, 7, 12, 16, 20, 25, 31 and 38 hours after imbibition, with the peripheral endosperm and cotyledons measured at 3, 16 and 31 hours after imbibition the transcriptomics levels within the lateral endosperm and cotyledons were taken. At the 25 hour samples, the seeds were segregated into two groups depending on whether they had undergone testa rupture, similarly at 38 hours the seeds were split according to whether they had undergone endosperm rupture.

The *Lepidium* data array comprises of twenty-seven conditions, designed to be directly comparable to the *Arabidopsis* time points. Since *Lepidium* seeds germinate over a shorter period of time, the radicle and micropylar endosperm samples were collected at 1, 3, 5, 7, 10, 13 and 16 hours after imbibition, with the cotyledons and lateral endosperm also taken at 3, 7 and 13 hours. As with *Arabidopsis* the seeds are segregated by testa and endosperm rupture at 7 hours and 16 hours respectively. As the *Arabidopsis* ATH1 micro-array was used for the closely related species *Lepidium*, probes may be unresponsive for *Lepidium* genes and so are removed during the post-hybridisation processing of data. An analysis of variance (ANOVA) was used to find probes which did not show differential expression across the 27 samples and these probes were subsequently removed, with a False Discovery Rate of 1%, genes with at least three probes showing differential expression were kept. Although the two species are closely related, they are not identical, and this significantly reduces the accuracy of the *Lepidium* data produced using the *Arabidopsis* chips.

1.4 Enzyme Kinetics

The Michaelis-Menten kinetics describes the creation of a product, P , from the interaction of a substrate, S , and its related enzyme, E . This form of kinetics considers the association rate, k_a , of the enzyme with the substrate and reverse rate or disassociation rate, k_d , and the rate, k_c at which a substrate/enzyme complex sequesters to form the product and original enzyme. The previously described reactions are illustrated below, (1.1).



Where k_a is the rate at which E and S associate, with the reverse k_d , the disassociation rate. The rate k_c is the rate at which $E : S$ is be converted into E and P . These rates are difficult to find, methods employed to estimate these rates take advantage of the reactions by-products such as p-nitrophenol [75] or the change in pH, as used by Chisari [14].

The ordinary differential equations (1.2)-(1.5) represent the kinetics of the reactions shown in equation (1.1) under the assumption that the law of mass action is sufficient. These equations are constructed by looking at the enzyme, E , substrate, S , product, P , and Complex, ES , separately and considering what alters their concentration over time.

$$\frac{d[E]}{dt} = -k_a[E][S] + k_d[ES] + k_c[ES], \quad (1.2)$$

$$\frac{d[S]}{dt} = -k_a[E][S] + k_d[ES], \quad (1.3)$$

$$\frac{d[ES]}{dt} = k_a[E][S] - k_d[ES] - k_c[ES], \quad (1.4)$$

$$\frac{d[P]}{dt} = k_c[ES], \quad (1.5)$$

where k_i are the previously discussed reaction rates and $[y]$ is the concentration of substance y . It is important to note that this system conserves the quantity of enzyme present, in mathematical terms:

$$[E] + [ES] = [E]_0 \quad (1.6)$$

this is referred to as a conservation law and the conservation law along with the so called Michaelis constant, K_m ,

$$K_m = \frac{k_d + k_c}{k_a}, \quad (1.7)$$

can approximate the rate of change of the product of the reaction, by equation (1.8).

$$\frac{d[P]}{dt} = \frac{V_{max}[S]}{K_m + [S]}. \quad (1.8)$$

where $V_{max} = k_c[E]_0$. The Michaelis-Menten approach is discussed fully by Murray [57].

Chapters 3, 4 and 5 consider enzyme based reactions and are modelled using differential equations, however this Michaelis-Menten approach is not used since the enzyme and substrate levels are of interest, as well as

the end product. The Michaelis-Menten simplification does not reduce computation times when this is the case and the added flexibility of the complete set of differential equations is an advantage over the Michaelis-Menten equation.

1.5 Thesis Outline

Through the course of this thesis elements of seed germination are introduced and analysed using mathematical techniques.

Chapter 2 considers the cells within a radicle. The aim of the chapter is to construct a systematic approach, using principle component analysis, to simplify each cell and categorise the cells by their shape.

The following three chapters construct a mathematical model to consider the cell wall weakening within the endosperm. Chapter 3 begins by constructing a network around PME activity, as introduced in section 1.2.2, and, through the use of activity data, parameter fitting and model simplification are undergone. The model resulting from chapter 3 is expanded, and used to inform new networks, in chapter 4. Chapter 4 results in three networks, built around the main components of the endosperm's cell walls and uses these models to consider cell wall properties during the germination process. In chapter 5, a spatial dimension is introduced to the three modelled networks developed in chapter 4 and further discussion on the implications on cell wall properties are discussed.

This thesis creates a starting framework, from which biochemical cell wall models can be developed to better understand, initially the importance of the endosperm to germination and later the contribution cell walls make to the properties of different tissues.

2. CELL SHAPE ANALYSIS

2.1 Introduction

During the germination process, an embryo's axis undergoes growth to promote the germination event; It is currently unknown when cells within the axis grow and whether it is a particular group of cells or the whole axis. This chapter aims to find a systematic approach to differentiate between the different cell types within a embryo's radicle; this method can be used to identify the location and time of cell growth by analysing the shape of individual cells, at different times after imbibition. Finding these times and locations may inform where and when cell wall remodelling occurs for the further work in this thesis.

Confocal imaging in combination with suitable software, such as MorphoGraphX [39], enables the digitalisation of the seed embryo, Figure 2.1 shows an *Arabidopsis* radicle as seen in MorphoGraphX and provided for use in this thesis by Dr Bassel (University of Birmingham, Unpublished).

Each cell shape is then simplified in Section 2.3 and the simplified shapes are compared with other cells in the same seed. These comparisons are then analysed to look for differentiating features, such as, volume or shape.

From observation of the MorphoGraphX images, there appear to be four distinct sections of the radicle: the centre of the radicle seems to consist of very long thin cells running the length of the radicle, Moving

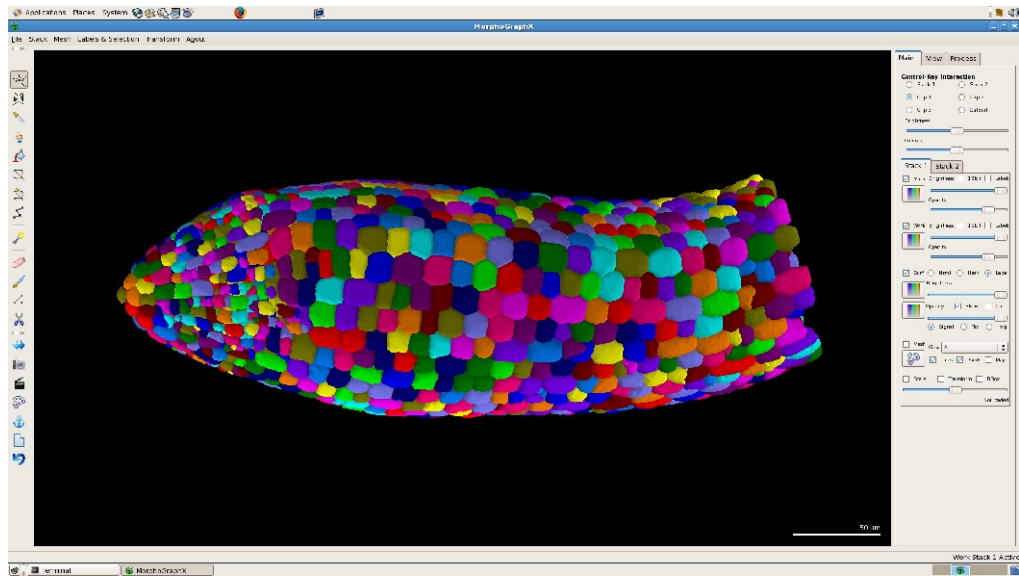


Fig. 2.1: An *Arabidopsis* embryo's radicle, three hours after imbibition, plotted using MorphoGraphX. The colours denote different cells.

out radially there appears to be rings of well organised roughly cuboid cells which make up the majority of the radicle's size, on the outer surface of the radicle is a single cell layer of less organised cells and the meristem at the tip of the radicle. Figure 2.2 shows the outer cell layer and organised layer below as they appear in a radicle. No differences are obvious when comparing cells from the different ends of the radicle; with the exception of the meristem, which is comprised of more densely packed cells.

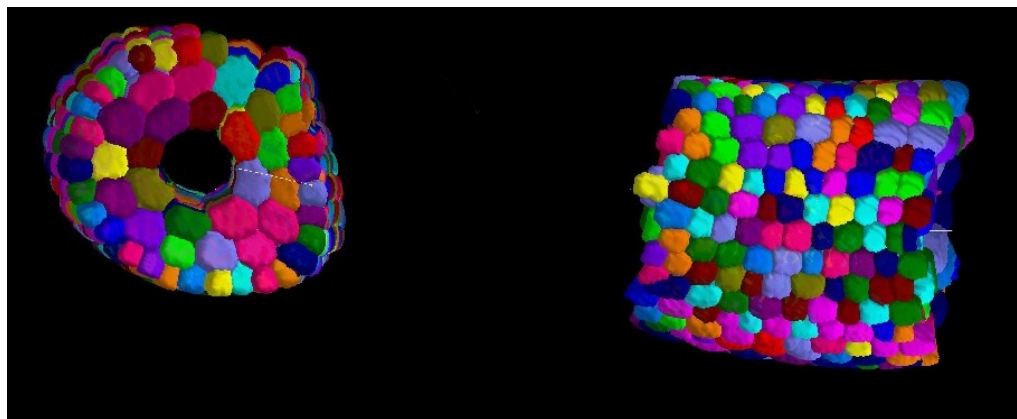


Fig. 2.2: A cross section of an *Arabidopsis* embryo's radicle, three hours after imbibition, plotted using MorphoGraphX. The central cells have been removed. The colours denote different cells.

2.2 *Digitalising the Cells*

The radicle is imaged using confocal microscopy. The advantages in clarity between this method and other methods is clearly shown, through image comparison, by White [81]; this produces grey-scale image stacks. These stacks are imported into the MorphoGraphX software. This software has been used for similar analysis for leaf growth in plants [39].

The MorphoGraphX software performs the operation of ‘colour seeding’ the image stack, which involves spreading very small spots of colour through the images. These colour seeds then undergo ‘bleeding’, which allows the spots of colour to begin spreading until they reach a significant grey-scale contrast, at which point this grey-scale contrast is considered a barrier to the spreading colour. Any two colours which meet, and are not separated by a grey-scale contrast, become one colour so as to avoid redundancies. MorphoGraphX can then establish which parts of the images constitute different cells and produces vertex-vertex surface meshes for all the individual cells and allocates a unique cell identification number.

2.3 *Shape Simplification*

Having discussed the existing MorphoGraphX software, the following steps have been implemented in order to analyse the cell shapes within a radicle. The vertex-vertex meshes, from MorphoGraphX, describe the surface of each cell, with around 800 vertices to each cell and more than 2000 cells to a radicle. For speed of computation, each cell needs to be simplified. Each cell is reduced to a centre, and three eigenvectors with associated eigenvalues, in the following way.

The centre referred to is simply the mean value of the vertices which

comprise its surface. This assumes that the vertices which make up the meshes are evenly spread across its surface. the cell centre is denoted as $\mathbf{M}_i = (M_{x,i}, M_{y,i}, M_{z,i})$, where $M_{x,i}$ is the x coordinate of the centre of cell i and with n_i the total number of vertices which comprise cell i . Each vertex, $\mathbf{u}_{i,j}$ is comprised of $x_{i,j}$, $y_{i,j}$ and $z_{i,j}$ coordinates where j ranges from 1 to n_i and so the centre can be computed by equation (2.1).

$$\mathbf{M}_i = \frac{\sum_{j=1}^{n(i)} (x_{i,j}, y_{i,j}, z_{i,j})}{n_i}. \quad (2.1)$$

Principle component analysis is used to simplify each cell in the following way: Eigenvalues and eigenvectors of each cell are calculated by looking at the square of the difference between each vertex and the centre. This is done by setting up a $3 \times n_i$ matrix, \mathbf{d} , which consists of a row for each vertex making up the cells surface and is calculated as in equation (2.2). This method finds three eigenvectors, orthogonal to one another, with there respective eigenvalues, for each cell.

$$\mathbf{d}_j = \mathbf{M}_i - \mathbf{u}_{i,j} \quad (2.2)$$

where \mathbf{d}_j is the j^{th} row of matix \mathbf{d} .

The transpose \mathbf{d}^T is multiplied by matrix \mathbf{d} and this creates the square 3×3 matrix, \mathbf{A}_i .

$$\mathbf{A}_i = \frac{\mathbf{d}^T \mathbf{d}}{n_i}, \quad (2.3)$$

from which the eigenvalues and eigenvectors are calculated:

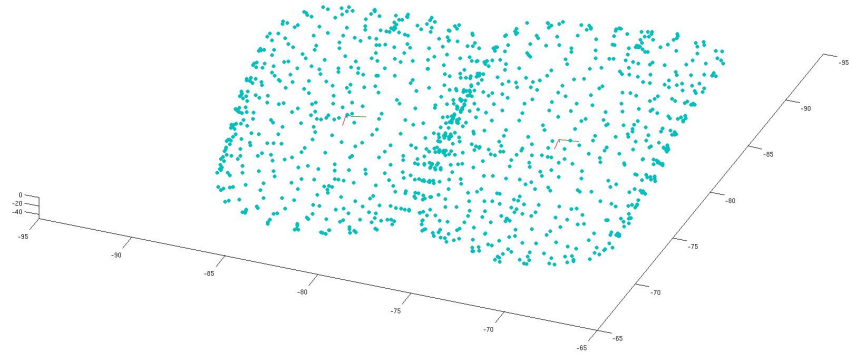
$$\mathbf{A}_i \mathbf{V}_{i,k} = \lambda_{i,k} \mathbf{V}_{i,k} \quad (2.4)$$

with $k \in \{1, 2, 3\}$. Figure 2.1 shows two typical, adjacent cells plotted as the vertices produced by MorphoGraphX and the eigenvectors plotted at the centre of each cell, from three different perspectives. The eigenvalues are labelled by dominance, meaning that the largest, middle, and smallest of a cell's three eigenvalues are $k = 1$, $k = 2$ and $k = 3$ respectively.

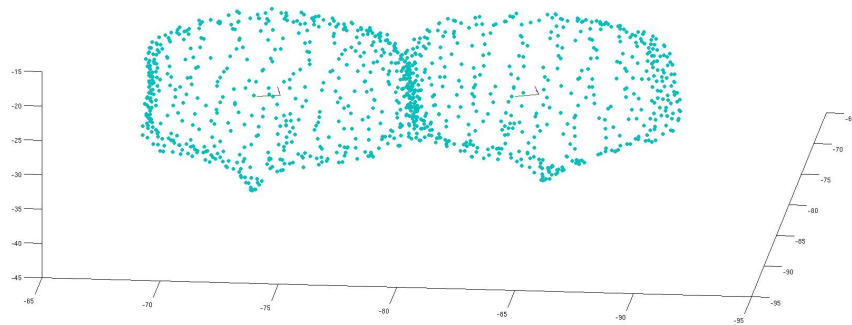
Figure 2.2 shows an axis, with all cells represented as three eigenvectors plotted at the centre of their respective cell. The meristem of this radicle can be seen as the dense distribution of cells in the upper right section of the graph, Figure 2.2. It is difficult to distinguish where the meristem ends and the rest of the radicle begins.

2.4 Analysis

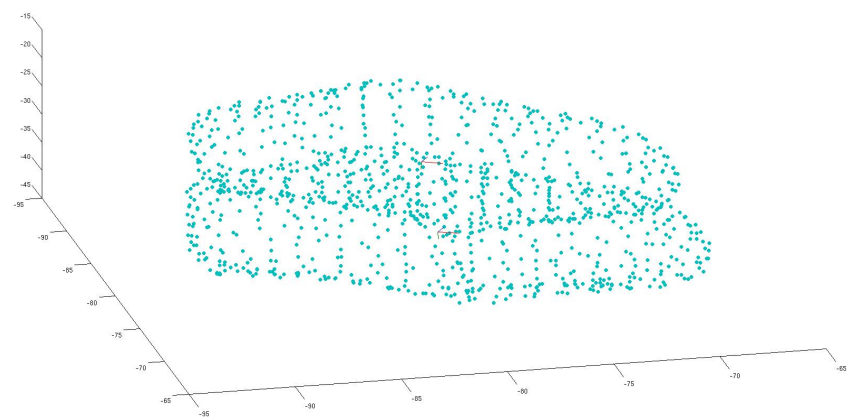
The following analysis will be done on a cross section of an *Arabidopsis* radicle, three hours after imbibition, that excludes the central cells; The central cells are not used in this preliminary analysis due to their low imaging quality. A relatively small cross section was used to reduce computing time while establishing a systematic technique for defining the cell properties of the distinct layers. A radicle, in an early stage development, was chosen since this is likely to be prior to any differentiating growth which may occur during germination. The cell ID, i , is allocated by MorphoGraphX, from smallest z coordinate to largest; there is an element of randomness to this ordering to ensure that all cells and vertices are labelled.



(a)



(b)



(c)

Fig. 2.1: Two adjacent radicle cells plotted as the MorphoGraphX vertices and derived eigenvectors from three perspectives. The cells were taken from an *Arabidopsis* radicle, three hours after imbibition.

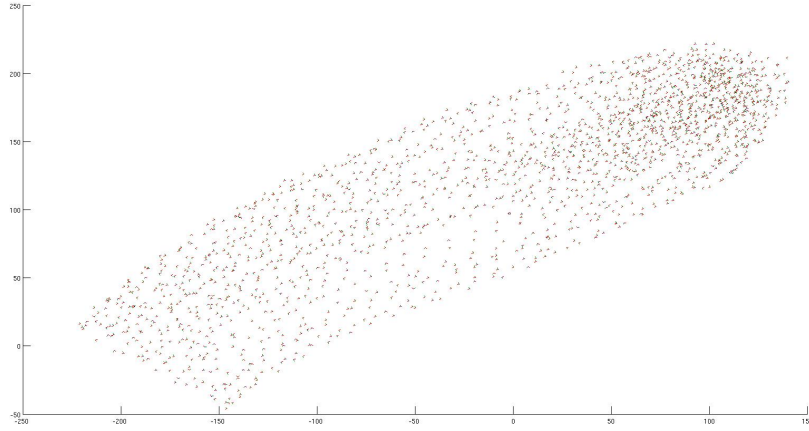


Fig. 2.2: An *Arabidopsis* embryo's radicle, three hours after imbibition, with each cells eigenvectors plotted at that cells centre.

The three eigenvalues can be used to calculate the volume assuming regular shapes. So, assuming cell i is a regular cuboid, the volume, $Vol_{i,c}$, of the cell is:

$$Vol_{i,c} = 2 \sqrt{\lambda_{i,1} \lambda_{i,2} \lambda_{i,3}}, \quad (2.5)$$

the equation for each cells' volume, when assuming each cell is an ellipsoid can be calculated by equation (2.6).

$$Vol_{i,e} = \left(\frac{4}{3}\right)\pi \sqrt{\lambda_{i,1} \lambda_{i,2} \lambda_{i,3}}. \quad (2.6)$$

The scatter graph in Figure 2.3 shows each cells volume as calculated in equation (2.5). These volumes are measured in pixels and are subject to the resolution and grey scale used during the digitalisation step.

There appears to be a cyclic behaviour within these cells, Figure 2.3: the first one hundred cells increase in volume as the CellID increases.

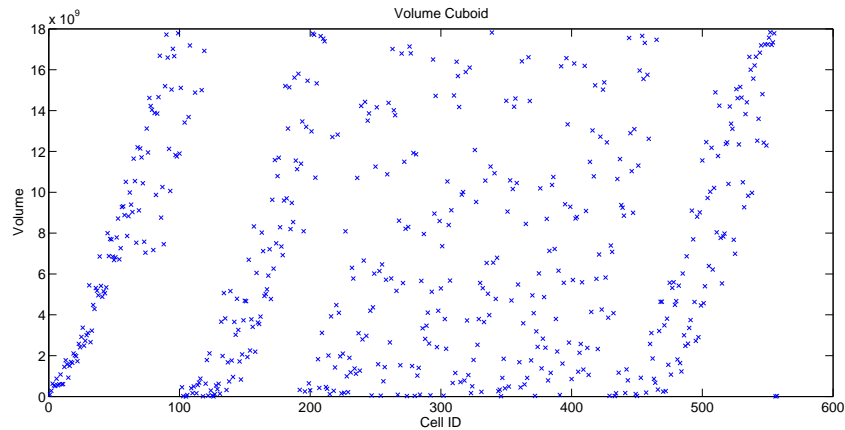
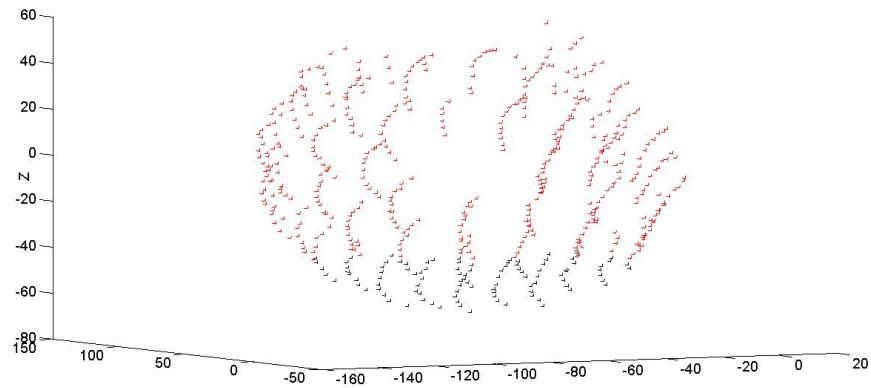


Fig. 2.3: Cell volumes, assuming the cells are cuboids, by location along the axis.

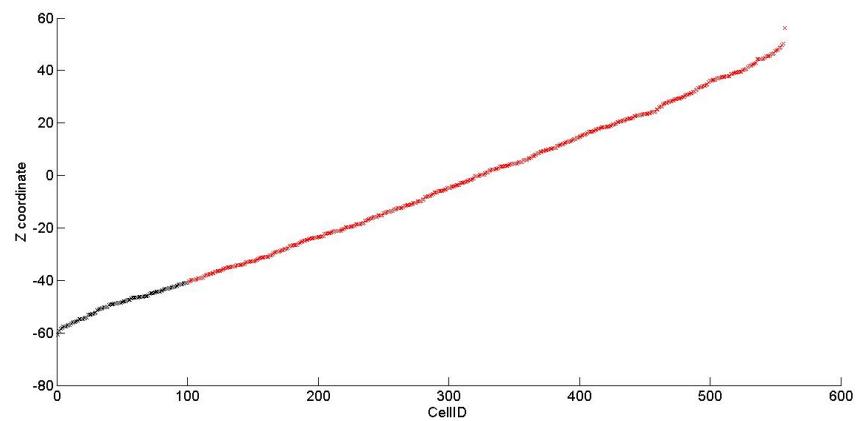
The cells, $i \in \{101, \dots, 200\}$, look to have the same although slightly weaker correlation between increase in CellID and volume. Cells, $i \in \{201, \dots, 400\}$, do not show any pattern, it is possible that there are several overlapping patterns here. The last hundred cells appear to show the previously seen cyclic pattern.

Figure 2.3 (a) shows the considered section of radicle, plotted as the cells' eigenvectors positioned about each cells' centre. The first one hundred cells have black eigenvectors and all other eigenvectors are red. This is a 3D plot and has been orientated to look down the radicle. The position of the first one hundred plotted cells suggests that either the near end of the radicle has smaller cells or the cells in the outer layer are smaller in volume than the layer beneath it. Either of these hypothesis would result in the discontinuity in the cyclic pattern seen for the mid ranged CellIDs, $i \in \{201, \dots, 400\}$. The last one hundred cells, $i \in \{458, \dots, 557\}$, resume the cyclic pattern, rather than producing a negative version of the correlation, implying that the near cells, as Figure 2.3 (a) is orientated, are smaller in volume than the further cells. Without more data it is possible that this is simply an artifact of the data and no cyclic pattern is present biologically. Figure 2.3 (b) confirms that with this data set the CellIDs are

allocated by z value.



(a)



(b)

Fig. 2.3: Section of *Arabidopsis* radicle, three hours after imbibition, (a) shows the three eigenvectors of each cell positioned from the centre of their cell and (b) shows the CellID plotted against the z-coordinate of the cell centre. In both graphs the first one hundred CellIDs are black and all others coloured red.

As well as volume, cell shape can be analysed to determine whether the cell is regular (length, height and depth are all equal) or whether the cell favours one of the axis of growth (one of the eigenvectors is larger than the others). To analyse the cell shapes across the axis, the elongation in each of the cell's primary directions is considered. For the three eigenvalues in perpendicular directions, the elongation in the

respective direction is calculated using equations (2.7) - (2.9).

$$E_{1,i} = \frac{\lambda_{1,i}}{\sum_{k=1}^3 (\lambda_{k,i})}, \quad (2.7)$$

$$E_{2,i} = \frac{\lambda_{2,i}}{\sum_{k=1}^3 (\lambda_{k,i})}, \quad (2.8)$$

$$E_{3,i} = \frac{\lambda_{3,i}}{\sum_{k=1}^3 (\lambda_{k,i})}. \quad (2.9)$$

Each cells' elongation values are compared in the scatter graphs in Figure 2.4, 2.5 and 2.6.

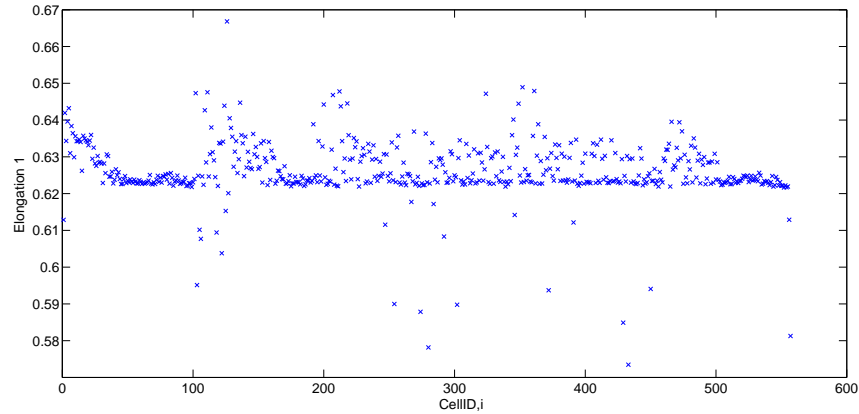


Fig. 2.4: Plot of each cells $E_{1,i}$

An $E_{1,i} \approx 1$ means that the dominant eigenvalue is far larger than the other two, $\lambda_{2,i} \approx \lambda_{3,i} \approx 0$, and will correspond to a long thin cylindrical cell whereas $E_{1,i} \approx \frac{1}{3}$ would suggest a cube or sphere since $\lambda_{2,i} \approx \lambda_{3,i} \approx \frac{1}{3}$, due to the eigenvalues being ordered by dominance. Figure 2.4 shows a very dense grouping of cells with $E_{1,i} \approx 0.624$. There are signs of the previously seen cyclic pattern: the first set of smaller cells in Figure 2.3 have larger $E_{1,i}$ values, suggesting that the cells along a cell file increase in magnitude on one or both of the two non-dominant axis. When the cells whose $E_{1,i} \leq 0.62$ are used to colour the MorphGraphX image no localisation or pattern is discernible.

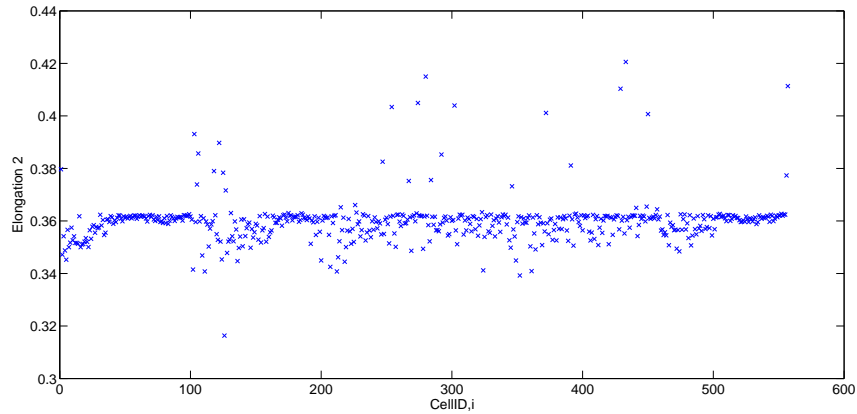


Fig. 2.5: Plot of each cells $E_{2,i}$

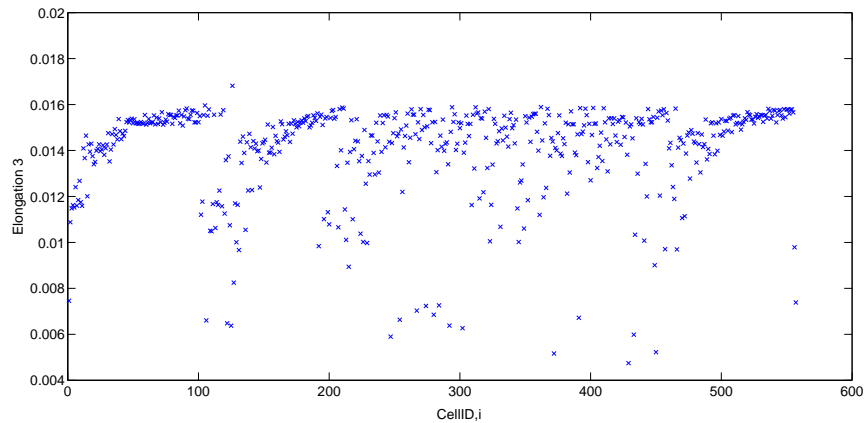


Fig. 2.6: Plot of each cells $E_{3,i}$

Both $E_{2,i}$, Figure 2.5, and $E_{3,i}$, Figure 2.6, increase where $E_{1,i}$ decreases, in the cyclic pattern observed previously. This suggests that the near cells, as Figure 2.3 (a) is orientated, are longer and thinner than the more regularly shaped further cells. The cells change as progress is made down the cell files. The near cells are more than twice as long as they are wide, with minimal depth. The farther cells increase in volume and probably remain at the same length, while increasing width and a small amount of depth. This may be due to the position of the cells within the seed, the near cell would lie closer to the cotyledons and so may be compressed by the rest of the embryo; in comparison the farther cells,

closer to the meristem have more room to expand freely.

2.5 Cell Orientation

With the shape analyses so far, we have not considered orientation within the axis and by analysing which direction the cell is elongated in we hope to be able to separate the three cell types within the axis. The cortical cells are very long and thin, elongated in the primary elongation direction, being the direction in which the axis grows. The other cells appear to be elongated in the radial direction.

Due to these differences, relabelling the existing eigenvalues so that $\lambda_{1,i}$ points closest to the primary growth direction, $\lambda_{2,i}$ points closest to the radial direction and leaving $\lambda_{3,i}$ to point in a circumferential direction, could enable the separation of the three cell types by their shape alone.

In order to relabel the eigenvalues, finding a curve that follows the centre of the axis at all points is essential in order to establish orientation of each cell relative to the whole tissue. Once this curve has been found, the eigenvalue to be labelled $\lambda_{1,i}$ is associated with the eigenvector closest to tangential with the closest point on the central curve. The eigenvalue to be labelled $\lambda_{2,i}$ is associated with the eigenvector closest to the vector from the centre of the cell to the central curve. The remaining eigenvector should be closest to the circumferential direction of the radicle.

2.5.1 Curve of best fit

Assuming that the cells are evenly distributed around the centre of the radicle, we look for the curve which minimises the distance between all the cell centres, the curve of best fit; this curve is found by minimising $F(s)$ as defined in equation (2.10), where $f_x(s)$ is a function used to map

the curve in the x direction, likewise, $f_y(s)$ and $f_z(s)$ are functions used to map the curve in the y and z direction respectively and x_i , y_i and z_i are the x , y and z coordinates of the centre of cell i .

$$F(s) = \sum_{i=1}^n \left(\begin{pmatrix} x_i \\ y_i \\ z_i \end{pmatrix} - \begin{pmatrix} f_x(x_i) \\ f_y(y_i) \\ f_z(z_i) \end{pmatrix} \right)^2 + \kappa \int \begin{pmatrix} \frac{d^2 f_x(x_i)}{ds^2} \\ \frac{d^2 f_y(y_i)}{ds^2} \\ \frac{d^2 f_z(z_i)}{ds^2} \end{pmatrix} ds, \quad (2.10)$$

with κ a constant to be estimated. The last term in this equation is a differential penalty as discussed by Jupp [37], to encourage a more linear solution; the components of the solution, $f_x(s)$, $f_y(s)$ and $f_z(s)$, can be linear, quadratic or even polynomials of higher order. The final term in equation (2.10), therefore contributes to $F(s)$ and this contribution is larger for higher order polynomials this method is used in a book by Green and Silverman [31]. This $F(s)$ is minimised using MatLab's builtin Nelder-Mead search function (`fminsearch`) on a test sample of radicle cells and a variety of starting parameter sets which include a small κ (between 0.5 and 2) and $f_x(s)$, $f_y(s)$ and $f_z(s)$ set to be general fourth order polynomials, cubics and quadratics. After using a variety of starting parameter sets the algorithm finds a straight line through the centre of the radicle orthogonal to the desired line more frequently than the curve of best fit is found; this suggests a better set of starting parameters is required to find the desired fit for a general three dimensional vertex cloud.

Bézier curves were considered, since the MorphoGraphX software, used to visualise the data, was already programmed to draw these parameterised curves, and they can be uniquely defined with a small series of points. Bézier curves are commonly used in computer graphics for

smoothing edges. The general Bézier curve is parameterised in t , with $0 \leq t \leq 1$, with an ordered set of Bézier points, P , each point consisting of an x, y and z coordinate; these points are connected to their neighbour(s) and these connecting lines are independently scaled to range from 0 to 1 and a point, $T_{i,1}$, lies upon each line. All neighbouring $T_{i,1}$ s are connected with a straight line, which will shift as all T s travel along their lines. Again, these lines connecting neighbouring $T_{i,1}$ s are scaled so that a point $T_{i,2}$ ranges from 0 to 1 and these $T_{i,2}$ s are further connected to their neighbours. This process is continued until one is left with one line whose point is $T_{1,n}$, where n is one less than the size of the set P . The Bézier line is then the course which $T_{1,n}$ takes as all the T s simultaneously increase in value from 0 to 1 and we refer to this $T_{1,n}$ simply as $B(t)$. Bézier curves are discussed in depth by Yamaguchi [82], with the primary focus being on their use in computer graphics and Zhao [85] suggests a method for using Bézier curves to find the line of best fit in a two-dimensional space, which we extend to include a third dimension.

The general form of the Bézier equation is:

$$B(t) = \sum_{i=0}^n \frac{n!}{i!(n-i)!} t^i (1-t)^{n-i} P_i, \quad (2.11)$$

$$B(t) = (1-t)^4 P_1 + 4t(1-t)^3 P_2 + 6t^2(1-t)^2 P_3 + 4t^3(1-t) P_4 + t^4 P_5. \quad (2.12)$$

For the section of radicle being considered in this section, the Bézier points, P , are shown in Table 2.1 and the Bézier curve is plotted in Figure 2.7.

With a complete radicle these Bézier points would be optimized in

Bézier Points	X	Y	Z
P_1	-115.641	-48.3234	-13.0475
P_2	-85.7865	4.60143	-6.25558
P_3	-69.2044	39.5959	0.0402638
P_4	-50.8854	81.4062	3.93641
P_5	-25.6222	125.522	10.7155

Tab. 2.1: Table of bezier points determined by Dr Bassel (university of Birmingham)

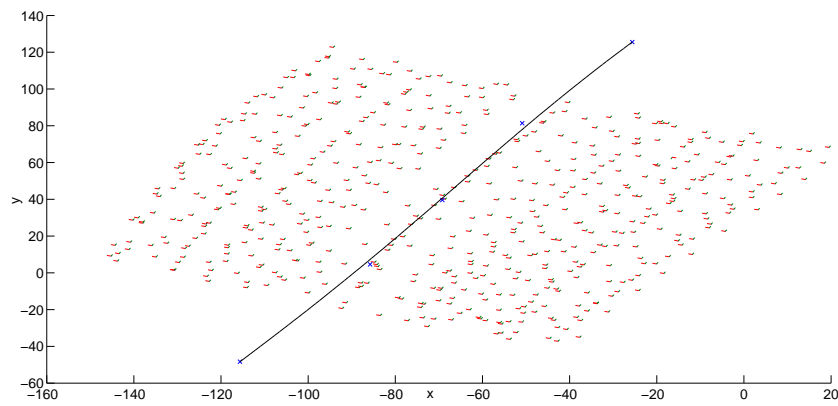


Fig. 2.7: The considered section of radicle with bezier curve.

matlab, using the built in genetic algorithm function (ga) however, since this section of radicle does not include the central cells and all eigenvectors for one cell are orthogonal to one another, the curve is of sufficient accuracy to continue without optimizing the curve.

2.5.2 Relabelling The Eigenvalues

The next step in relabelling the eigenvectors is to assign each cell a t -value, t_i , to each cell, i , this t -value denotes the closest point on the Bézier to the cell.

Once this is done, inequalities (2.14), (2.15) and (2.16) are defined from the geometric definition:

$$\mathbf{A} \cdot \mathbf{B} = |\mathbf{A}||\mathbf{B}| \cos(\theta), \quad (2.13)$$

where θ is the angle between lines **A** and **B**.

Each cell's eigenvector which points closest to the axis's growth direction will be named $\hat{V}_{i,1}$. The three eigenvectors for cell i are considered and the eigenvector for which inequality (2.14) is true will be the desired eigenvector, $\hat{V}_{i,1}$, its related eigenvalue will be labelled $\hat{\lambda}_{i,1}$.

$$\frac{\pi}{4} > \left| \cos^{-1} \left(\frac{\mathbf{V}_{i,k} \cdot \frac{d(B(t_i))}{dt}}{\left| \frac{d(B(t_i))}{dt} \right| \|\mathbf{V}_{i,k}\|} \right) \right| \geq \frac{7\pi}{4}. \quad (2.14)$$

Inequality (2.14) looks for the eigenvector which is within the 90° cone, emanating from the centre of the cell, centred about the direction of the gradient of the Bézier curve at point t_i . There will be one and only one such eigenvector for each cell, since the three eigenvectors are orthogonal to one another. This is illustrated in Figure 2.8 with the red line the centre of the inequality (2.14).

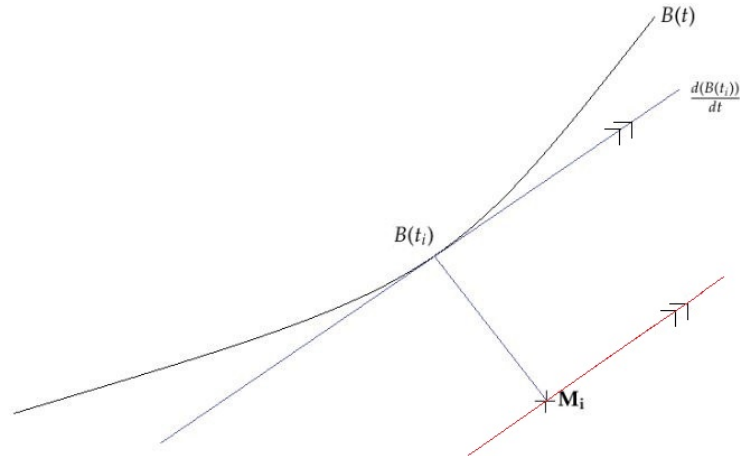


Fig. 2.8: An illustration of a cell centre and the Bézier curve with the red line the centre of the 90° cone used to calculate which eigenvalue and eigenvector are labeled $\hat{\lambda}_{i,1}$ and $\hat{V}_{i,1}$, respectively

The second of the directionally labelled eigenvectors will be in the radial direction or the eigenvector which is closest to the vector joining

the centre of the cell i to the point $B(t_i)$ and as such satisfies inequality (2.15).

$$\frac{\pi}{2} > \left| \cos^{-1} \left(\frac{(\mathbf{V}_{i,k} \cdot (B(t_i) - \mathbf{M}_i))}{|(B(t_i) - \mathbf{M}_i)| |\mathbf{V}_{i,k}|} \right) \right| \geq \frac{7\pi}{4}. \quad (2.15)$$

The eigenvector which lies within 45° of the vector $B(t_i) - \mathbf{M}_i$ as seen in Figure 2.9, is labelled $\hat{V}_{i,2}$ and its related eigenvalue, $\hat{\lambda}_{i,2}$.

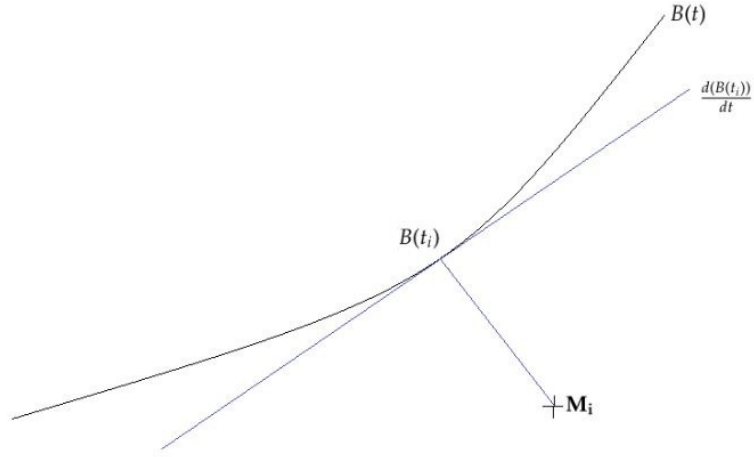


Fig. 2.9: An illustration of a cell centre, \mathbf{M}_i and point $B(t_i)$, for use in calculating $\hat{V}_{i,1}$ and $\hat{V}_{i,2}$

Finally eigenvector $\hat{V}_{i,3}$, and consequently eigenvalue $\hat{\lambda}_{i,3}$, will then be the remaining eigenvector which is closest to the radial direction or closest to the vector orthogonal to both $\frac{d(B(t_i))}{dt}$ and $B(t_i) - \mathbf{M}_i$ and so satisfies the inequality (2.16).

$$\frac{\pi}{2} > \left| \cos^{-1} \left(\frac{(\mathbf{V}_{i,k} \cdot ((B(t_i) - \mathbf{M}_i) \times \frac{d(B(t_i))}{dt}))}{|((B(t_i) - \mathbf{M}_i) \times \frac{d(B(t_i))}{dt})| |\mathbf{V}_{i,k}|} \right) \right| \geq \frac{7\pi}{4}. \quad (2.16)$$

With all of the eigenvectors and eigenvalues labelled by direction it is easy to plot the recalculated elongation values using the new labelling, with the added advantage that the cells can be ordered by the position

along the Bézier curve, t -value, or distance from the Bézier curve, $B(t_i) - \mathbf{M}_i$.

2.6 Separation of Cell Types

The surface layer of cells is by definition further away from the central Bézier curve than the inner cells. In Figure 2.10, this distance is plotted against each cells' t -value.

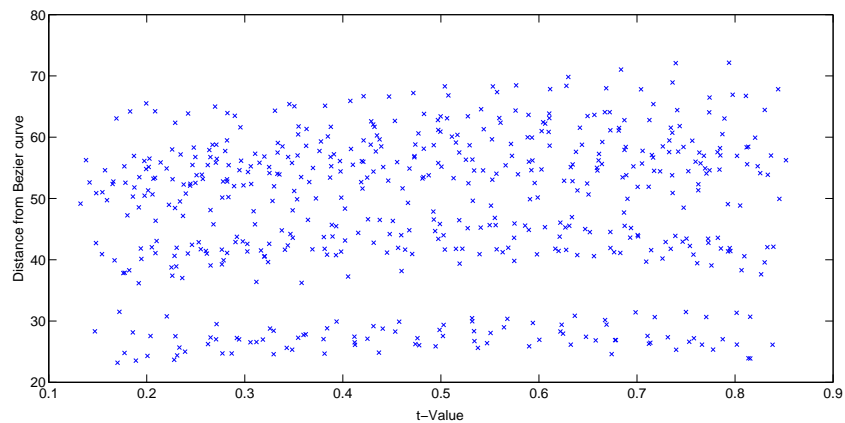


Fig. 2.10: The distance of each cell centre away from the Bézier curve plotted against its position along the radicle, t -value.

Figure 2.10 shows three bands of vertices. The inner cell files lie between twenty and thirty units of distance, the next circle of cell files lie between thirty five and forty eight units of distance. The outer cells are far more varied in distance, from forty five to seventy five units away from the Bézier curve: this larger width for each radial layer of cells highlights the outer cells' disorder when compared to the inner cell files. These clear bands of cell files allow the subsequent graphs to be plotted against distance to easily distinguish the surface cells from the inner cells.

With the exception of the order in which the points are plotted, Figure 2.11 is the same as the graph in Figure 2.5, suggesting that all the cells are second longest in the growth direction.

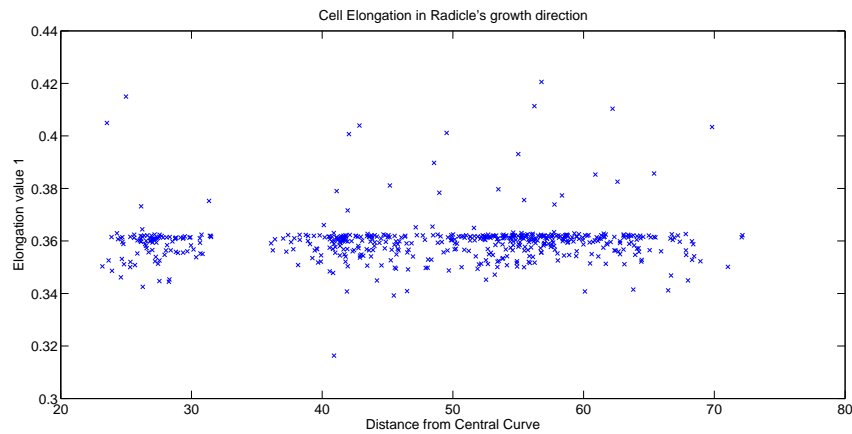


Fig. 2.11: Each cell's elongation in the radicle's primary growth direction against the distance of each cell centre away from the Bézier curve.

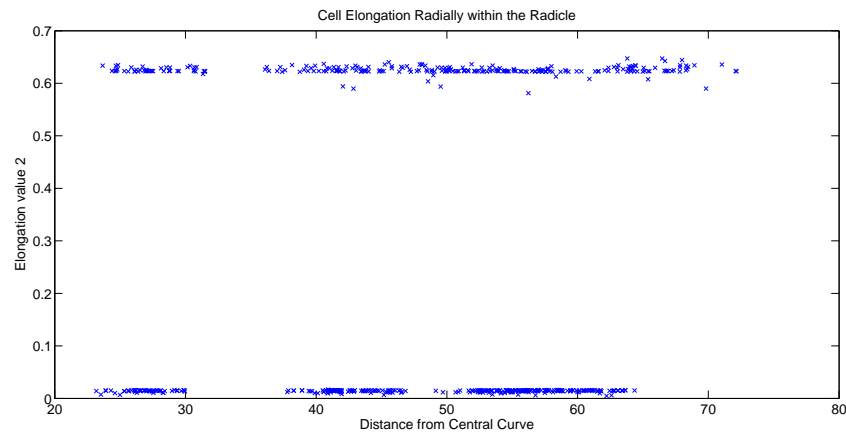


Fig. 2.12: Each cell's elongation radially from the Bézier curve, against distance of each cell centre away from the Bézier curve.

Figures 2.12 shows that the cells are either longest or shortest in the radial direction. The split between which cells are longest and which are shortest in this direction does not coincide with any positional pattern. The remaining elongation values, in the circumferential direction, are shown in Figure 2.13.

This method does not distinguish the two types of cells in the considered section of radicle. It is perhaps surprising that the organised interior cells do not seem to have similar shapes to their neighbours but conversely it is expected that some of the less ordered cells may be similar

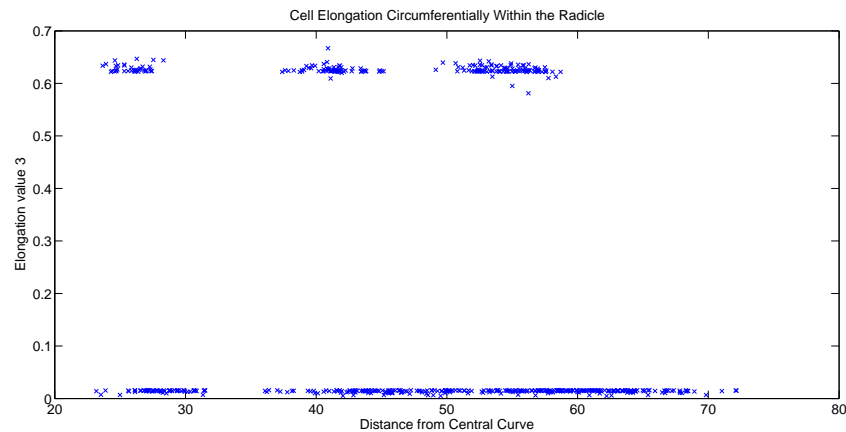


Fig. 2.13: Each cell's elongation circumferentially around the radicle, against distance of each cell centre away from the Bézier curve.

in shape to the interior cells.

2.7 Conclusion

This chapter considers the vertex-vertex mesh of cells within the radicle of an *Arabidopsis*, three hours after imbibition, and simplifies each cell into a cell centre, three eigenvalues and the three associated eigenvectors. The simplified cells are then analysed but found to have fairly similar shapes. The labelling of the eigenvalues and eigenvectors is altered so that instead of dominance they are labelled by direction relative to the radicle. Although this reordered the eigenvalues, the different cell types were not found to be distinct in shape or size. This radicle was early in the germination process and so may have no major distinction between cell shapes at this stage, data from a late radicle could show this method to be sufficient to separate cells types and so highlight the lack of distinction in earlier seeds.

The method of creating a Bézier curve through the radicle, as a curve of best fit, enables the cell distance from the centre to be calculated and did successfully separate the cells by their each layer within the radicle.

Additionally, the Bézier curve is used to assign each cell a t -value, from 0 to 1, which denotes its position along the length of the radicle. This t -value will be useful when comparing cells from other radicles i.e. radicles at different developmental stages or from different species altogether.

The central cells of the radicle have severely different cell shapes and as such this method would be sufficient to differentiate these cells if more data is produced.

A more accurate cell simplification would improve the method but whether the cells are uniformly different between the two cell types is hard to say. The cell simplification can be done by weighting each vertex by the area of the triangles this vertex helps to form; this would remove the assumption that the vertices are evenly spaced on the surface of the cell.

The considered radicle was from a seed, three hours after imbibition. This is early in the germination process and as such the two cell types may not have differentiated themselves significantly from one another, especially when compared to the two cell types of a radicle further along the germination process. The method described in this chapter may be sufficient to separate the two tissues of a more developed radicle.

3. ORDINARY DIFFERENTIAL EQUATION MODEL

INVESTIGATING THE ROLE OF PECTIN METHYLESTERASE IN THE CELL WALL

The aim of this chapter is to consider whether the two different groups of pectin methylesterase (PME) have unique functions. The two groups differ as the first group can perform only PME-like activity, as explained 1.2.2, the second group can prevent PME-like activity (inhibitors) as well as perform the same PME-like activity; there is no literature analysing the capacity of the second group to inhibit PME activity, it is only known that they have the required domain.

Firstly, a biologically informed network of reactions is constructed (Section 3.1) and this network is converted into a system of ordinary differential equations (section 3.2). The data provided in Figure 3.1 will be used to inform the constructed model by parameter fitting, more precisely by using MatLab's builtin genetic algorithm. Finally, in order to try and discover the significance of the separate groups of PME a model simplification is attempted with a view to prepare the network for expansion in future models.

Data derived from the vSEED consortium [21], discussed in section 1.3, is used to approximate the levels of each protein over time and included in the ODE model constructed in section 3.2.

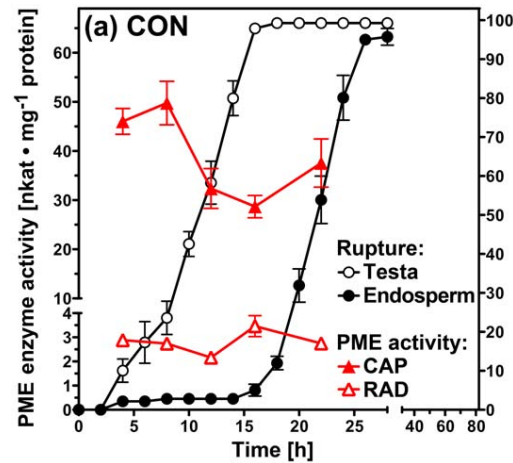


Fig. 3.1: Activity of all PME_s during the germination process, shown using triangles and measured in nKat/mg of protein. Circles indicate testa and endosperm rupture and are measured in percentage of total seeds. The image and data are provided by Prof. G Leubner (Royal Holloway University), unpublished

3.1 Biological Network

Homogalacturonan, as explained in section 1.2.1, is synthesised in a highly methylsterified form. Some cell wall remodelling enzymes, such as polygalacturonase (PG), are unable to access the relevant activity sites until this methylesterified homogalacturonan (MeHG) undergo demethylesterification to become de-methylesterified homogalacturonan (dHG). The polysaccharide MeHG is de-methylesterified by an enzyme to become dHG; the enzyme family responsible for this is called pectin methylesterase (PME). We assume that this reaction is irreversible following discussions with Professor Paul Knox (University of Leeds); this hypothesis will not be tested.

The PME family can be split into two groups, both of which can be inhibited by a pectin methylesterase inhibitor (PMEI). The exact method of inhibition is unknown but it is assumed that the PMEI protein binds with the PME domain, removing its ability to convert MeHG into dHG. The first set of enzymes in the PME family is called PME group 1 (GI) and

these are comprised solely of a PME domain and differ from the second group (GII), as GII comprises of both a PME and a PMEI domain; the GII protein is assumed to be self inhibiting but not able to inhibit GI proteins; again, this inhibition is assumed to be the GII PME domain binding with its PMEI domain and removing the protein's ability to convert MeHG to dHG. These proteins and their domains are illustrated below in Figure 3.2.

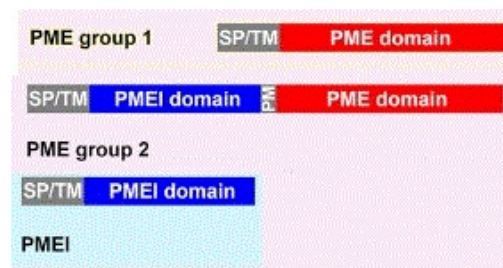


Fig. 3.2: Illustration of the two different *PMEs* with the *PMEI* protein and the domains they are comprised of, provided by Prof. G Leubner (Royal Holloway University), unpublished. In this illustration, SP denotes the signal peptide, TM the transmembrane and PM the processing motive

The presence of two opposing domains making up GII group *PMEs* implies a role for the GII proteins that the GI proteins cannot fulfil. They may simply be a self regulating protein, meaning they inhibit themselves after removing a methylester side chain from MeHG and so preventing GII from having traditional enzyme activity.

The network diagram below (Figure 3.3) shows the considered interactions of the *PME* (GI and GII) and *PMEI*.

3.2 Mathematical model

We convert the network diagram in Figure 3.3 into a system of eight ordinary differential equations (ODEs). Each equation considers the rate of change of the respective protein, protein complex or polysaccharides.

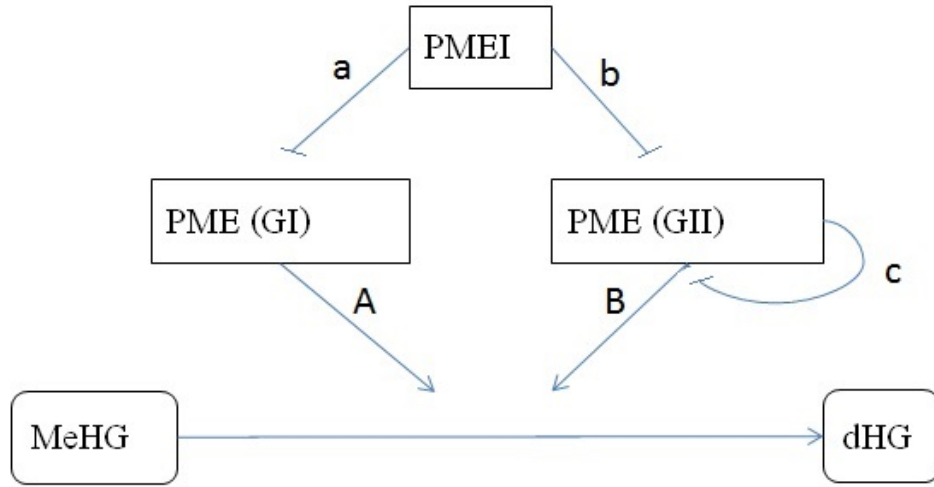


Fig. 3.3: Network Diagram, where a , b and c are the rates at which a PME_I domain binds with a PME domain and A and B the rates at which MeHG is de-methylesterified.

This model does not include production of polysaccharides since this is assumed to be slow when compared with protein production and activity. As discussed in section 1.4, Michealis-Menten is not used here since it does not reduce computation times due to our interest in all variables but the law of mass action is used in these equations.

Equation (3.1) considers the MeHG polysaccharides, with $[MeHG]$ denoting the mass pre volume of cell wall. Since MeHG is a long chain with multiple activity sites, it is more useful to consider the locations that PME interacts with than the amount of MeHG present: it is likely that the concentration of activity sites is proportional to the concentration of MeHG but their distribution is unknown. Thus we take

$$\frac{d[MeHG]}{dt} = -A[GI][MeHG] - B[GII][MeHG]. \quad (3.1)$$

The presence of GI converts $MeHG$ into dHG at a rate of A and likewise the presence of GII converts $MeHG$ into dHG at a rate of B . The $MeHG$ polysaccharide's activity sites converted in these reactions to become de-

methylesterified homogalacturonan activity sites (mass per volume of cell wall) dHG is modelled by equation (3.2). The sum of $MeHG$ and dHG should be constant, providing a simple check on the numerics.

$$\frac{d[dHG]}{dt} = A[GI][MeHG] + B[GII][MeHG]. \quad (3.2)$$

The PMEs required for $MeHG$ conversion are enzymes and therefore are not consumed by the reactions described above; they can, however, create complexes whereby the $PMEI$ proteins inhibit the PME and prevent the PME from cleaving methyl side chains from the homogalacturonan. $PMEI$ is taken to create complexes with GI and GII irreversibly at rates a and b respectively. As GII proteins contain both PME and $PMEI$ domains, we include a term allowing GII to inhibit itself. This inactive form of GII is a modelling choice and denoted as $IGII$. The PME inhibition can be seen in equations (3.3) and (3.4), while equation (3.5) describes the $PMEI$ reactions. The inactive $[IGII]$, $[PMEI : GI]$ and $[PMEI : GII]$ complexes are described by equations (3.6), (3.7) and (3.8).

$$\frac{d[GI]}{dt} = -a[GI][PMEI] + \alpha_s \beta_{GI,s}(t) \quad (3.3)$$

$$\frac{d[GII]}{dt} = -b[GII][PMEI] - c[GII] + \alpha_s \beta_{GII,s}(t) \quad (3.4)$$

$$\frac{d[PMEI]}{dt} = -a[GI][PMEI] - b[GII][PMEI] + \alpha_s \beta_{PMEI,s}(t) \quad (3.5)$$

$$\frac{d[IGII]}{dt} = c[GII] \quad (3.6)$$

$$\frac{d[PMEI : GI]}{dt} = a[GI][PMEI] \quad (3.7)$$

$$\frac{d[PMEI : GII]}{dt} = b[GII][PMEI] \quad (3.8)$$

The β_i terms are production rates of gene i dependent on time t .

These functions β are found using the cumulative values of the protein i from the vSEED (section 1.3) transcriptomics data of species s , with each point connected by straight lines to its neighbours to create continuous functions. These $\beta_{i,s}$ functions are plotted in Figure 3.4 for *Arabidopsis* and in Figure 3.5 for *Lepidium*. Since transcriptomics measures mRNA levels, we assume a constant translation of protein from all present mRNA. The non-dimensional parameter α_s converts the activity levels from the transcriptomics data to protein levels relative to polysaccharide activity sites, for species s ; this quantity is unknown and not practical to find. It is likely that the α_s value for *Arabidopsis*, α_A , and *Lepidium*, α_L , are different, so the two distinct α_s will be reduced to a single parameter by using cross species house keeping genes (Section 3.3); parameter fitting will be relied upon to produce the value of this remaining parameter.

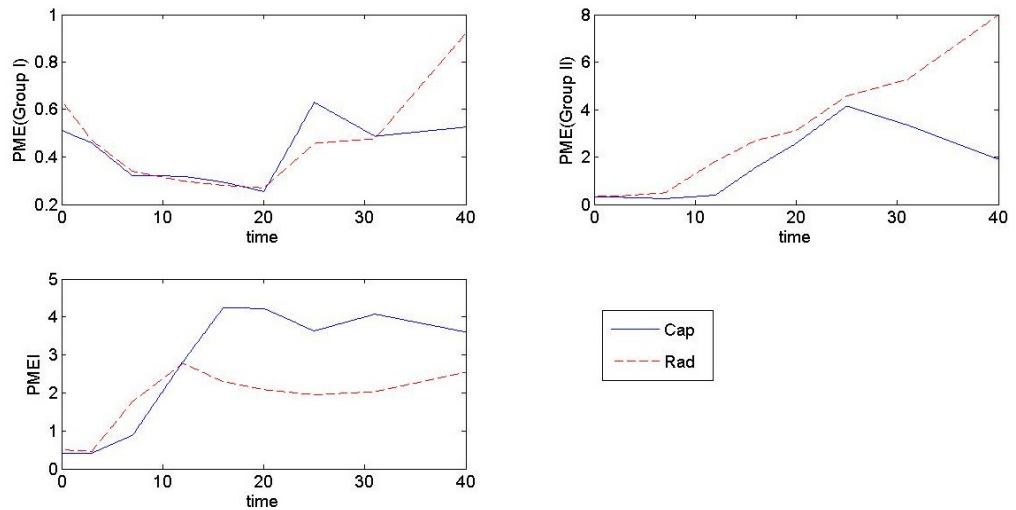


Fig. 3.4: β functions: mRNA levels, within the cap and radicle of *Arabidopsis*; these levels are used as approximations of protein production

We set the initial conditions to be 100 sites (mass per volume) for the $[MeHG]$, 0 sites (mass per volume) of $[dHG]$ and all proteins will be considered to be initially absent. All activity rates, A and B , are set to $0.6 \mu\text{m}^3/\text{mg s}$ and the inhibition rates, a , b and c , set slightly lower at

0.4 $\mu\text{m}^3/\text{mg s}$; these activity rates are set to promote the conversion of *MeHG* to *dHG*, within the values found for *PME* activity (being 0.117 $\mu\text{m}^3/\text{mg s}$ and 0.84 $\mu\text{m}^3/\text{mg s}$ [60]), it should be noted that these values are approximations as they are found using cowpea pectins and citrus *PME*.

The mRNA levels of the three protein families are shown in Figure 3.4 and assumed to be proportional to protein production. The group I *PMEs* are produced throughout the forty hour time period at relatively low levels, when compared to the group II *PMEs*. The production of *PME* group II proteins is constantly higher in the radicle than in the cap.

The first *Arabidopsis* seeds are said to start germinating at roughly 32 hours and so it is interesting that at this time the *GI* mRNA switches to being more abundant in the radicle than the cap; this could reflect the endosperm's redundancy post-germination. By this 32 hour mark, the *GII* mRNA in the radicle are also outnumbering those of the micropylar endosperm or cap, and so production in the radicle will be greater.

The *PMEI* proteins are more prominent in the cap; the loss of methylester side chains initially allows for calcium cross-linking [11], which would strengthen the cell walls although it also allows cleaving by other cell wall remodelling proteins, such as polygalacturonase, which is thought to separate cells completely. The purpose of high *PMEI* activity in the micropylar endosperm region is unknown.

The protein production within *Lepidium* (Figure 3.5) appears to be phasic: first the group I *PMEs* are produced, then the *PMEI* proteins and finally the group II *PMEs*. This is clearer in the radicle data, since the group II *PMEs* do not seem to have the same escalation within the cap, after the testa rupture. As with the *Arabidopsis*, the *PMEI* within the *Lepidium* seems to be more prominent in the cap.

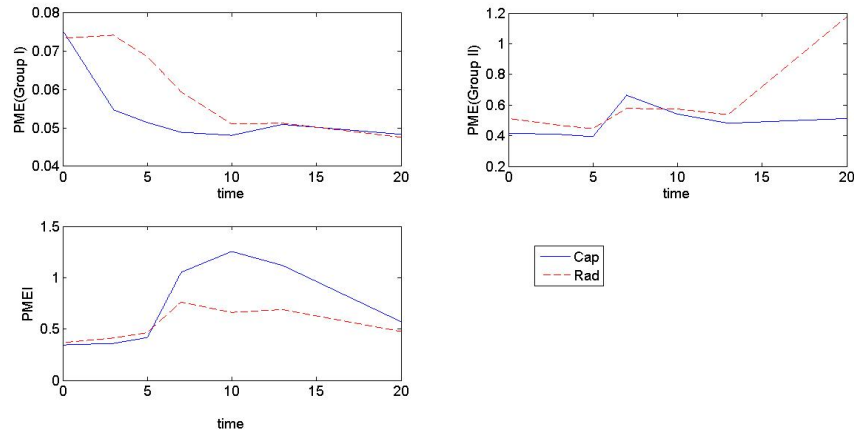
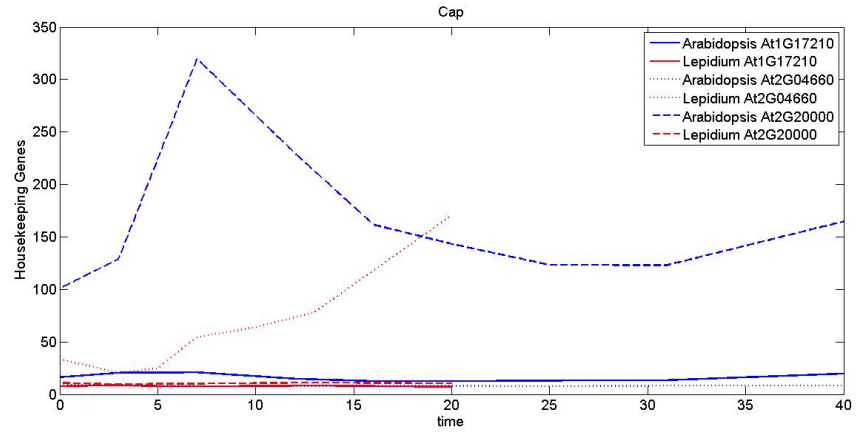


Fig. 3.5: β functions: mRNA levels, within the cap and radicle of *Lepidium*; these levels are used as approximations of protein production

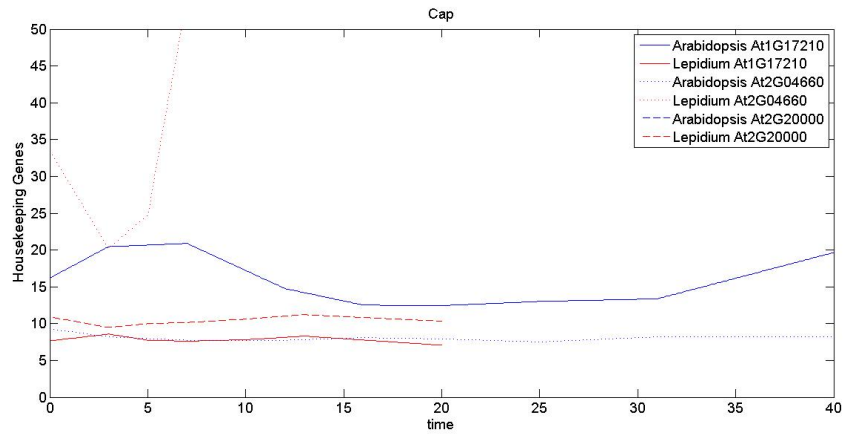
3.3 Cross-species house keeping genes

The vSEED transcriptomics data have been normalised within each species, as described in section 1.3, but using different normalisation techniques, making comparison between species difficult. The article by Graeber [30] points to some genes whose expression is present at constant levels between *Arabidopsis* and *Lepidium*. Figures 3.5 and 3.6 show the transcriptome levels, from the vSEED data, of three genes (At1G17210, At2G04660 and At2G20000) reported to be most stable by Graeber [30], the former of these graphs compares the cap or micropylar endosperm while the latter shows the levels within the radicle.

From observation of the Figures 3.5 and 3.6 it is clear that the transcriptome levels of two of these three genes (AT2G20000 and AT2G04660) are not level or indeed do not have conserved gradients. The third gene, AT1G17210, has a similar mRNA level profile for both tissues and so four lines of best fit are plotted, one through each of the AT1G17210 sets of data points; a further requirement is included, that the gradient of the lines should be conserved within each tissue type, the lines of best fit for the micropylar endosperm are plotted in Figure 3.7.



(a)



(b)

Fig. 3.5: Three cross species housekeeping genes from the micropylar endosperm of *Arabidopsis* and *Lepidium*. (b) is a close up of the lower portion of the graph in (a).

This results in a fold change between the two species, in each tissue and the mean of these fold changes, m , is used to set α_L proportional to α_A , as in equation (3.9).

$$\alpha = \alpha_A = m\alpha_L \quad (3.9)$$

The parameter m is found to be 2.1827, in this way.

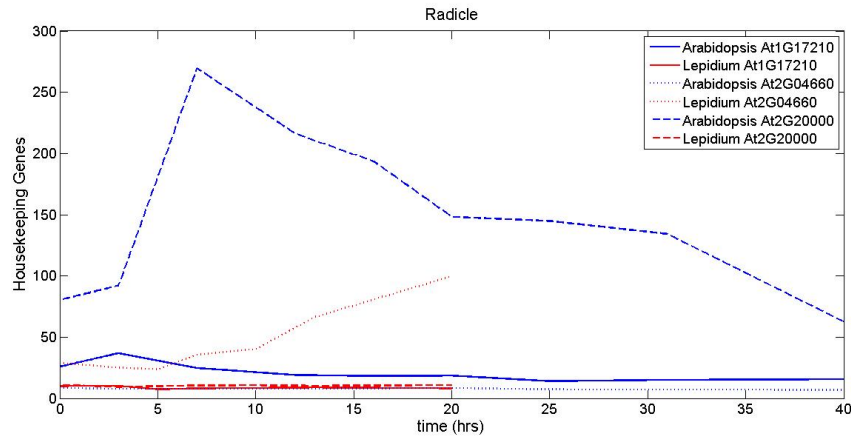


Fig. 3.6: Three cross species housekeeping genes from the radicle of *Arabidopsis* and *Lepidium*

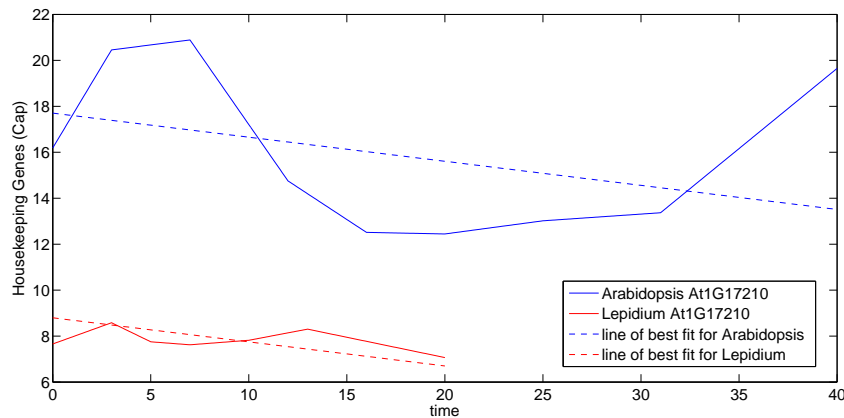


Fig. 3.7: mRNA levels of AT1G17210 from the micropylar endosperm of *Arabidopsis* and *Lepidium*, with lines of best fit

3.4 Results

Due to the detailed spatial sampling of the vSEED data we may compare the activity within the two tissue types, the micropylar endosperm and the radicle, for *Arabidopsis* and *Lepidium*.

The graphs (Figure 3.8) show the numerical simulation of the ODE system described in section 3.2 when considering *Arabidopsis* and comparing both tissue types, namely radicle and micropylar endosperm (or cap); the only change between the two models is the production rates of the proteins, the β functions (Figure 3.4). The PME activity is increasing

with time during the germination process.

In the cap, Group I PMEs protein is produced with imbibition and accumulate steadily through the germination process whereas the group II PMEs seem to have very little effect until around fifteen hours when they quickly accumulate to similar levels to those of group I PMEs. The PMEIs within the cap seem to have similar behaviour to the group II PMEs, although roughly five hours in advance.

The activity within the radicle is somewhat different to that in the cap. Where both PME groups are approaching a plateau in the cap, the same proteins are still accumulating in the radicle; the PME activity, however, reaches a far lower level within the radicle than within the cap. The impact of these differences is marginal when considering the changes in *MeHG* and *dHG* levels. PME group I and PMEI begins to accumulate early after imbibition, whereas the PME group II protein is more abundant earlier in the radicle than in the cap.

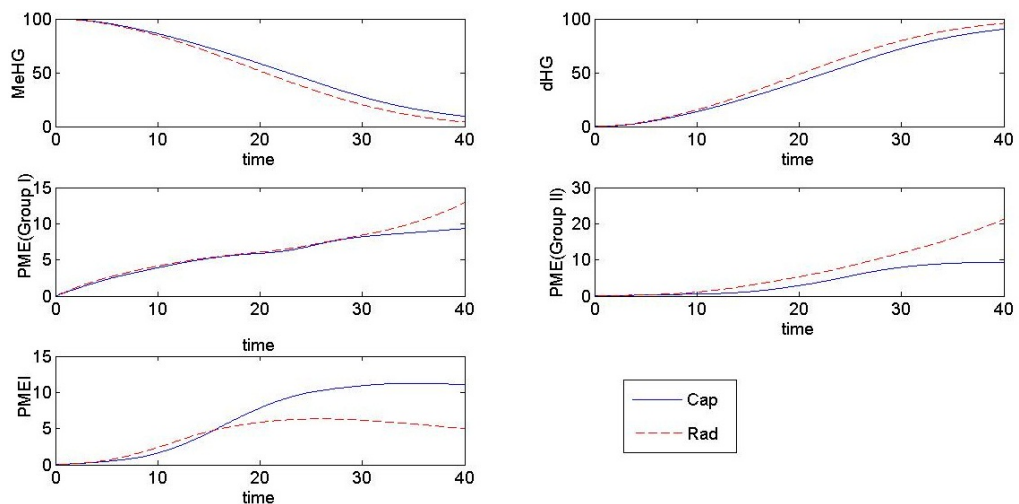


Fig. 3.8: Change in protein and polysaccharides levels over time, within the cap and radicle of Arabidopsis

When considering the same protein activity in both radicle and cap of *Lepidium* (Figure 3.9) it is important to note that first *Lepidium* seeds

germinate at 16 hours and testa rupture occurs after 7 hours, whereas the first *Arabidopsis* seeds germinate at 34 hours after testa rupture at 22 hours. The *Lepidium* activity profiles match that of the *Arabidopsis* activity, with the exception that the group II PME begins from the outset in *Lepidium*. The levels of protein within *Lepidium* are significantly lower than those within *Arabidopsis*; this may be due to the cross-species hybridisation process used for the *Lepidium* transcriptomics, as explained in section 1.3.

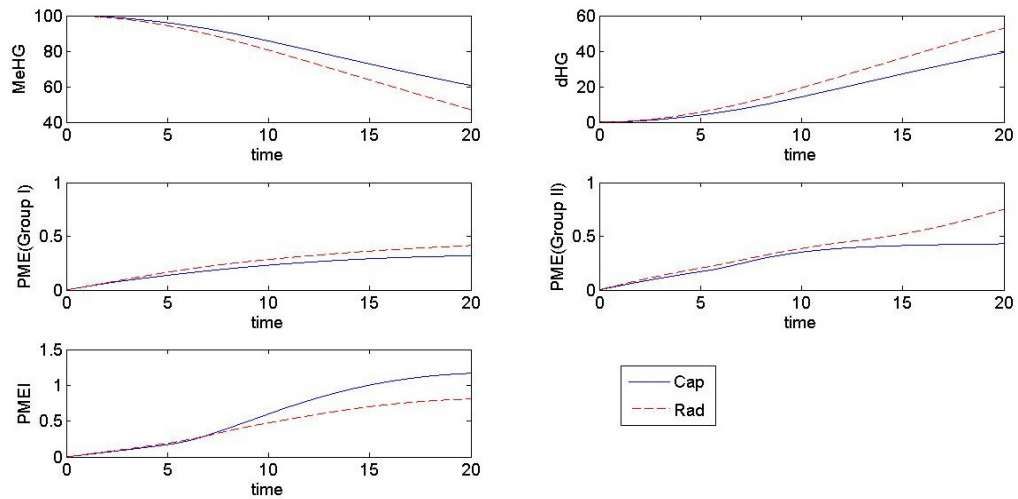


Fig. 3.9: Change in protein and polysaccharides levels over time, within the cap and radicle of *Lepidium*

3.5 Parameter Sensitivity Analysis

For any mathematical model, it is important to understand how altering a parameter affects the model, with special notice taken of the key variables, in this case the change in the level of each polysaccharide. This parameter fitting section will focus on *Lepidium* in order to align the work with the data available in Figure 3.1; the parameter changes when using *Arabidopsis* data have similar impacts on the various curves, as expected since the model, with the exception of input, is the same. Each parameter

has been doubled, halved, multiplied by ten and divided by ten from the standard values described in section 3.2.

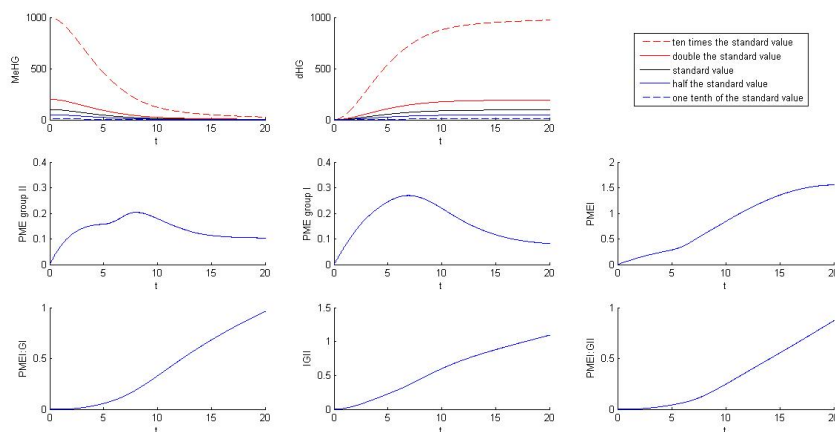


Fig. 3.10: Parameter sensitivity of the initial quantity of *MeHG*, using the vSEED *Lepidium* endosperm data

Figure 3.10 shows that by altering the initial level of *MeHG* we see no change in the protein levels; this is expected since they are enzymes and not consumed by altering the *MeHG* polysaccharide. The profile of the two polysaccharide levels is very similar, the only change being the availability of more *MeHG* allows there to be more *dHG*, due to conservation of mass. The time taken to reach the steady state does not shift linearly with the change in initial condition; indeed the time taken for *dHG* to approach steady state changes very little.

The alterations caused by varying α are seen in Figure 3.11. Increasing α accentuates the profile of the enzymes and increases the production of these enzymes, as such, this speeds up the conversion of the polysaccharide. Estimating the real value of α is therefore important and will be attempted in the following parameter fitting section (Section 3.6). The current standard value of α has been selected by noting that, in the data provided by Prof. G Leubner (Royal Holloway University, Figure 3.1), there is a reasonable step down in PME activity by 10hrs

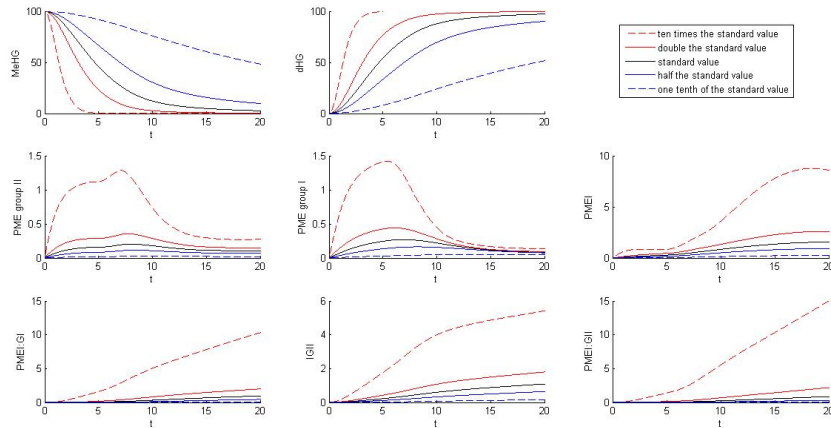


Fig. 3.11: Parameter sensitivity of the α , using *Lepidium* endosperm data

and assuming that this relates to there being little *MeHG* left for PME to de-methylesterify by this time point.

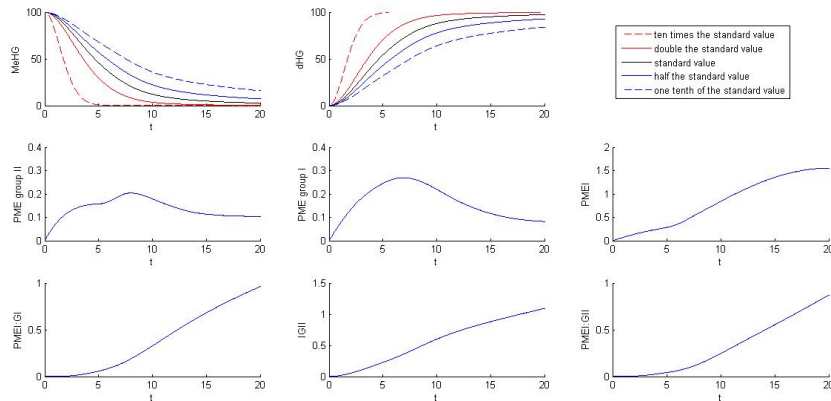


Fig. 3.12: Parameter sensitivity of A , using *Lepidium* endosperm data

Figure 3.12 shows the affects of varying A , the reaction rate at which *GI* de-methylesterifies *MeHG* (Figure 3.3); the equivalent graphs for parameter B are very similar, though with less impact on the polysaccharide levels. Decreasing A slows the rate of conversion of the polysaccharide but has no effect on the level of enzymes, as expected since equations (3.3) - (3.8) are not dependant on A , or B .

As expected, Figure 3.13 shows that increasing the rate of inhibition

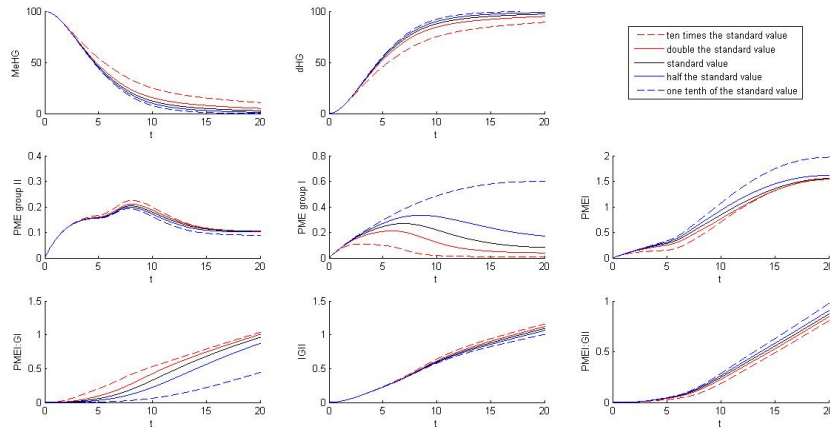


Fig. 3.13: parameter sensitivity of a , using *Lepidium* endosperm data

slows the rate of conversion from $MeHG$ to dHG , as a faster uptake of GI by $PMEI$ reduces the amount of GI , proteins available to react with $MeHG$, the 'one tenth the standard value' curve for GI is noteworthy as it appears to have an exaggerated reaction to the change in a , when compared to the other GI curves; the curve in question is reflected in the $PMEI : GI$ graph, the profile of this curve is the same if we consider a longer time course. Since GI and GII are both inhibited by the same pool of available $PMEI$ it is not surprising that an increase in a increases the available GII proteins, although we might have expected this increase to be larger; the minimal change in GII levels can be explained by GII 's ability to inhibit itself, but again this is possibly more subdued than expected.

Parameter b is the binding rate of GII to $PMEI$, Figure 3.3. Changes in parameter b , as shown in Figure 3.14, have little effect on the levels of dHG suggesting that the polysaccharides are insensitive to variations in b . Increasing the affinity of GII to $PMEI$ has the obvious effect of reducing both GII and $PMEI$ levels. In contrast to altering parameter a , reducing b increases the level of GII and the self inhibiting complex

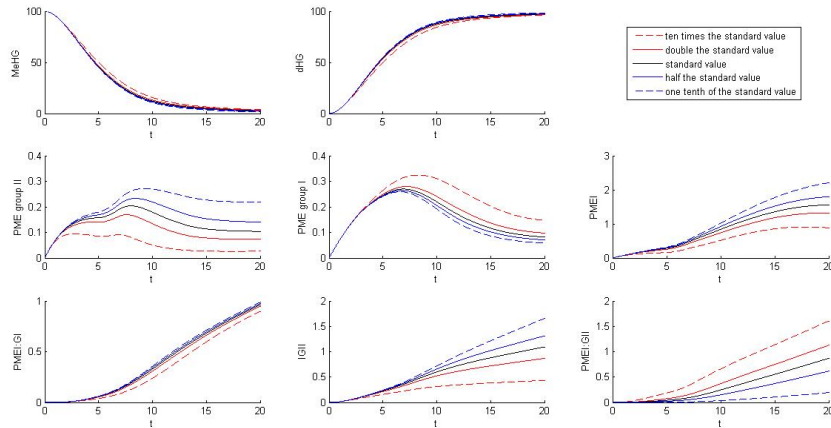


Fig. 3.14: Parameter sensitivity of b , using *Lepidium* endosperm data

IGII. When increasing b the level of *GI* increases notably more so than increasing a affects *GII*. The relatively large variations in the level of *GII* proteins combined with virtually no change in the polysaccharide levels suggests that *GII* proteins play a minor role in the de-methylesterification process, meaning that the *GI* proteins should be the focus of following discussion; this is supported in Figure 3.13, where the change in dHG levels is greater than in Figure 3.14 and the variance of *GII* proteins is comparably minimal.

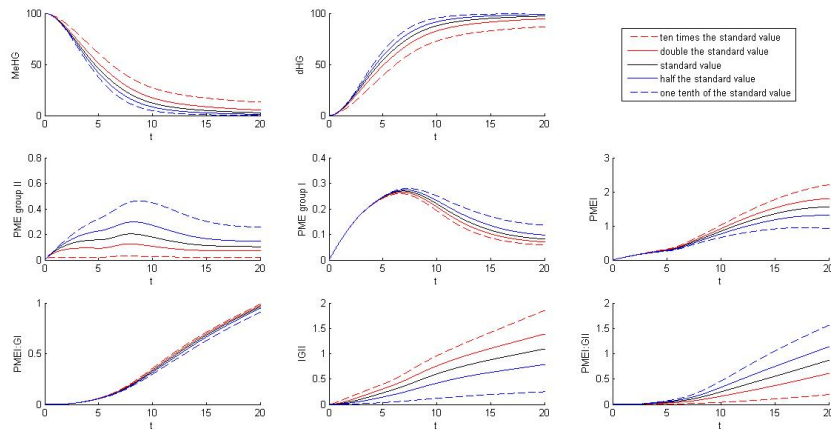


Fig. 3.15: Parameter sensitivity of c , using *Lepidium* endosperm data

When considering parameter c , Figure 3.15, the level of *GII* decreases

as c increases as expected, but perhaps surprisingly, the level of GI also decreases. The decrease in GI can be explained by the increased availability of $PMEI$; with less GII available to compete for $PMEI$, there is more $PMEI$ to react with the GI proteins. The hypothesis that GII proteins have little impact on the polysaccharide levels when compared to GI is not supported by Figure 3.15; Figure 3.15 displays the smallest change in GI levels out of the inhibition reaction rate constants yet it can be seen that the levels of polysaccharides are most sensitive to parameter c , where GII show the greatest variations.

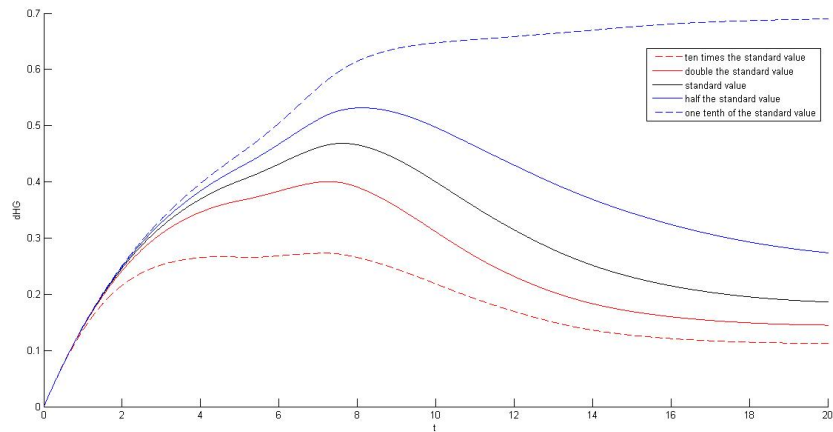
From Figure 3.15 we can see that the total level of PME , being the sum of GI and GII , is likely to be a better variable to control the change in polysaccharide levels than either GI or GII independently. This is not surprising but may point to a model simplification.

3.6 Parameter fitting

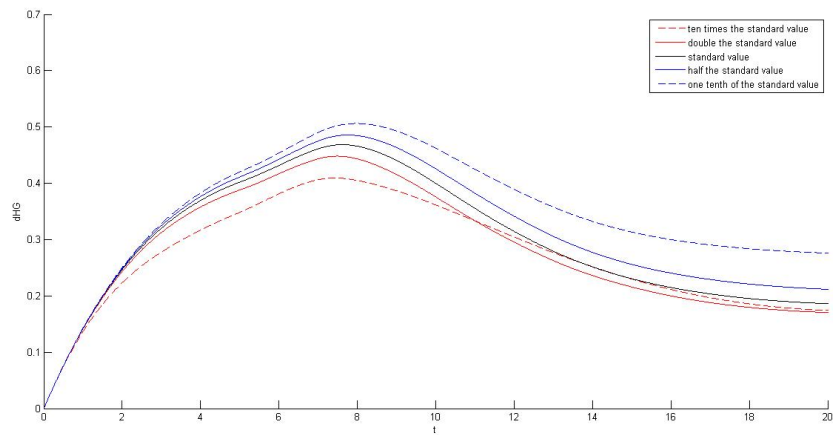
Here, the model constructed in section 3.2 is used to replicate the activity displayed by the data, in Figure 3.1 and table 3.1. Efforts will then be made to simplify the model, without altering the profile of dHG or $MeHG$.

This so called PME activity level, referred to in table 3.1, is proportional to the rate of de-methylesterification, since that is the activity of $PMEs$.

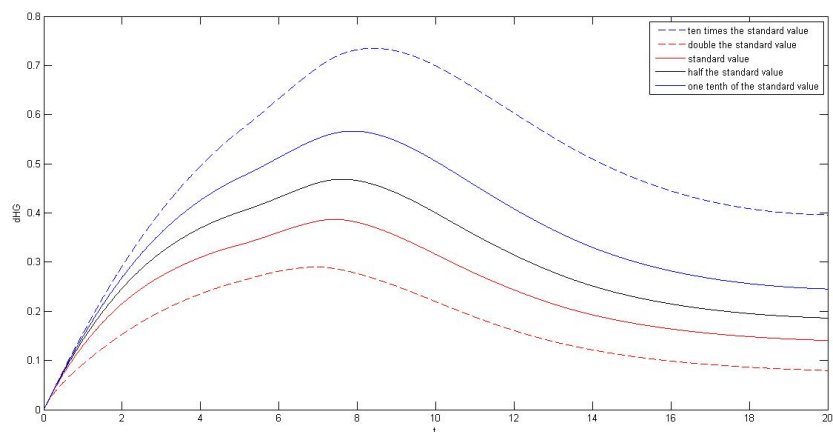
The first attempt to fit the data in table 3.1 focuses on the micropylar endosperm, since the endosperm will be the tissue of most interest in future chapters. Matlab's built-in genetic algorithm package 'ga' was chosen for convenience and is used to minimise the objective function, f , in equation (3.10), where the system of equations (3.1) - (3.8), with the *Lepidium* endosperm data (vSEED data explained in section 1.3), is used



(a)



(b)



(c)

Fig. 3.15: The total PME (both GI and GII) when considering the parameter sensitivity of the inhibiting reaction constants: Figure (a) parameter a , Figure (b) parameter b and Figure (c) parameter c

Time(hr)	Radicle			
	replicate 1	replicate 2	replicate 3	mean
4	2.56	3.11	2.98	2.88
8	3	2.53	2.7	2.74
12	1.82	2.54	2.12	2.16
16	4.29	3.28	2.82	3.46
22	2.63	2.86		2.745

Time (hr)	Cap			
	replicate 1	replicate 2	replicate 3	mean
4	45.57	41.75	50.8	46.04
8	55.51	41.06	52.74	49.77
12	40.39	27.29	29.44	32.37
16	25.87	27.03	33.17	28.69
22	28.79	45.77	38.1	37.55

Tab. 3.1: PME activity level in nKatal/mg, within *Lepidium micropylar* endosperm and radicle, provided by Prof. G Leubner (Royal Holloway University)

to calculate $\frac{d[dHG]_e}{dt}$.

$$f = \sum_{i=1}^5 \left(P \frac{d[dHG]_e}{dt} \Big|_{time_{i-1}}^{time_i} - mean_e(time_i) \right)^2 \quad (3.10)$$

where

$$\begin{aligned} time &= \{4, 8, 12, 16, 22\} \quad \text{and} \\ mean_c &= \{46.04, 49.77, 32.37, 28.69, 37.55\} \end{aligned} \quad (3.11)$$

The non-dimensional constant P , to be fitted, is included since the change of $\frac{d[dHG]_e}{dt}$ from one time point to the next is proportional to activity levels over that time step, which is what is being fitted to. The initial conditions used are in table 3.2.

Parameter	$[MeHG]_0$	$[dHG]_0$	$[GI]_0$	$[GII]_0$
Parameter value	1000 mg / μm^3	0 mg / μm^3	0 mg / μm^3	0mg / μm^3
Parameter	$[PMEI]_0$	$[IGII]_0$	$[PMEI : GI]_0$	$[PMEI : GII]_0$
Parameter value	0 mg / μm^3	0 mg / μm^3	0 mg / μm^3	0 mg / μm^3
Parameter	A	B	a	
Parameter value	0.6 $\mu\text{m}^3/\text{mg s}$	0.6 $\mu\text{m}^3/\text{mg s}$	0.4 $\mu\text{m}^3/\text{mg s}$	
Parameter	b	c	α	P
Parameter value	0.4 $\mu\text{m}^3/\text{mg s}$	0.4 $\mu\text{m}^3/\text{mg s}$	0.0005	1

Tab. 3.2: Parameters used to begin parameter fitting

The starting parameters for quantity of *MeHG* is set to be a sufficiently large number to ensure that the reaction occurs, bearing in mind that there is no input from production for the polysaccharides, with the initial conditions for *dHG* set to zero since any initial quantity will have no impact of the model. Initial conditions for the proteins are set to zero to ensure that the vSEED transcriptomics data is a substantial contributor to the activity, with *alpha* set to slow production, so that at its fastest production is of $O(1)$. The reaction rate constants are informed by data from Mondal, who investigate the reaction rates of Guava *PME* with Apple pectin (*in vitro*) [54] and Nighojkar, who uses Cowpea *PME* and citrus pectin (*in vitro*) [60] which provide a range of between 0 $\mu\text{m}^3/\text{mg s}$ and 0.8 $\mu\text{m}^3/\text{mg s}$, in order to ensure reactions occur the activating reaction constants, A and B , are set to 0.6 $\mu\text{m}^3/\text{mg s}$ and the inhibiting reaction rates, a , b and c are set slower at 0.4 $\mu\text{m}^3/\text{mg s}$. This parameter fitting results in Figure 3.16

From the data points alone we expect a fairly constant activity but that is not what is predicted by the model, Figure 3.16. This can easily

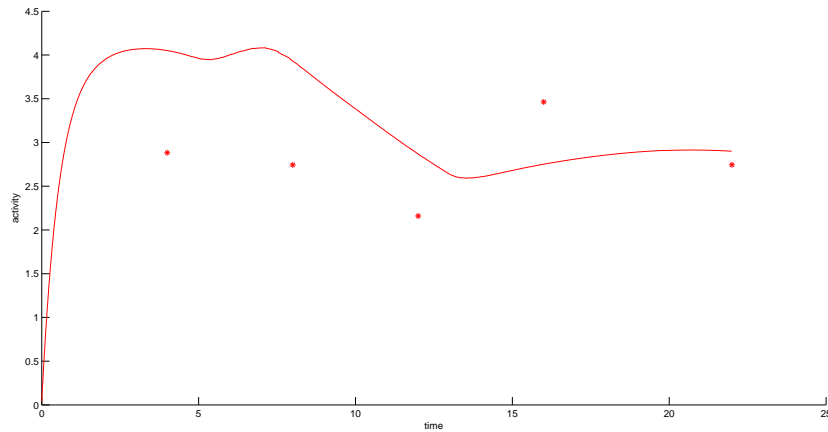


Fig. 3.16: PME activity when using the *Lepidium* PME model and fitting to the *Lepidium* data for PME activity within the cap, provided by Prof. Leubner (Royal Holloway University)

be tested by finding PME activity at key times, such as the peak between 6 and 7 hours. It is possible that the profile of the fitted curve is due to production of polysaccharides not being included in the model. If production were to be included, an equilibrium could be found where by conversion from *MeHG* to *dHG* happened at a constant rate in line with production, which should result in more constant activity as we would expect from the data available.

Parameter	$[MeHG]_0$	$[dHG]_0$	$[GI]_0$
Parameter value	8626.2293 mg / μm^3	5.0471 mg / μm^3	0.0027 mg / μm^3
Parameter	$[GII]_0$	$[PMEI]_0$	$[IGII]_0$
Parameter value	0.0104 mg / μm^3	50.9901 mg / μm^3	4.3177 mg / μm^3
Parameter	$[PMEI : GI]_0$	$[PMEI : GII]_0$	A
Parameter value	3.1764 mg / μm^3	1.7847 mg / μm^3	0.061 $\mu\text{m}^3/\text{mg s}$

Parameter	B	a	b
Parameter value	$0.0483 \mu\text{m}^3/\text{mg s}$	$0.665 \mu\text{m}^3/\text{mg s}$	$0.5226 \mu\text{m}^3/\text{mg s}$
Parameter	c	α	P
Parameter value	$0.5323 \mu\text{m}^3/\text{mg s}$	0.0415	45.2168

Tab. 3.3: Optimal solution to four decimal places

The fit to the data points is good, Figure 3.16 and better than expected for the radicle's data points considering that they have not been fitted to. Figure 3.17 shows the protein and polysaccharide levels for the model when the optimal solution is used (parameter values shown in table 3.3).

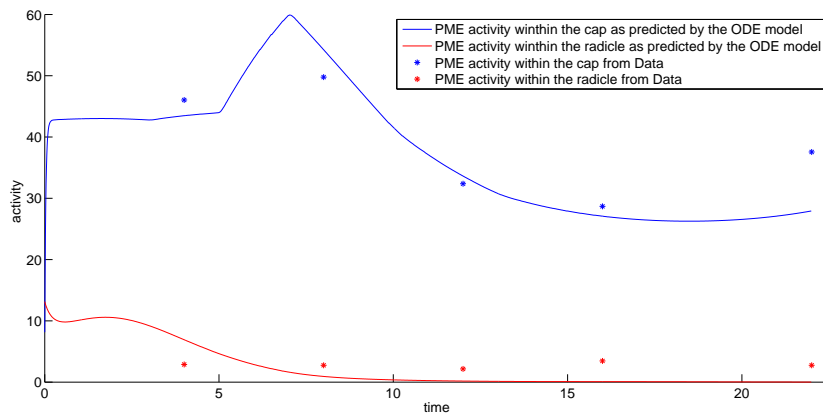


Fig. 3.17: Results from fitting the *Lepidium* PME model to the *Lepidium* data for PME activity within the cap over time (hours), provided by Prof. Leubner (Royal Holloway University)

In an attempt to improve the parameter fitting, The Matlab ga function is used to fit both sets of data points; to fit to the data in table 3.1, the model constructed in section 3.2 will be run twice in parallel, once using the *Lepidium* micropylar endosperm transcriptomics data and once using *Lepidium* radicle transcriptomics data, giving the complete model

as equations (3.12) - (3.19):

$$\frac{d[MeHG]_s}{dt} = -A[GI]_s[MeHG]_s - B[GII]_s[MeHG]_s \quad (3.12)$$

$$\frac{d[dHG]_s}{dt} = A[GI]_s[MeHG]_s + B[GII]_s[MeHG]_s \quad (3.13)$$

$$\frac{d[GI]_s}{dt} = -a[GI]_s[PMEI]_s + \alpha\beta_{GI,s}(t) \quad (3.14)$$

$$\frac{d[GII]_s}{dt} = -b[GII]_s[PMEI]_s - c[GII]_s + \alpha\beta_{GII,s}(t) \quad (3.15)$$

$$\frac{d[PMEI]_s}{dt} = -a[GI]_s[PMEI]_s - b[GII]_s[PMEI]_s + \alpha\beta_{PMEI,s}(t) \quad (3.16)$$

$$\frac{d[IGII]_s}{dt} = c[GII]_s \quad (3.17)$$

$$\frac{d[PMEI : GI]_s}{dt} = a[GI]_s[PMEI]_s \quad (3.18)$$

$$\frac{d[PMEI : GII]_s}{dt} = b[GII]_s[PMEI]_s \quad (3.19)$$

with the subscript s relating to the tissue being considered. Equations (3.12)-(3.19) are run once for the radicle, subscript r and again with subscript e relating to the cap or micropylar endosperm. It should be noted that the reaction rates are assumed to be the same in both tissues, although the pH differences between the tissues may have an effect on the reaction rates. The starting parameter values for the reaction rates and cap initial conditions are the results from the previous parameter fitting (table 3.3), the radicle initial conditions $[MeHG]_{r,0} = 1000$ and all others were set to 0 as with the original fit to the cap.

The activity levels described in table 3.1 are proportional to the rate of change of $MeHG$ to dHG , meaning the objective function to be minimised is:

$$f = \sum_{i=1}^5 \left(P \frac{d[dHG]_e}{dt} \Big|_{time_{i-1}}^{time_i} - mean_c(time_i) \right)^2 \quad (3.20)$$

$$+ \sum_{i=1}^5 \left(P \frac{d[dHG]_r}{dt} \Big|_{time_{i-1}}^{time_i} - mean_r(time_i) \right)^2$$

where

$$time = \{4, 8, 12, 16, 22\}, \quad (3.21)$$

$$mean_r = \{2.88, 2.74, 2.16, 3.46, 2.745\}, \quad (3.22)$$

$$mean_e = \{46.04, 49.77, 32.37, 28.69, 37.55\} \quad (3.23)$$

from the data provided in table 3.1. The constant P is included to shift the results since f is proportional to activity, as in the first parameter fitting.

The graph 3.18 shows the mean data points from table 3.1, and the activity curves found using the model described above, equations (3.12) - (3.19) with the parameter set from table 3.4.

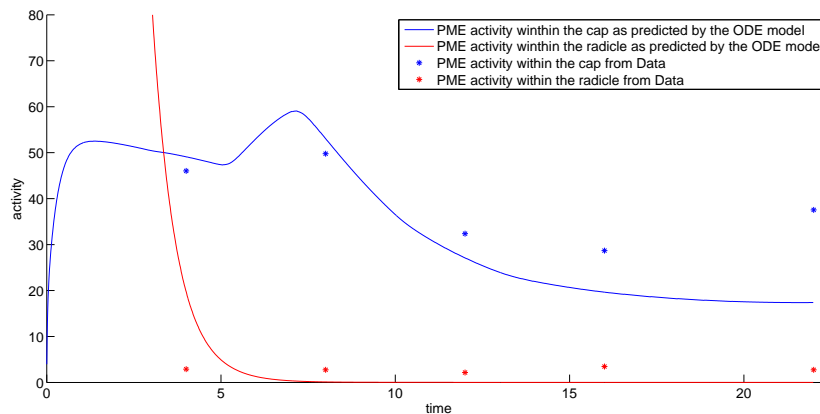


Fig. 3.18: Results from fitting the *Lepidium* PME model to the *Lepidium* data for PME activity within the cap and radicle, provided by Prof.G Leubner (Royal Holloway University)

The profile of the curve showing cap PME activity is similar in both

parameter fittings, although the fit shown in Figure 3.18 is worse when only looking at the cap activity. Where the activity in the cap shows a reasonable fit to, the activity within the radicle seems very unlikely. The vastly different starting points of the two activity curves is due to the initial level of *PMEI*, *GI* and *GII*; the initial value of *PMEI* within the endosperm is over 100 fold higher than that of the levels within the radicle, allowing both *PME* groups to be more highly inhibited within the endosperm. Compounding the difference in initial activity level, the level of *GI* is five orders of magnitude higher in the radicle and *GII* is two orders of magnitude higher in the radicle, all of which ensures that the radicle is converting *MeHG* to *dHG* quickly from the outset whereas the endosperm has to produce *PMEs* of both groups before de-methylesterification can occur.

Previously, the possibility of including production of polysaccharides has been highlighted as an extension to the model although this activity within the cap would seem to be counter productive to a germinating seed; however, this activity would be essential to a growing radicle and as such production of *MeHG* should certainly be included in the radicle model in order to produce a close fit. If this production were to be included, it is likely that a balance could be found between the production of *MeHG* and de-methylesterification, via *PME* groups, to sustain a constant *PME* activity as implied by the radicle data.

Parameter	$[MeHG]_{e,0}$	$[dHG]_{e,0}$	$[GI]_{e,0}$
Parameter value	8797.0552 mg / μm^3	0.6963mg / μm^3	0.0007 mg / μm^3
Parameter	$[GII]_{e,0}$	$[PMEI]_{e,0}$	$[IGII]_{e,0}$
Parameter value	0.0181 mg / μm^3	39.2946 mg / μm^3	2.3048 mg / μm^3

Parameter	$[PMEI : GI]_{e,0}$	$[PMEI : GII]_{e,0}$	$[MeHG]_{r,0}$
Parameter value	2.6749 mg / μm^3	2.8807 mg / μm^3	6771.1779mg / μm^3
Parameter	$[dHG]_{r,0}$	$[GI]_{r,0}$	$[GII]_{r,0}$
Parameter value	0.6219 mg / μm^3	11.0852 mg / μm^3	8.1561 mg / μm^3
Parameter	$[PMEI]_{r,0}$	$[IGII]_{r,0}$	$[PMEI : GI]_{r,0}$
Parameter value	0.3689 mg / μm^3	0.2982 mg / μm^3	7.6944 mg / μm^3
Parameter	$[PMEI : GII]_{r,0}$	A	B
Parameter value	0.9789 mg / μm^3	0.1265 $\mu\text{m}^3/\text{mg s}$	0.0259 $\mu\text{m}^3/\text{mg s}$
Parameter	a	b	c
Parameter value	0.9966 $\mu\text{m}^3/\text{mg s}$	0.0602 $\mu\text{m}^3/\text{mg s}$	0.9906 $\mu\text{m}^3/\text{mg s}$
Parameter	α	P	
Parameter value	0.0212	16.216	

Tab. 3.4: Optimal solution when fitting to both the radicle and cap data, to four decimal places

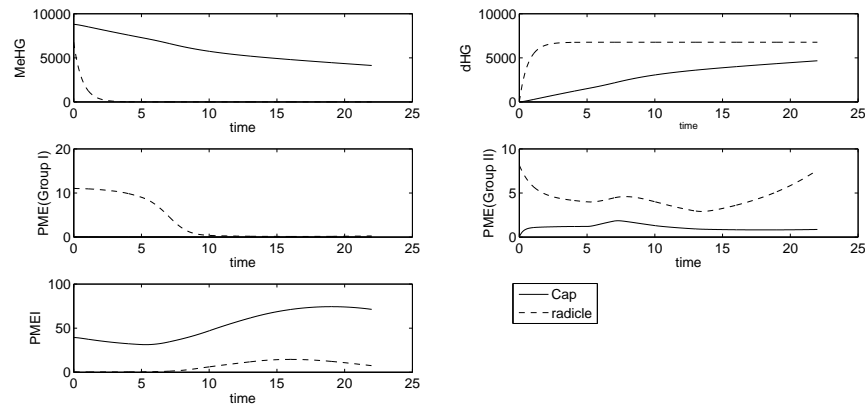


Fig. 3.19: Protein and polysaccharide levels within *Lepidium* cap and radicle as predicted by the PME model for parameters in table 3.4

The model predicts that the polysacchrides within the radicle are

de-methyl-esterified more quickly than in the endosperm. Levels of both forms of *PME* are lower in the cap than the radicle, allowing for a sustained conversion without consuming all the *MeHG* quickly. The profiles of the *PMEI* levels are similar in both the radicle and endosperm.

3.7 Model Simplification

Before expanding this model to incorporate more cell wall remodelling processes, this section will attempt to simplify the *PME* model constructed in section 3.2 without reducing accuracy. The focus through this section will be on the micropylar endosperm since this will be the model taken forward into future chapters.

The previous sections have pointed to the total amount of *PME* being more important than just focusing on the group I or group II *PMEs* and so the simplified model will include a single *PME* term as illustrated in Figure 3.20.

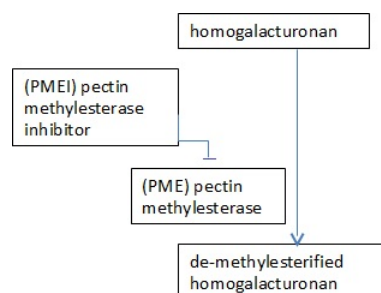


Fig. 3.20: Simplified *PME* network

This network reduces the number of parameters from fourteen to eight and the number of variables from eight to five and results in the

following equations (equations (3.24) - (3.28)):

$$\frac{d[MeHG]_{(s)}}{dt} = -D[MeHG][PME], \quad (3.24)$$

$$\frac{d[dHG]_{(s)}}{dt} = D[MeHG][PME], \quad (3.25)$$

$$\frac{d[PME]_{(s)}}{dt} = -d[PMEI][PME] + \alpha_2\beta_{GI,r}(t) + \alpha_2\beta_{GII,r}(t), \quad (3.26)$$

$$\frac{d[PMEI]_{(s)}}{dt} = -d[PMEI][PME] + \alpha_2\beta_{PMEI,r}(t), \quad (3.27)$$

$$\frac{d[PMEI : PME]_{(s)}}{dt} = d[PMEI][PME]. \quad (3.28)$$

Here α_2 converts the vSEED transcriptomics data into a production level proportional to polysaccharides levels; this parameter has the same purpose as the previous α but may not have the same value. The reaction rates D and d are simplified constants for the de-methyl-esterification rate and the inhibitor binding rate respectively. The subscript (s) denotes the simplified model.

The polysaccharide levels are considered to be the most important element of this model as they will inform the cell wall properties and as such the function to be optimised is:

$$f = \sum_t \left([dHG]_e - [dHG]_{(s)} \right)^2 \quad (3.29)$$

with $[dHG]_e$ found from equations (3.12)-(3.19), using parameter values from Table 3.4, in section 3.6. The starting $[MEHG]_{(s),0} = 1000$ and all the other initial conditions are set to zero, parameter $D = d = 0.5$.

The resulting protein and polysaccharide levels are shown in Figure 3.7 and the optimal parameter set can be seen in table 3.5, below.

Parameter	$[MeHG]_{(s)}$	$[dHG]_{(s)}$	$[PME]_{(s)}$
Parameter value	9355.3350 mg / μm^3	0.0047 mg / μm^3	0.0001 mg / μm^3
Parameter	$[PMEI]_{(s)}$	$[PMEI : PME]_{(s)}$	D
Parameter value	40.207 mg / μm^3	0.1011 mg / μm^3	0.3586 $\mu\text{m}^3/\text{mg s}$
Parameter	d	α_2	
Parameter value	0.8775 $\mu\text{m}^3/\text{mg s}$	0.0078	

Tab. 3.5: Optimal solution when fitting to both the radicle and cap data, to four decimal places

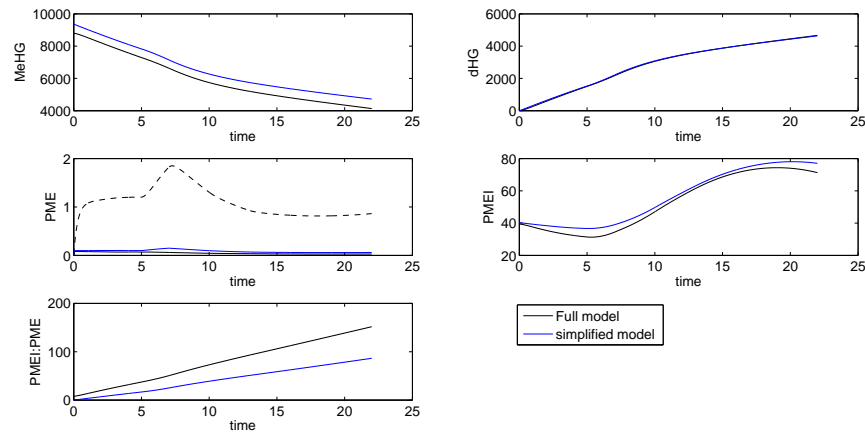


Fig. 3.21: Protein and polysaccharide levels predicted by the full and simplified model. The PME graph separates the group I (solid black line) and group II (dotted black line) as well as the simplified PME (blue line)

The dHG levels for both the full and simplified model are very similar suggesting that the simplified model is a good substitute for the full model. The profile of the two $MeHG$ curves are the same, as are the two $PMEI$, although not as closely related as the two dHG curves. The complex $PMEI : PME$ curves are not as closely related as the other elements of the model but since this variable is used solely as a check for numerical error, with no variable dependant upon $PMEI$, the difference between the simplified and full model is incidental to any model extensions. The simplified model appears to fulfil the requirements of reproducing the

full models results accurately and so will be used in future chapters. Since the simplified model was sufficient to reproduce the full model, we assume the two *PME* groups have the same activity, suggesting that, at least in the tissues we have considered, the *PMEI* domain in group II *PMEs* is inactive.

3.8 Conclusion

In this chapter, an ordinary differential equation model was constructed to replicate the activity of two forms of pectin methylesterase within a germinating seed. Activity data was used to attempt to find parameters for the constructed model and then this model was simplified for future use.

It is hypothesised that the group II *PMEs* are self controlling since they are produced towards the end of the process to avoid remodelling areas which should not be remodelled.

The model assumes a well mixed solution of polysaccharides and proteins with no polysaccharide production. Reactions considered in the models are thought to be fully irreversible. The reality of these assumptions is predominately unknown but it is likely that including production of polysaccharides in the model would improve the fit to the data, especially for the radicle cell walls, and should be considered for future models. A well mixed assumption is usual for first models and expanding the model to include spatial elements is a lot more complicated but attempted in section 5.

The pH change within a cell wall can have major repercussions on the reaction rate of *PMEs* but the lack of data as to pH micropockets within the cell wall makes this model refinement difficult, as does the need for

including spatial variations to properly model this.

De-methyl-esterified homogalacturonan can be acted upon by other cell wall remodelling enzymes and the model is expanded to reflect this in section 4.

4. ORDINARY DIFFERENTIAL EQUATION MODEL OF CELL WALL BEHAVIOUR DURING GERMINATION

4.1 Introduction

In order to consider cell wall remodelling during germination, biological interaction networks are constructed to capture the predominant elements of the endosperm. These networks are converted into ordinary differential equations (ODEs) in order to analyse a well mixed homogeneous solution of key polysaccharides and proteins. The aim of these ODEs is to improve our understanding of the physical properties of the endosperm and their changes during germination, as such vSEED transcriptomics data, as described in Section 1.3, for the *Arabidopsis* endosperm will be used.

Parameter estimation will be used to try to accurately represent each parameter; this will be done through considering the prior model in chapter 3 and the available literature.

With this system of ODEs constructed, the parameter space will be explored to identify the variables which inform cell wall properties.

The important elements of the networks are the state of the polysaccharides, as the polysaccharides are the structural components of the cell wall. As such, the networks will be built around: homogalacturonan, for its volume within the cell wall, arabinan, as a defining feature of endosperm cell walls, and hemicellulose or xyloglucan, as a controlling

factor for cell wall expansion. Cellulose itself will not be considered due to its inability to be broken down, although expansin proteins will be included in the xyloglucan network.

These networks will be converted into mathematical equations using the law of mass action and considering the rates of change of the polysaccharides.

4.2 Homogalacturonan Network

This homogalacturonan network takes the simplified model constructed in section 3.7 and expands the network to consider the remodelling processes which follow.

The homogalacturonan element of pectin is abundant within most plant cell walls and this is the case for the endosperm. Homogalacturonan has three major remodelling enzymes: pectin methylesterase (*PME*), polygalacturonase (*PG*) and pectin lyase (*PL*).

Homogalacturonan is synthesized with roughly 70% of its molecules methylesterified, this state being referred to as methylesterified homogalacturonan (*MeHG*). In this state the methylesterification does not allow polygalacturonase or pectin lyase to act upon it or for calcium crosslinking to occur and so pectin methylesterase is used as a catalyst to de-methylesterify the homogalacturonan. Pectin methylesterase works at an optimal pH of 7 and by-products of the de-methylesterification are acidic. This change from a neutral pH to a slightly acidic environment improves the polygalacturonase activity. Polygalacturonase cannot cleave the homogalacturonan without homogalacturonan first being de-methylesterified. We consider the de-methylesterification to occur blockwise, which means that several adjacent methylesterified molecules

are de-methylesterified at once. It is important to consider the pectin methylesterase inhibitor (*PMEI*) protein, which can bind with pectin methylesterase and by doing so prevents the pectin methylesterase from de-methylesterifying the homogalacturonan.

When the homogalacturonan chain has a de-methylesterified section of eight to fifteen consecutive monomers we consider this section to be in the next state of the network, called de-methylesterified homogalacturonan (*dHG*), since this is the approximate length of block required for calcium cross-linking [67]. Once in this state a process of calcium cross-linking is assumed to be immediate, binding two homogalacturonan chains together irreversibly and reinforcing the wall structure. We consider calcium cross-linking to happen immediately due to the abundant presence of calcium, meaning that the de-methylesterified homogalacturonan is always calcium cross-linked.

In this state pectin lyase and polygalacturonase are able to catalyse the cleaving of de-methylesterified homogalacturonan giving the new state of cleaved homogalacturonan (*cdHG*). The polygalacturonase inhibitor protein can create a complex with polygalacturonase to prevent the cleaving of homogalacturonan, however, there is no known inhibitor of pectin lyase.

The network we are using is that, *MeHG* can be de-methyl-esterified by *PME*, creating *dHG*, and this process is slowed by *PMEI* binding with *PME* which prevents *PME* from acting on available *MeHG*. The then present *dHG* is assumed to be calcium cross-linked and the polysaccharides can be cleaved into *cdHG* by either *PG* or *PL*, the former, *PG*, can be inhibited by the presence of *PGI* through *PGI* binding with available *PG* and removing its ability to cleave *dHG*. This is summed up in Figure 4.1 below.

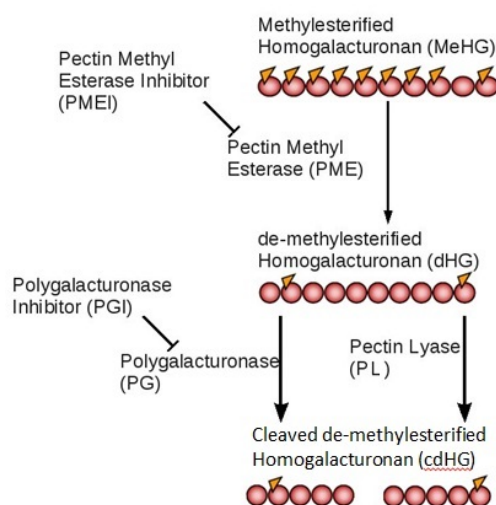


Fig. 4.1: A summary of the homogalacturonan network considered in this model. Edited from an image provided by Kieran Lee (University of Leeds), unpublished

In this network the important quantities are the different homogalacturonan states, as each state contributes differently to the cell wall properties: De-methylesterified homogalacturonan is thought to be less permeable than the methylesterified state as calcium cross-linking has occurred, this permeability is then increased by the cleaving process of PL and PG.

The reactions discussed are considered to be irreversible since the germination process is a cascade process; the seed will desire the endosperm to be broken down quickly so that it does not slow germination once the seed has decided to go through this expensive process. The endosperm is not required post-germination and so the germination process is a primarily a degradation of the endosperm, with little concern for the endosperm's longevity.

The law of mass action is used to produce the first order differential equation which explain the rate of change of methylesterified homogalacturonan ($MeHG$),

$$\frac{d[MeHG]}{dt} = -D[PME][MeHG]. \quad (4.1)$$

In this equation $[MeHG]$ is the quantity of methylesterified homogalacturonan as it changes over time, with $[PME]$ the quantity of pectin methylesterase and D is a rate constant; D is the rate at which pectin methylesterase will catalyse the de-methylesterification of the homogalacturonan, an approximation for its value has been found in section 3.7. It is clear that as $[MeHG]$ is reduced, de-methylesterified homogalacturonan, $[dHG]$, is increased directly and so this becomes the first term in the second equation, the equation for how $[dHG]$ changes over time.

$$\frac{d[dHG]}{dt} = D[PME][MeHG] - (E[PL] + F[PG])[dHG], \quad (4.2)$$

the second and third terms on the right hand side of this equation deal with the effect of pectin lyase, $[PL]$ and polygalacturonase, $[PG]$ respectively. The rate constant E is time that pectin lyase takes to cleave the dHG and F is the rate at which polygalacturonan cleaves the $[dHG]$. Since the reduction in $[dHG]$ directly increases the amount of cleaved homogalacturonan $[cdHG]$, we can again use these terms from equation (4.2) to determine the change in $[cdHG]$ over time.

$$\frac{d[cdHG]}{dt} = (E[PL] + F[PG])[dHG]. \quad (4.3)$$

Next we consider pectin methylesterase, $[PME]$, and its inhibitor $[PMEI]$. Noting that both these variables decouple from the rest of the

system. Since $[PME]$ is a catalyst to the de-methylesterification it is not consumed by this reaction. So with this in mind we get the following three equations:

$$\frac{d[PME]}{dt} = -d[PMEI][PME] + \alpha\beta_{PME}, \quad (4.4)$$

$$\frac{d[PMEI]}{dt} = -d[PMEI][PME] + \alpha\beta_{PMEI}, \quad (4.5)$$

$$\frac{d[PME : PMEI]}{dt} = d[PMEI][PME], \quad (4.6)$$

where $[PME : PMEI]$ is the heterodimer of $[PME]$ with $[PMEI]$ and d the rate at which the two elements, $[PME]$ and $[PMEI]$ dimerise. The $\alpha\beta_i$ terms relate to the production of proteins, where the vSEED transcriptomics, as described in section 1.3, are introduced as β_i for protein i . The non-dimensional constant α is used to relate the relative mRNA levels to actual protein production and is assumed to be found in section 3.7. We can create a similar group of equations for the dimerisation of Polygalaturonase $[PG]$ and its inhibitor $[PGI]$.

$$\frac{d[PG]}{dt} = -c[PGI][PG] + \alpha\beta_{PG}, \quad (4.7)$$

$$\frac{d[PGI]}{dt} = -c[PGI][PG] + \alpha\beta_{PGI}, \quad (4.8)$$

$$\frac{d[PGI : PG]}{dt} = c[PGI][PG], \quad (4.9)$$

with c being used as the rate that PG dimerises with PGI . The remaining equation calculates the PL available to cleave the pectin and is simply a production term, equation (4.10).

$$\frac{d[PL]}{dt} = \alpha\beta_{PL}. \quad (4.10)$$

Equations (4.1), (4.4), (4.5) and (4.5) are taken directly from section 3.7 and similarly equation (4.2) is expanded from equation (3.25) in section 3.7. The model assumes a well mixed solution of polysaccharides and proteins with degradation not included as it is assumed to be negligible over the time scale we are considering, for simplicity; they are no known decay rates for the proteins considered here. We continue to use the assumption that all the equations are fully irreversible.

Once these equations have been input into Matlab, the ode45 function was used to find numerical solutions to this system. The protein PL was included although its presence in the system is not certain experimentally. The parameter values used are listed in Table 4.1.

Initially, we set $[MeHG]_0$, $[PME]_0$, $[PMEI]_0$, $[dHG]_0$, $[PME : PMEI]_0$, α , D and d to the parameter values found in section 3.7. The remaining initial conditions are set to zero, $[PG]_0 = [PL]_0 = [PGI]_0 = [PG : PGI]_0 = [cdHG]_0 = 0$ sites (mass per volume), since we have no other information.

The reaction constants c , E and F are informed by literature and the previous models in chapter 3.

Ortega [63] considers the reaction rates of pectin lyase in a variety of different plants, at temperatures of between 50 °C and 80 °C and although rates found are higher than that of the previously discussed PME, 50 °C is well above 'normal' temperature for seeds. The parameter E is then set to 0.4 $\mu\text{m/s}$ for the following model, since this is higher than parameter D but not to the same degree as suggested by Ortega to compensate for the temperature disparity.

Polygalacturonase (*PG*) reaction kinetics are investigated by Bonnin, Chisari and Gummadi [7], [14] and [33], for a variety of substrates under differing conditions resulting in a large range of possible rate constants associated with *PG* activity and with the *PME* rate constant, $0.4 \mu\text{m/s}$, falling within the range of possible rate constants *F* is chosen to be $0.4 \mu\text{m/s}$. The reaction rates of *PGI* is not so widely studied and so *c* is set to $0.8 \mu\text{m/s}$ in order to keep in line with the *PME* and *PMEI* rate constant.

The complete parameter set is below:

Parameter	$[MeHG]_0$	$[dHG]_0$	$[cdHG]_0$	
Parameter value	$9355.3350 \text{ mg}/\mu\text{m}^3$	$0.0047 \text{ mg}/\mu\text{m}^3$	$0 \text{ mg}/\mu\text{m}^3$	
Parameter	$[PME]_0$	$[PMEI]_0$	$[PMEI : PME]_0$	
Parameter value	$0.0001 \text{ mg}/\mu\text{m}^3$	$40.207 \text{ mg}/\mu\text{m}^3$	$0.1011 \text{ mg}/\mu\text{m}^3$	
Parameter	$[PG]_0$	$[PGI]_0$	$[PGI : PG]_0$	$[PL]_0$
Parameter value	$0 \text{ mg}/\mu\text{m}^3$	$0 \text{ mg}/\mu\text{m}^3$	$0 \text{ mg}/\mu\text{m}^3$	$0 \text{ mg}/\mu\text{m}^3$
Parameter	<i>D</i>	<i>E</i>	<i>F</i>	
Parameter value	$0.3586 \mu\text{m}^3/\text{mg s}$	$0.4 \mu\text{m}^3/\text{mg s}$	$0.4 \mu\text{m}^3/\text{mg s}$	
Parameter	<i>d</i>	<i>c</i>	α	
Parameter value	$0.8775 \mu\text{m}^3/\text{mg s}$	$0.9 \mu\text{m}^3/\text{mg s}$	0.003573	

Tab. 4.1: Parameter values used for the homogalacturonan model

The production terms, $\alpha\beta_p$ are plotted below, Figure 4.2, with the data points from the vSEED transcriptomics, discussed in section 1.3, being connected linearly to create a continuous function.

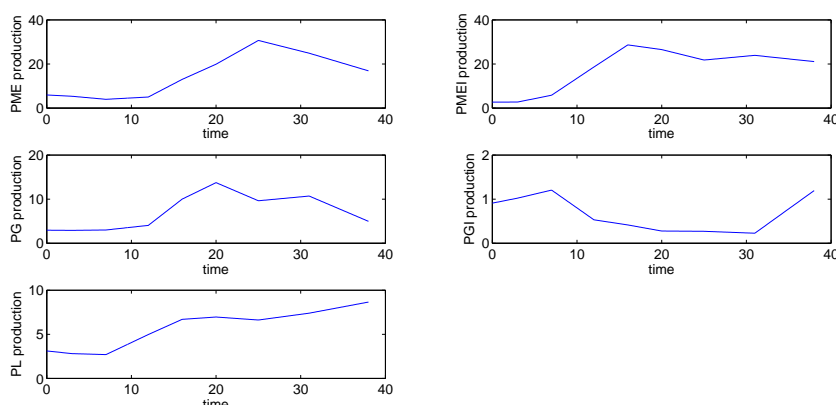


Fig. 4.2: Graphs showing the change in protein production, over time (hr). As informed by the vSEED transcriptomics data [21]

The *PME* and *PME1* production seem to occur at a similar level with *PME1* slightly exceeding *PME* production at most time points except around the twenty-five hours after imbibition, which is the expected time for testa rupture. The *PG* production is at background levels until twelve hours after imbibition when the production rapidly increases to over ten times the production of its inhibitor *PGI*, while *PL* steadily increases from seven hours after imbibition but does not reach the same peak production level as *PG*.

Graphs of each variable change over time have been produced (Figure 4.3) and are analysed below.

These polysaccharides are altered by the proteins whose changing levels, with respect to time, are shown in the Figures 4.4 and 4.5, below. The de-methylesterification begins immediately after imbibition and so the level of *MeHG* decreases and conversely the product of this process, *dHG*, increases. At around ten hours after imbibition the conversion from *MeHG* to *dHG* slows and the process further slows around the thirty one hour mark. The de-methylesterified form of homogalacturonan is cleaved to become *cdHG*; this cleaving does not begin as quickly as the

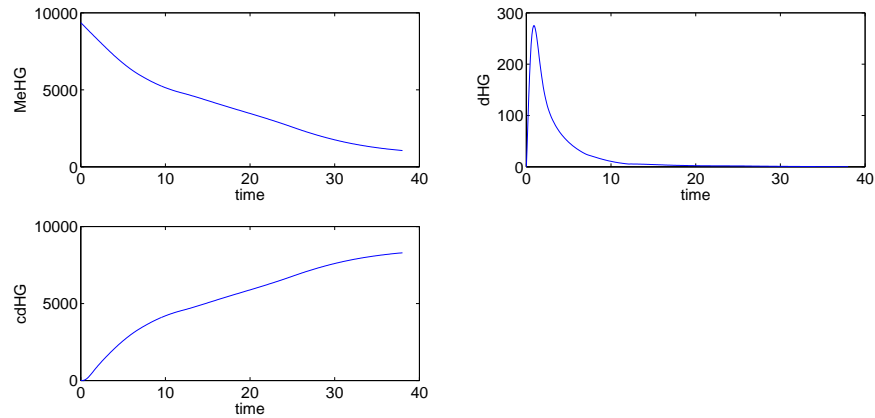


Fig. 4.3: Graphs showing the change in homogalacturonan polysaccharide activity sites, over time (hr)

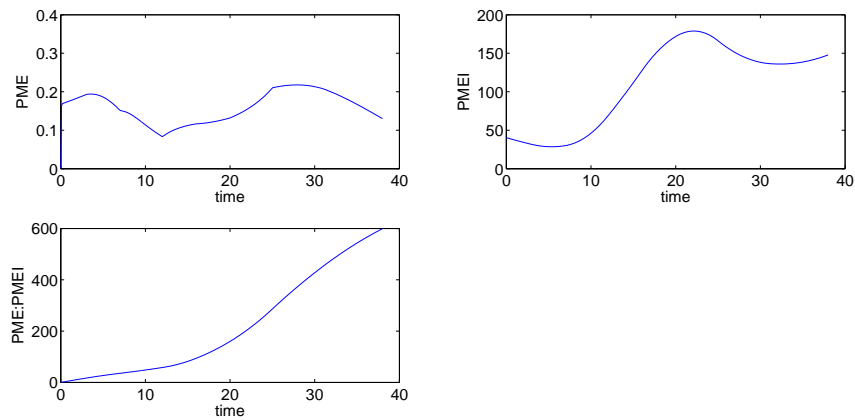


Fig. 4.4: Graphs showing the change in *MeHG* altering enzymes and their inhibitors, over time (hr)

de-methylesterification due to the need for HG to be de-methylesterified prior to cleaving. The creation *cdHG* slows at similar times to *MeHG* conversion, with the exception of the initial delay. These polysaccharides will be considered with respect to their contribution to cell wall properties in section 4.5.

The graphs in Figure 4.4 are the *Arabidopsis* counterparts to the simplified model created in Section 3.7, created using *Lepidium*. The wave-like features seen in the changes of *PME* and *PMEI* levels are created from the transcriptomics production data. The level of *PMEI* is monotonically

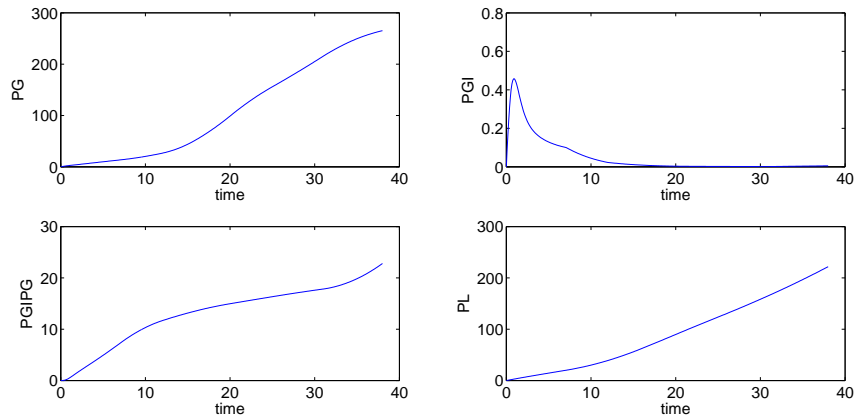


Fig. 4.5: Graphs showing the change in dHG altering enzymes and their inhibitors, over time(hr)

increasing. There is significantly less PME in the system than any other protein which may be surprising since it is the only protein de-methyl-esterifying $MeHG$ into dHG .

At twelve hours after imbibition, there is a relatively sharp change in the level of PME , it is possible that this indicates the divergence from dormancy to germination; since the data do not distinguish dormant and germinating seeds it is difficult to tell but mRNA levels of dormant seeds could be investigated, possibly with a focus around twelve hours.

Polygalacturonase and pectin lyase are initially produced in low levels but after twelve hours the production is increased to increase the amount of present PG and PL , the change in PG being more significant, in spite of the inhibitor. This could lend weight to the notion that twelve hours after imbibition is the point at which a germinating seeds activity alters from that of a dormant seed. The protein PGI appears to be a lot more prominent in the early germination process, the free PGI being available in the system; by twenty hours, PGI creates a complex with PG as fast as it is produced, with plenty of PG left over for cleaving of dHG .

The proteins PME , $PMEI$ and $[PME : PME I]$ graphs in Figure 4.4 are

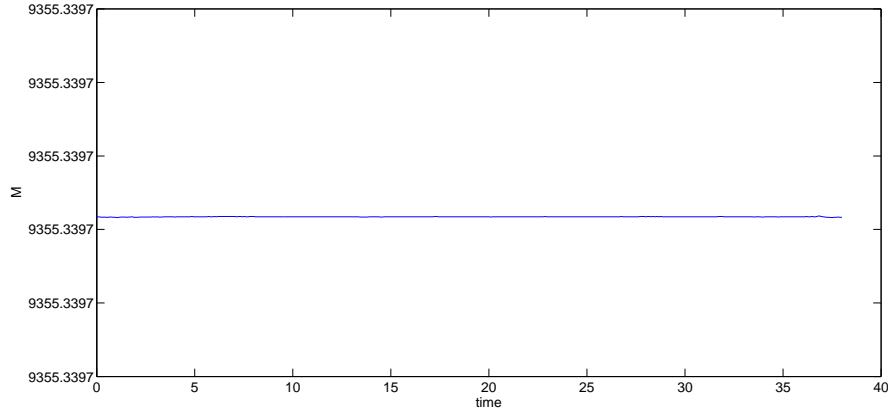


Fig. 4.6: Graph showing M .

directly comparable to the proteins PG , PGI and $[PG : PGI]$ graphs in Figure 4.5 since the equations for both groups are so similar, the main difference being the production, through transcriptomics data.

Looking at the three polysaccharide states, $MeHG$, dHG and $cdHG$, together we can see:

$$[MeHG] + [dHG] + [cdHG] = M,$$

for M constant due to the lack of decay or production rates, this M provides a simple check on numerics and the plot of M against time is shown in Figure 4.6.

4.2.1 Parameter Sensitivity

The following section explores the parameter space of the model described in section 4.2; this exploration will highlight which parameters are most important to get accurate.

The altering of the reaction rate of PME de-methyl-esterifying homogalacturonan, D , we see the affects reflected in the $cdHG$ level, suggesting that the PG and PL are working very quickly and are available in

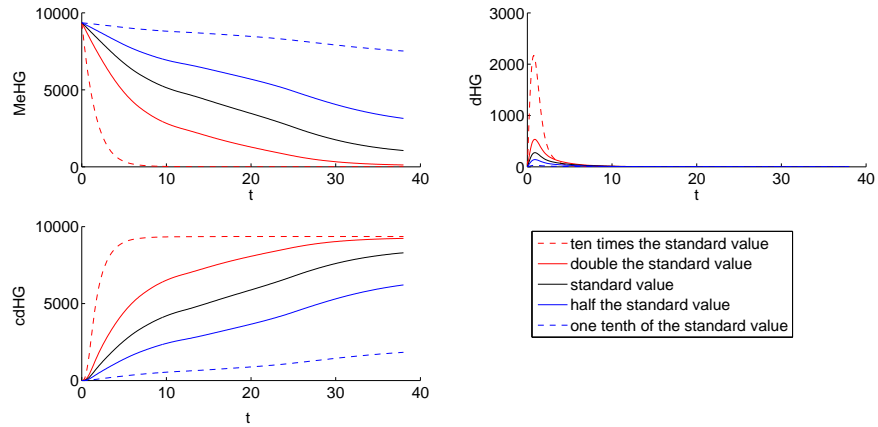


Fig. 4.7: Parameter sensitivity of D , on the polysaccharide state levels

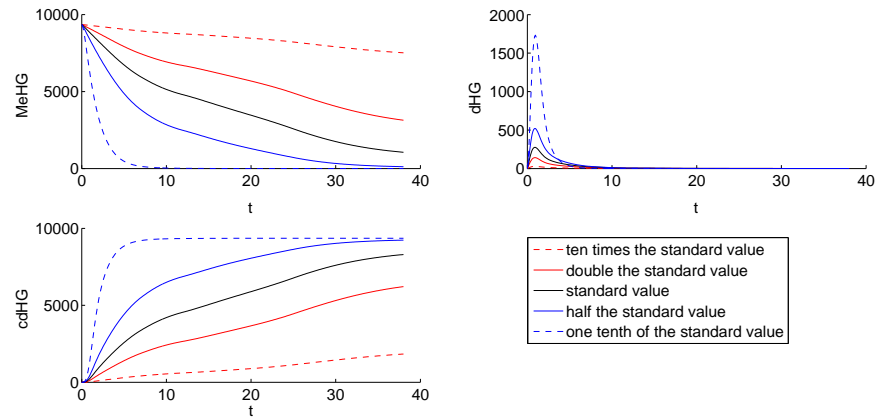


Fig. 4.8: Parameter sensitivity of d , on the polysaccharide state levels

abundance to cleave homogalacturonan, certainly from ten hours after imbibition. This is unlikely to be the case in practice as PG is reported to be involved with cell separation and so we would expect plants to be more controlled in its use, this may however be explained if these cleaving enzymes are targeted to specific areas of the cell wall which cannot be captured with this model; another explanation is that the hemicellulose and cellulose in the system are sufficient to maintain the cell walls until the germination (separation) event. Parameter D does not impact any other elements of the system.

The differences between changing parameter D , Figure 4.7, and d ,

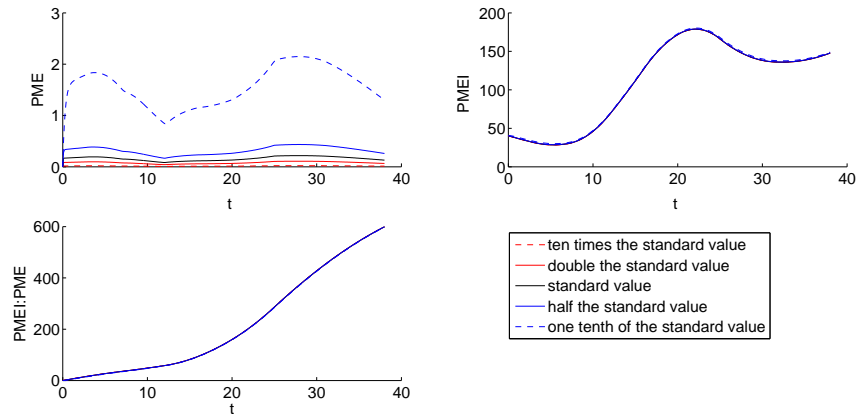


Fig. 4.9: Parameter sensitivity of d , on the enzyme levels

Figure 4.8, are subtle, with the exception that increasing D is similar to decreasing d and vice versa. Further to this, changing D to be ten fold its standard value speeds up the de-methyl-esterification more than making d a tenth of its standard value, which in turn creates a higher peak of dHG without changing the timing of the peak. Since d is the rate of binding between PME and $PMEI$, changing d effects the available PME level as seen in Figure 4.9, below.

From Figure 4.9 it can be seen that with d one tenth of its standard value, the PME profile is accentuated, as expected and even with low affinity between PME and $PMEI$ results in PME levels being vastly lower than any other enzyme. Due to the low levels of PME , changing d has very little affect on $PMEI$ levels.

Figure 4.10 shows the effect of altering the rate at which PL cleaves the de-methyl-esterified homogalacturonan; the result is seen clearly in the dHG levels but even when E is a tenth of the standard value, the peak of dHG increases by one and a half times and the shift in the timing of the peak is less than an hour later for the lower reaction rate. This parameter does not alter the $MeHG$ levels and by twenty hours after imbibition no effect is seen from any of the polysaccharide states, with minimal effect

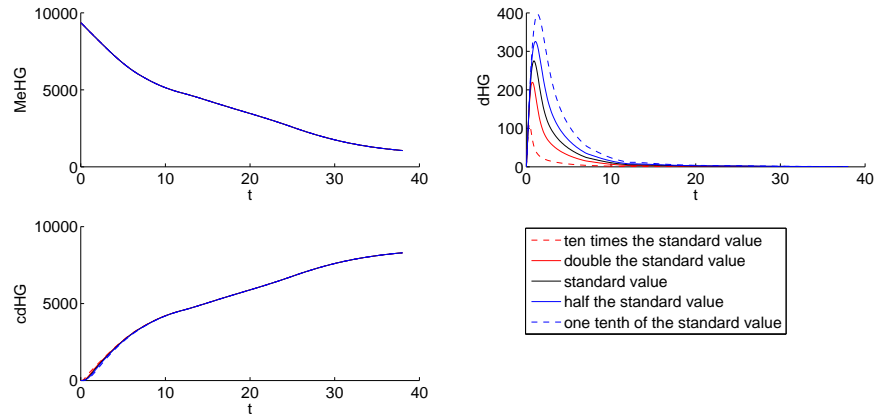


Fig. 4.10: Parameter sensitivity of E , on the polysaccharide levels

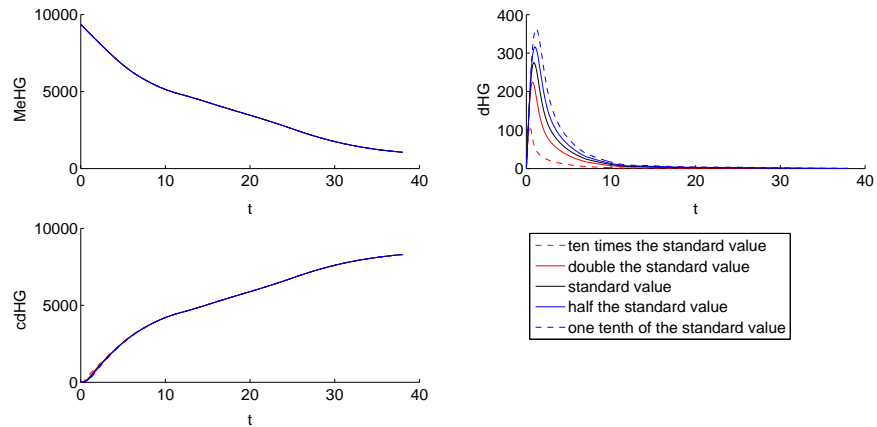


Fig. 4.11: Parameter sensitivity of F , on the polysaccharide levels

after ten hours.

Perhaps unsurprisingly, the impact of altering F , as shown in Figure 4.11, is similar in profile yet a reduction in magnitude to that of changing E . This is due to the similarities in the PL and PG curves and reaction rates; this is an argument for simplifying the model so that PL and PG are considered one family of proteins, given our current limited knowledge about the PL family.

Parameter c , the reaction rate of PG creating a complex with PGI , Figure 4.12, has no significant affect on the polysaccharide states up to an order of magnitude change in the value and as such its value is

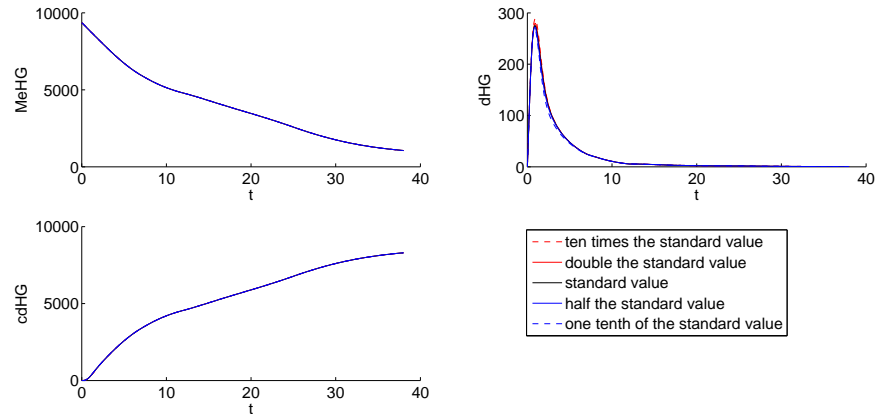


Fig. 4.12: Parameter sensitivity of c , on the polysaccharide levels

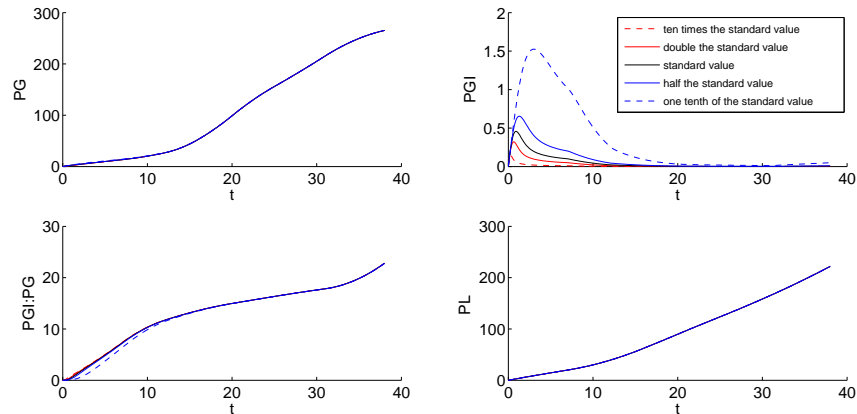


Fig. 4.13: Parameter sensitivity of c , on the enzyme levels

incidental to the model. This is likely to be due to the low levels of PGI mRNA within the endosperm, as seen in Figure 4.13. The model could be constructed with a high initial quantity of PGI , making parameter c more important to the model but without evidence to suggest this and with such low levels of mRNA it would lack biological relevance.

The parameter α is present in all of the single protein equations and as such has an effect on every variable: it aims to translate the mRNA levels from the vSEED data (Section 1.3) to protein levels; this parameter has been estimated through parameter fitting in section 3.7. Parameter sensitivity of α is shown in Figures 4.14 - 4.16.

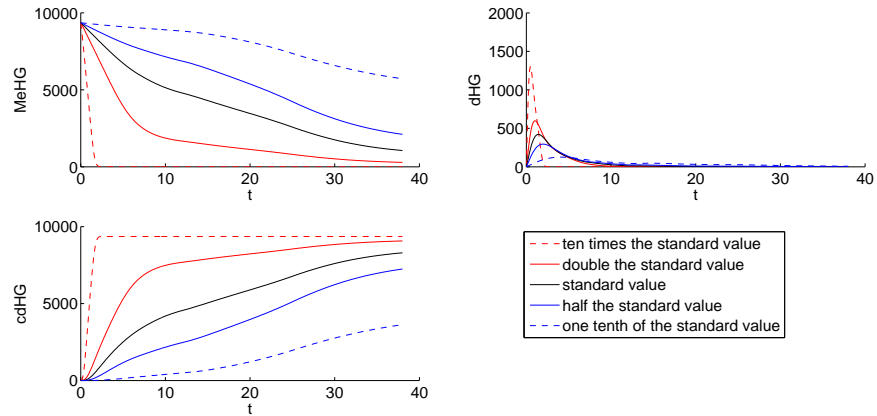


Fig. 4.14: Parameter sensitivity of α , on the polysaccharide levels

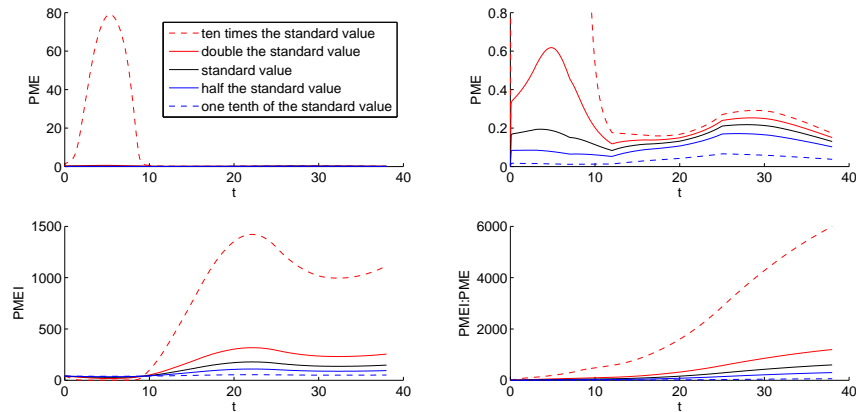


Fig. 4.15: Parameter sensitivity of α , on the PME , $PMEI$ and $PMEI : PME$ levels. The top right graph being a close up of the top left.

Altering the parameter α has a vast affect on the polysaccharide levels, Figure 4.14, from converting all the homogalacturonan to its cleaved state in the first two hours to barely converting a third of the available homogalacturonan to its de-methyl-esterified form. The level of dHG is minimal after ten hours for all α values, this is due to the tissue we are considering; in the radicle vSEED transcriptomics, PG and PL levels of mRNA are severely reduced.

Figure 4.15 highlights the availability of PME in the first ten hours after imbibition and, after this, the level of $PMEI$ controls the PME levels for the remainder of the germination process. For the first twelve hours,

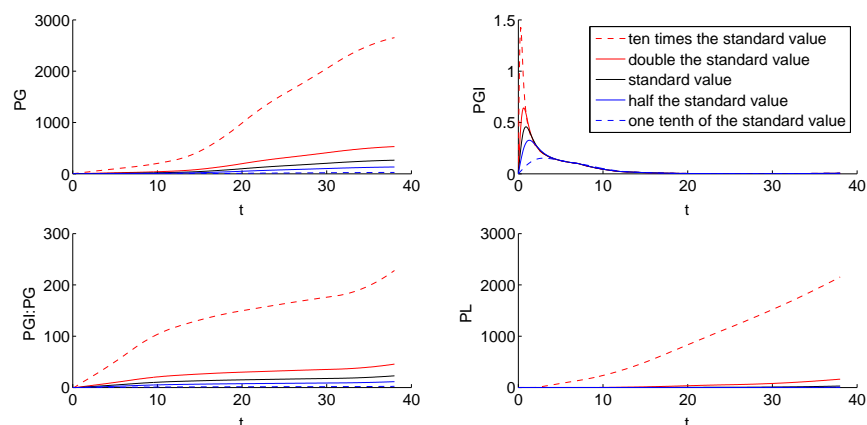


Fig. 4.16: Parameter sensitivity of α on the PG , PGI and $PGI : PG$ levels

PME levels spike, with a ten fold increase in the parameter α resulting in a forty fold accumulation of PME at its peak, five hours after imbibition; from twelve hours onwards the protein curve profiles are very similar and the same tenfold increase in α results in a twenty percent increase in protein accumulation. The $PMEI$ graph show the same profile for all values of α , higher values simply accentuating this profile.

The PGI protein levels from three hours after imbibition seem invariant to alterations in α , Figure 4.16, this is not the case but the increase parameter α causes is counter acted by the same increase in PG resulting in additional $PGI : PG$ and leaving the PGI level unchanged.

4.3 Arabinan Network

The arabinan polysaccharide and arabinase protein are discussed in Section 1.2. Arabinan is a member of the pectin group of cell wall polysaccharides along with homogalacturonan although there are no known interactions between the two polysaccharides.

Work produced by Lee [44] has shown, by using fluorescent markers, that the abundant arabinan in the endosperm is altered in some way. To

support this, the transcriptomics data has highlighted arabinase activity and Minic [51] highlights the importance of arabinase, however, the form of alteration is currently undetermined. So, the following network (Figure 4.17) is converted into a mathematical model.

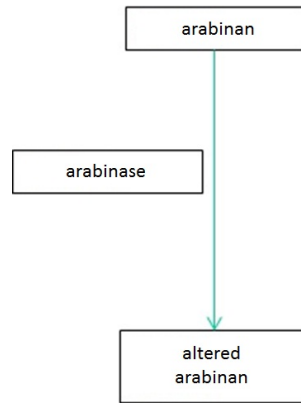
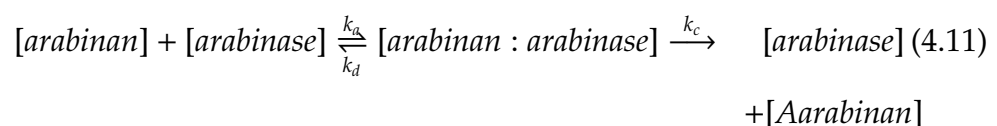


Fig. 4.17: The arabinan network

The network begins with arabinan in its synthesised form, a generic arabinase is used to create an altered state of arabinan, which we will refer to as altered arabinan (Aarabinan). This leads to one of the most basic forms of a conservation of mass model but without more biological knowledge additional complexity may be unproductive. Lee [44] used immunocytochemistry to establish the presence of arabinan in the endosperm cell walls and found, even at three hours after imbibition, that arabinan is present in its altered form; this may point to arabinan remodelling occurring during seed maturation and not early germination.

In equation form, we look at the rate of change of arabinan or $\frac{d[\text{arabinan}]}{dt}$ and consider what alters this state. Firstly, arabinase will bind to the arabinan and may then unbind or alter the arabinan into ‘altered arabinan’ (Aarabinan):



Statement 4.11 is a typical Michaelis-Menten model but will be modelled using the same method as the homogalacturonan network for comparability. In this section a simplified form is assumed where the reverse arrows are neglected; this results in equations (4.12) - (4.14), where k is a rate constant. There is a separate differential equation for both of the polysaccharide states as well as the enzyme.

$$\frac{d[arabanan]}{dt} = -k[arabanan][arabinese], \quad (4.12)$$

$$\frac{d[arabinese]}{dt} = \alpha\beta_{arabinese}, \quad (4.13)$$

$$\frac{d[Aarabanan]}{dt} = k[arabanan][arabinese]. \quad (4.14)$$

Literature surrounding arabinan enzyme kinetics is limited since it is considered a minor element of most cell walls, this is not the case for the endosperm cell walls. Spagnuolo [75] considers arabinase activity at a high temperature of 40 °C and the suggested reaction rate was 0.0167 $\mu\text{m}^3/\text{mg s}$. The suggested reaction rate appears slow if we are to assume that the arabinan is remodelled during germination and suggests that it is more likely to occur earlier in seed development, perhaps during seed maturation. We assume, given that arabinan is at most 20% of the cell wall, that $[arabanan]_0 = 4677.7\text{mg}/\mu\text{m}^3$, when compared to the value of $[MeHG]_0$, as 40% of the cell wall dry weight, used in section 4.2.

The standard result for our model as shown in Figure 4.18, with $k = 1 \mu\text{m}/\text{s}$ to keep within the order of magnitude found by Spagnuolo [75]. The initial value of arabinan, $[arabanan]_0 = 4677.7\text{mg}/\mu\text{m}^3$ and all other initial conditions are zero.

With the standard parameters used, arabinan is heavily remodelled before three hours after imbibition, as seen by Lee [44]. The level of

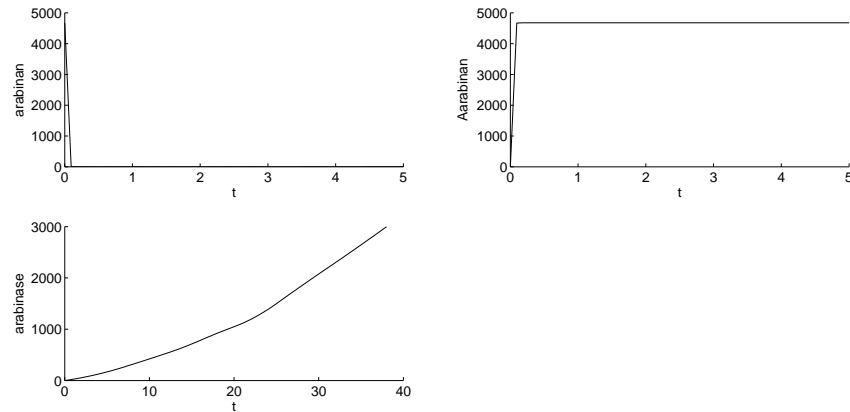


Fig. 4.18: Arabinan polysaccharide and protein levels over time (hr)

arabinase monotonically increases throughout the germination process. This increase seems biologically unnecessary, with all the arabinan remodelled so early. There is the possibility that immunocytochemistry may only illuminate the accessible molecules in the cell wall structure, meaning that as the other proteins remodel the wall more arabinan may become available and is therefore remodelled quickly with the abundance of available arabinase.

4.3.1 Parameter Sensitivity

This section will consider the parameters k and α with regard to their effect on the polysaccharide and protein levels and special attention given to the robustness of significant remodelling occurring before three hours after imbibition.

As expected, Figure 4.19 shows that increasing α speeds up the reaction process and even a tenth of the arabinase production results in remodel all of the arabinan by the three hour time; in order to have unmodified arabinan by three hours after imbibition α has to be decreased to a twentieth of the standard value.

Altering k has a similar effect on the polysaccharide to altering α , ow-

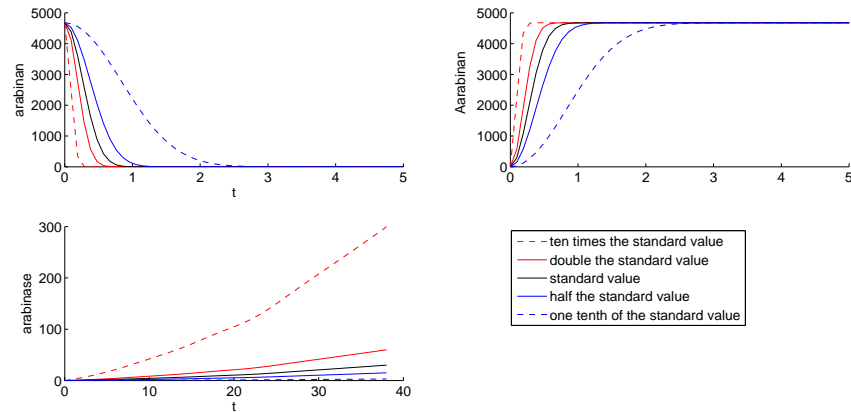


Fig. 4.19: Arabinan polysaccharide and protein levels over time (hr), while altering α

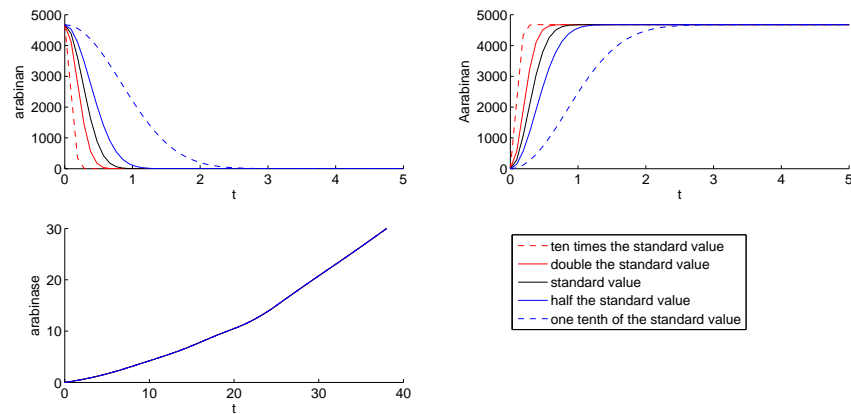


Fig. 4.20: arabinan polysaccharide and protein levels over time (hr), while altering k

ing to the expedient remodelling; meaning that since the initial value of the enzyme is zero, $[arabinase]_0 = 0\text{mg}/\mu\text{m}^3$, then for very early timepoints $[arabinase] = \alpha\beta_{arabinase}$. So, multiplying α by ten will simply increase $[arabinase]$ by ten and so has the same impact on the term $k[arabinan][arabinase]$ as multiplying k by ten.

This shows that, with the currently used standard values, the observed completely remodelled arabinan is a robust result of the model.

4.4 Xyloglucan Network

The xyloglucan has the potential to be remodelled by two different proteins, XTH and expansin, with differing results. Since these two proteins work in contrasting environments we will assume that xyloglucan affected by XTH cannot subsequently be the target of expansins and visa versa.

The resulting network is summarised in Figure 4.21. It shows a competition for the original xyloglucan between XTH and expansin, with the resulting states being cleaved xyloglucan ($cXylo$) and weakened xyloglucan ($wXylo$), respectively.

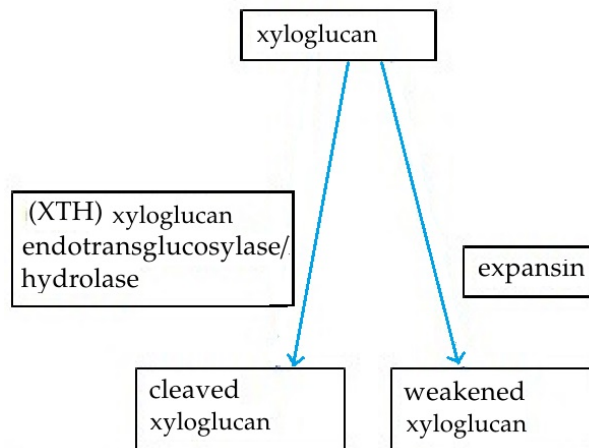


Fig. 4.21: A summary of the xyloglucan network

The xyloglucan has the potential to be remodelled in two different ways and has a term for every reaction it is involved with, giving:

$$\frac{d[Xylo]}{dt} = -(A[Expan] + B[XTH])[Xylo]. \quad (4.15)$$

In equation (4.15) the first term on the right hand side relates to the expansin reaction and is also seen in the expansin equation (4.16) since

Cosgrove [16] explains that the expansin activity of cell wall loosening requires the continued presence of the expansin protein and the complex of expansin and activity site becomes a new weakened xyloglucan state ($[wXylo]$) described in equation (4.18). The second term deals with the XTH interaction and is mirrored in equation (4.19), the equation for cleaved xyloglucan ($cXylo$); due to at least some XTH creating a covalent bond with the xyloglucan during its interaction, the amount of available XTH reduces as it interacts with the polysaccharide. Neither of the proteins, XTH or expansin, are true enzymes since they are required to maintain the xyloglucans altered state.

$$\frac{d[Expansin]}{dt} = -A[Xylo][Expansin] + \alpha\beta_{Expansin}, \quad (4.16)$$

$$\frac{d[XTH]}{dt} = -B[Xylo][XTH] + \alpha\beta_{XTH}, \quad (4.17)$$

$$\frac{d[wXylo]}{dt} = A[Xylo][Expansin], \quad (4.18)$$

$$\frac{d[cXylo]}{dt} = B[Xylo][XTH]. \quad (4.19)$$

Without any further knowledge, A and B are assumed to be equal to one another and of the same order as the previously discussed D , Section 4.2, so $A = B = 0.4\mu\text{m}^3/\text{mg s}$. The initial condition $[Xylo]_0 = 10000 \text{ mg}/\mu\text{m}^3$ to keep the complete cell wall in proportion and all other initial conditions are set to zero.

Figure 4.22 shows the results from the model constructed in equations (4.15) - (4.19). The polysaccharide xyloglucan is used up by ten hours after imbibition and the majority has been acted upon by expansins. Biologically, expansin is thought to relieve tension from the xyloglucan and so this an upper limit to the expansin activity during germination.

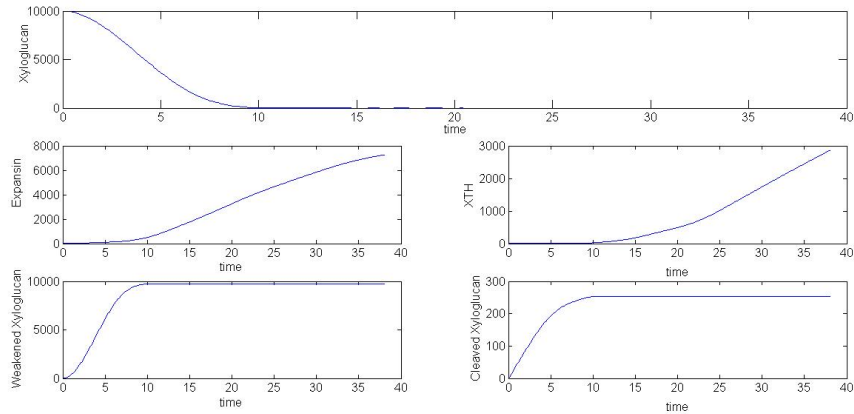


Fig. 4.22: Xyloglucan polysaccharide and protein levels over time (hr)

4.4.1 Parameter Sensitivity

Parameters A and B , the reaction rate constants, have little effect on the system as seen in Figures 4.23 and 4.24 meaning that estimating this parameter is unimportant especially when compared to other parameters.

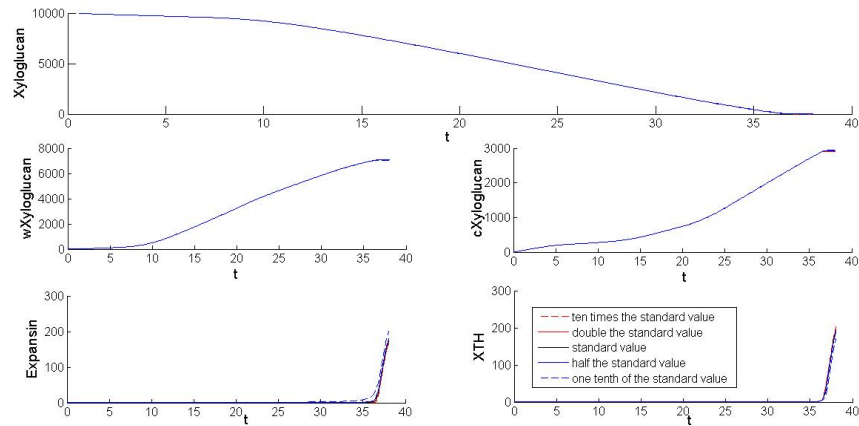


Fig. 4.23: Xyloglucan polysaccharide and protein levels over time (hr), while altering the initial condition A

Altering $[Xylo]_0$, Figure 4.25 shifts the initial level of xyloglucan and the gradient of the curve is the same; the lower values of $[Xylo]_0$ reach zero and then plateau, at this point the XTH and expansin begins to accumulate. The competitive nature of the two altered xyloglucan, $[wXylo]$ and $[cXylo]$ is unchanged by altering this initial condition of xyloglucan,

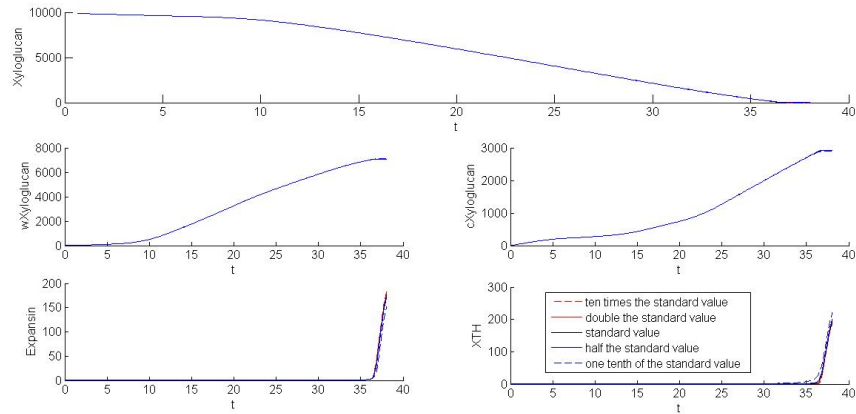


Fig. 4.24: Xyloglucan polysaccharide and protein levels over time (hr), while altering the initial condition B

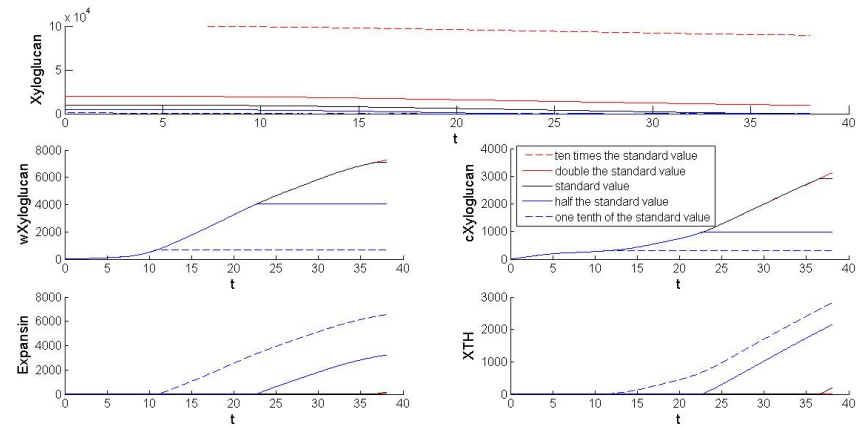


Fig. 4.25: Xyloglucan polysaccharide and protein levels over time (hr), while altering the initial condition $[Xylo]_0$

the only change is the time by which all the $[Xylo]$ is used up by the proteins.

The effect of changing α is shown in Figure 4.26, the obvious effects of increasing α resulting in faster remodelling of xyloglucan and higher levels of expansin and XTH can be seen as well as the more interesting effects on the level of the resulting polysaccharide states $[wXylo]$ and $[cXylo]$; the production of expansin and XTH helps to explain this behaviour, Figure 4.27. The first four hours of production show that XTH is produced at twice the rate of expansin, meaning that these first four

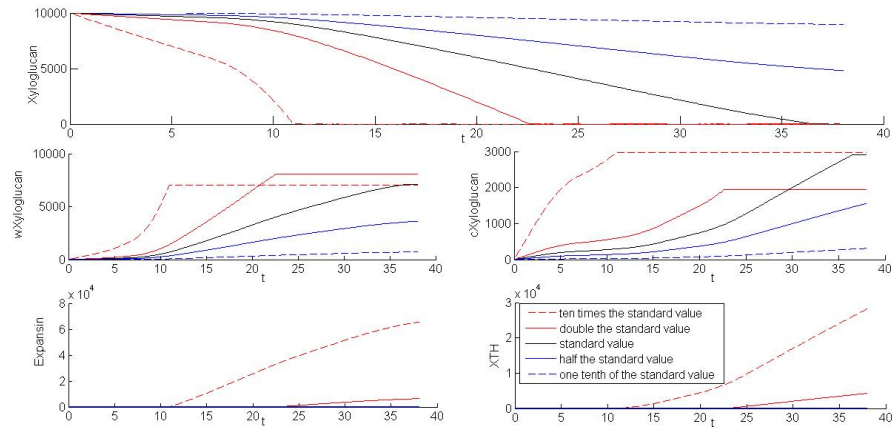


Fig. 4.26: Xyloglucan polysaccharide and protein levels over time (hr), while altering the initial condition α

hours we expect more $[wXylo]$ than $[cXylo]$ to be produced, however, this initial level of XTH is relatively small as by five hours expansin production has overtaken XTH production and by ten hours expansin production is eight times the level of XTH production and increasing. In Figure 4.26, there is sufficient xyloglucan to last more than ten hours, with the parameters used, if however the xyloglucan was remodelled before five hours, the $[cXylo]$ would exceed the $[wXylo]$ meaning that the quantity of xyloglucan activity sites, $[Xylo]_0$, is important to estimate especially when considered relative to α .

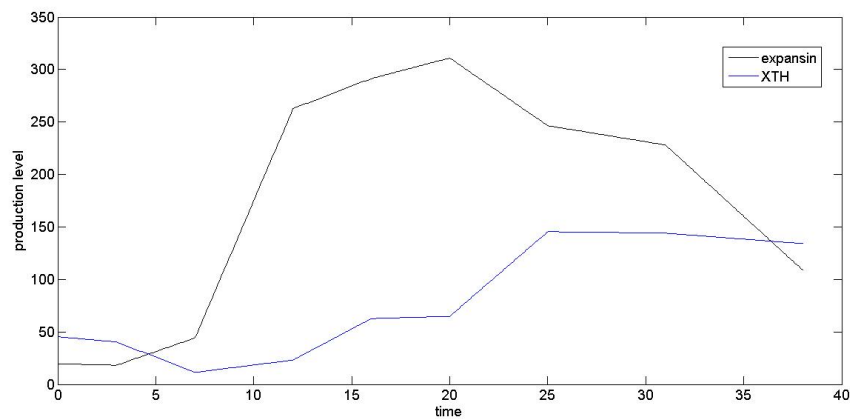


Fig. 4.27: Production of XTH and expansin over time, $\alpha\beta$ terms for XTH and expansin

4.5 Cell Wall Properties

In this section, the homogalacturonan network in Section 4.2, arabinan network in Section 4.3 and xyloglucan network in Section 4.4 are used to investigate some cell wall properties. First the germination event (or cell separation) is discussed, followed by an investigation of the cell wall permeability and finally the cell wall extensibility.

4.5.1 Cell Separation

The germination event (or cell separation) is thought to be a combination of cell wall weakening and pressure exerted by the radicle. There is evidence during other cell separation events that polygalacturonase is essential [69] and this, along with the site of separation being in the intercellular matrix between two cells, points to homogalacturonan being the main consideration for cell separation.

Arabinan may be present in the intercellular matrix and therefore at the site of cell separation but with the arabinan remodelling occurring before the third hour after imbibition, and possibly even during seed maturation, arabinan will not contribute significantly to a germination prediction. That is to say that the presence of arabinan may be necessary for germination in a biological sense but without additional information on its remodelling it will not contribute to the mathematical model. When considering other species and cell separation events, arabinan should be considered to differentiate the tissues.

The implication is that a cell separation prediction will be a function of $[cdHG]$.

Endosperms of *Lepidium* seeds were tested by Dr. Sebastian Busch and Dr. Kerstin Mueller (University of Friburg) to find the force required

to be exerted in order to cause a cell separation event at various hours after imbibition. A cylinder 0.3mm in diameter with a hemispherical tip of the same diameter is pushed into an endosperm until the endosperm ruptures, the force required to rupture the endosperm is recorded and the resulting data is shown using violin plots in figure 4.28. A violin plot shows the distribution of of data points at each time point; each time points distribution is calculated and then reflected to create the 'violins' seen in figure 4.28. The data was then analysed by Dr. Simon Pearce (University of Nottingham).

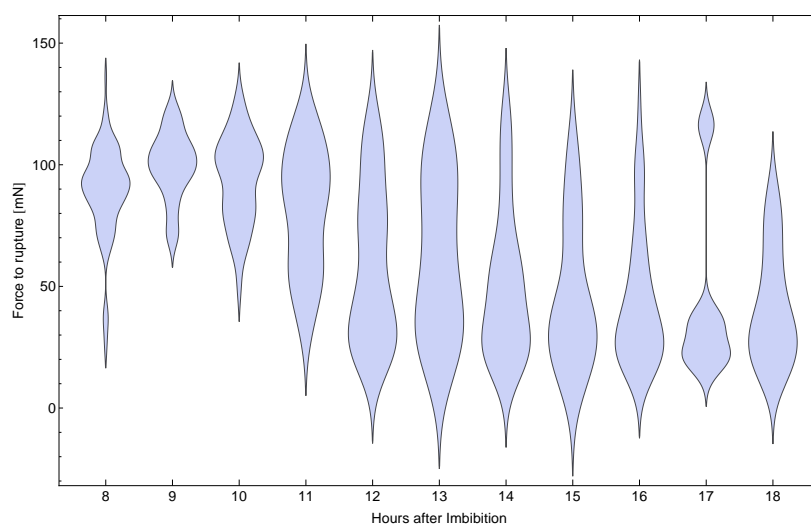


Fig. 4.28: Distribution of force exerted by a needle on *Lepidium* endosperm to cause endosperm rupture, separated by the endosperm's age in hours after imbibition. *Lepidium* seeds germinate at roughly sixteen hours after imbibition.

The distributions in Figure 4.28 reinforce the hypothesis that the cell wall remodelling weakens the endosperm in preparation for germination. The violin plots in Figure 4.28 show a bimodal distribution. For the first ten hours after imbibition the endosperms require roughly 100 mN to puncture: from twelve hours the mode force required decreases to around 30mN; this change in cell wall cohesion which causes the reduction in force required to puncture the endosperm may be a grad-

ual process which continually weakens the endosperm, alternatively, some threshold of cell wall cohesion could be reached which steps the endosperm from its stronger form requiring 100mN for rupture to the weaker form which requires only 30mN. The spread seen in Figure 4.28 is caused by biodiversity and the unavoidably destructive method of testing the endosperms. The two hypotheses are indistinguishable given the current data. The transition from the higher, 100 mN, mode to the lower, 30 mN, begins slightly before testa rupture.

Figures 4.29 and 4.30 show the change in polysaccharide and protein levels as predicted by the model constructed in this chapter (see Sections 4.2 and 4.4) using *Lepidium* vSEED data for all β terms. Using the change in puncture force required for germination and the change in polysaccharide levels, hypotheses can be drawn as to which polysaccharides most impact cell wall cohesion.

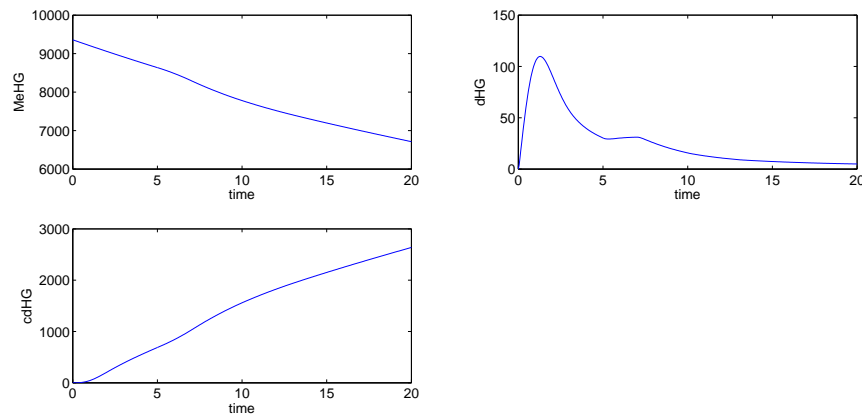


Fig. 4.29: Homogalacturonan polysaccharide levels over time (hr), for *Lepidium* endosperm during germination

The $[dHG]$ profile, as shown in Figure 4.29, is minimal from twelve hours onwards suggesting that the presence of non-cleaved de-methylated homogalacturonan prevents germination and supports the theory that the $[dHG]$ strengthens the cell wall cohesion through calcium

crosslinking. The cleaved form of homogalacturonan is continually increasing, the physical impact of which, on the cohesion of the wall, is difficult to determine and could result in either a gradual reduction in cohesion of a step change.

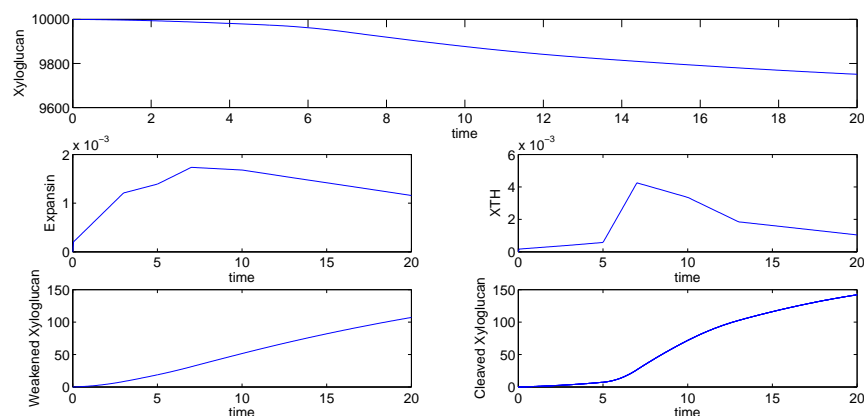


Fig. 4.30: Xyloglucan polysaccharide and related protein levels over time (hr), for *Lepidium* endosperm during germination

In Figure 4.30, the profile of the two altered polysaccharides is very different to the same graphs for *Arabidopsis*, Figure 4.22; the difference between these two sets of graphs results from the transcriptomics data i.e. the β functions, the slight differences in protein level profile caused by this change in transcriptomics are minor in comparison to the fact that in *Arabidopsis* the expansin protein is dominant in the competition for xyloglucan, three times the level of XTH at thirteen hours, a third of the way through the germination process. Conversely, XTH is the dominant protein in *Lepidium*, with twice the level of expansin at seven hours, roughly a third of the way through germination process.

When considering candidates for promoters of the cell separation event from the xyloglucan network, Figure 4.30, either of the altered forms of xyloglucan may contribute, although the cell separation is thought to occur in the intercellular matrix where there are no xyloglucan

polysaccharides. The sharp change in gradient of the cleaved xyloglucan polysaccharide level at six hours indicates a change in cell properties but is four hours before any notable change in cell cohesion.

The arabinan remodelling occurs in the first hour for *Lepidium* indicating that it has no impact on the change in cell wall properties, as hypothesised in section 4.3.

4.5.2 Cell Wall Permeability

Cell wall permeability is an important element of the cell wall properties since any alteration of the cell wall permeability will affect the mobility of all the enzymes considered in this chapter. Under the presented model conditions we would expect changes to occur in the cell wall permeability and assumptions are made below as to how each element of the model will impact the permeability, though the extent to which this is changed is unknown.

The permeability of the cell wall can be simply broken down into two elements.

Firstly, the cellulose and hemicellulose framework can be considered to form a porous structure, the pores of which will be variable and unknown in size. If the pore starts narrower than the protein size no protein movement will occur until alterations have been made to the porous structure. Conversely if the pores of the framework are sufficiently large any additional increase in size will have relatively little impact on protein movement. With the assumption that cellulose remains unchanged the pore sizes are controlled by the hemicellulose, i.e. in the case of this model, xyloglucan. The starting state of xyloglucan, $[Xylo]$, will therefore set some undefined pore size which is determined by the proximity to neighbouring xyloglucan and the tautness of the xyloglucan and its

neighbours, none of which is considered within the model discussed in this chapter. Expansin is thought to loosen xyloglucan and would therefore increase the pore size of the framework, whereas XTH performs a cleaving of the xyloglucan and so would increase the pore size more dramatically.

The second element of the cell wall permeability is the viscosity of the pectin and water structure. Due to the size of cell walls this is difficult to measure. In a paper by Dyson [23] the viscosity of plant cell walls is approximated to between 10^9 - 10^{11} kg $m^{-1}s^{-1}$ from tissue level measurements of tomato [78] and pea [77] cells. It is also important to note that the seed endosperm has a higher percentage make up of arabinan than either of the measured tissues: due to our lack of knowledge regarding arabinan it is difficult to guess what impact altering it has on the viscosity of the cell wall, but since the remodelling happens very early and quickly it is enough to assume that it has no impact on altering the cells viscosity. This leaves homogalacturonan as the main controller of cell wall viscosity, with the de-methyl-esterifying process reducing viscosity but calcium crosslinking increasing the viscosity again and the cleaving reducing the viscosity; the magnitude of these changes is unknown.

With so many unknowns the full extent of the cell wall permeability is not explored in this thesis, although a viscosity, independent of time, is included in Chapter 5. Permeability is likely to be altered by environmental factors as well as pH as discussed by Klis [40], who considered yeast cell walls.

4.5.3 Cell Wall extensibility

The endosperm's cell wall extensibility is assumed to change during germination since a vast portion of the cell wall is remodelled. The

de-methylesterification of homogalacturonan has been shown to change cell wall extensibility [65]. Hemicellulose and xyloglucan in particular has been shown as a controlling factor of elasticity [64]. Either of the altered forms of xyloglucan are more elastic than the [*Xylo*] state and it is assumed that XTH has a larger impact than expansin although this is not necessarily true; expansin is said to relieve tension in the hemicellulose with no documentation as to what degree. An article by Dyson [24] considers the impact of hemicellulose on cell wall extensibility in a growing cell while making similar assumption for how expansin and XTH activity occurs.

Arabinan is thought to be more elastic than other pectins [36] and its presence in the endosperm is a major difference between the cell wall of the endosperm and other tissues but the different impact of the altered form of arabinan compared to its unaltered form is unknown. Homogalacturonan will reduce the extensibility of the cell wall when calcium crosslinking occurs and increase extensibility through cleaving. The de-methylesterification process is not assumed to have an impact other than allowing further alterations.

In order to determine any change in endosperm extensibility experiments have been carried out by Sebastian Busch (University of Frieburg). A 0.3mm cylinder with a hemispherical tip of the same 0.3mm diameter is pushed into an endosperm and the displacement is measured as force is increased. The resulting data is plotted as a line of force against displacement. Simon Pearce (University of Nottingham) then normalised the data and the gradient of the lines is shown in Figure 4.31.

Figure 4.31 shows no significant change to cell wall extensibility with the given sample size. With the level of remodelling occurring in the model it is surprising that no change in extensibility is seen in these ex-

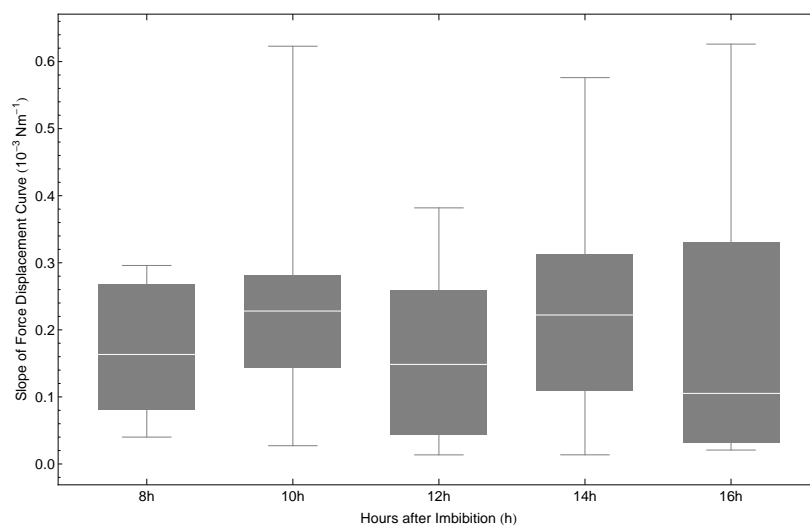


Fig. 4.31: Box and whisker graph of slope of the force displacement plot separated by hours after imbibition.

periments and this will be revisited with the partial differential equation model in Chapter 5.

4.6 Conclusion

The ODE model constructed in Chapter 3 was expanded to include the major cell wall proteins and polysaccharides with an aim to consider the impact of altering these polysaccharides on the mechanical properties of the cell wall. The well mixed assumption, as well as the reactions being fully irreversible remain. Data were introduced showing the change in required force, from the radicle, to cause cell separation and therefore germination, the exact nature of this change is difficult to distinguish between a step change or a gradual weakening. Endosperm extensibility has been measured and no significant change over time was seen. The final cell wall property, permeability, was discussed and suggested to be the combination of a varying viscosity of the pectin polysaccharides through a porous structure formed by the cellulose and hemicellulose structure, with changing pore sizes. With experiments aimed at measur-

ing cell wall permeability very difficult due to the size of the cell wall, no data is currently available on how, if at all, permeability changes during the germination process; some approximations have been made from other plant tissues as to general cell wall permeability but the distinct nature of the endosperm, being predominantly its differing components, means that these approximations may not be valid for the endosperm.

The arabinan polysaccharide is found to be altered by the available arabinase very quickly and in fact may begin imbibition in the altered form due to being altered during an earlier stage of seed development. Although arabinan is a distinguishing feature of the endosperm cell wall, the lack of change in the polysaccharide during the germination process makes it a poor candidate to explain any cell wall changes. Arabinan is thought to deform more, without breaking, than homogalacturonan and so when comparing the extensibility, and other cell wall properties, of the endosperm with other plant tissues, arabinan should be considered to explain any difference. Further experiments designed to establish when arabinase alters arabinan may help to clarify the purpose of arabinan and why it is present in the endosperm at higher levels than other cell walls.

Homogalacturonan is seen as highly important for the viscous element of cell wall permeability due to its abundance; without data it is difficult to suggest the significance of each polysaccharide state although an indication is made as to whether each state will increase or decrease viscosity.

Polygalacturonase activity is associated with many cell separation events and due to the perceived location of the rupture being in a pectin only region between primary cell walls, and arabinase's inactivity during germination, we expect polygalacturonase to be the major contributor to the cell separation associated with germination; the ODE model shows a

constant increase in cleaved de-methylesterified homogalacturonan, the product of polygalacturonase, supporting this hypothesis. These models do not consider the spatial elements of the cell wall and so although polygalacturonase is clearly active during the germination process it is unclear whether its activity can be seen at the site of the cell separation and so a spatial dimension is introduced in Chapter 5.

The xyloglucan network was introduced as a major component of the plant cell wall and thought to be a controlling factor in cell wall extensibility and we suggest its contribution to cell wall permeability to be the main element for controlling pore size. The significant increase in cleaved xyloglucan before the cell separation event may suggest that the cleaved form of xyloglucan allows polygalacturonan to move more freely through the wall and thus perform the separation event. Further work is needed on this to confirm or reject this hypothesis. The unchanging extensibility of the endosperm during germination suggests that xyloglucan does not control this cell wall property and arabinan is a more likely candidate; other plant tissues contain minimal arabinan resulting in a less elastic cell wall but may result in xyloglucan controlling the extensibility in these cells.

Establishing the cell wall permeability and how it changes during germination requires further modelling to consider the proposed structure but will not be presented in this thesis; in order for this model to be constructed more information is needed on distribution of hemicellulose along the cellulose and spatial elements would need to be incorporated.

The pH change within the cell walls has not been addressed and could prove to significantly alter the competitive nature of the xyloglucan network, with acidic cell wall regions favouring expansin and more neutral pH favouring XTH. This could be crudely achieved by using a complete

cell wall pH level. The pH preferences through the homogalacturonan network require knowledge of pH levels of micropockets within the cell wall and, although some information is available about the affect some of the discussed reactions have on pH, spatial structure is again required.

Proteomics data from a germinating seed would be useful to validate the vSEED transcriptomics data used in the model constructed in this chapter. This validation would go a step towards making the models more quantitative and therefore more easily testable.

Chapter 5 continues to build on this model by introducing a spatial dimension to further explore the cell separation event and other cell wall properties.

5. PARTIAL DIFFERENTIAL EQUATION MODEL OF CELL WALL BEHAVIOUR DURING GERMINATION

5.1 *Introduction*

This Chapter will revisit relevant background information before taking the ordinary differential equation model constructed in section 4 and expanding it to include spatial dependence. For this to be done partial differential equations will be used and diffusion terms are introduced.

Using the environmental scanning electron microscope (eSEM), as seen in Figure 5.1 provided by Dr. Simon Pearce and Dr. Nicola Everitt (University of Nottingham), it is thought that the embryo ruptures between two cells and so it is important to consider the junction between two cells. The aim of this is to consider whether this model can point to a candidate for cell separation given the hypothesis that the endosperm breaks between primary cell walls (intercellular matrix) in order to allow the seed radicle to emerge. The endosperm is the layer of cells surrounding the embryo before germination. It is a single cell thick in both *Arabidopsis* and *Lepidium*.

Section 5.2 reiterates the biological networks introduced in previous chapters and explains the spatial domain before section 5.3 defines the partial differential equations, boundary conditions and initial conditions which represent the biological networks.

This model will be used, primarily to investigate the importance of

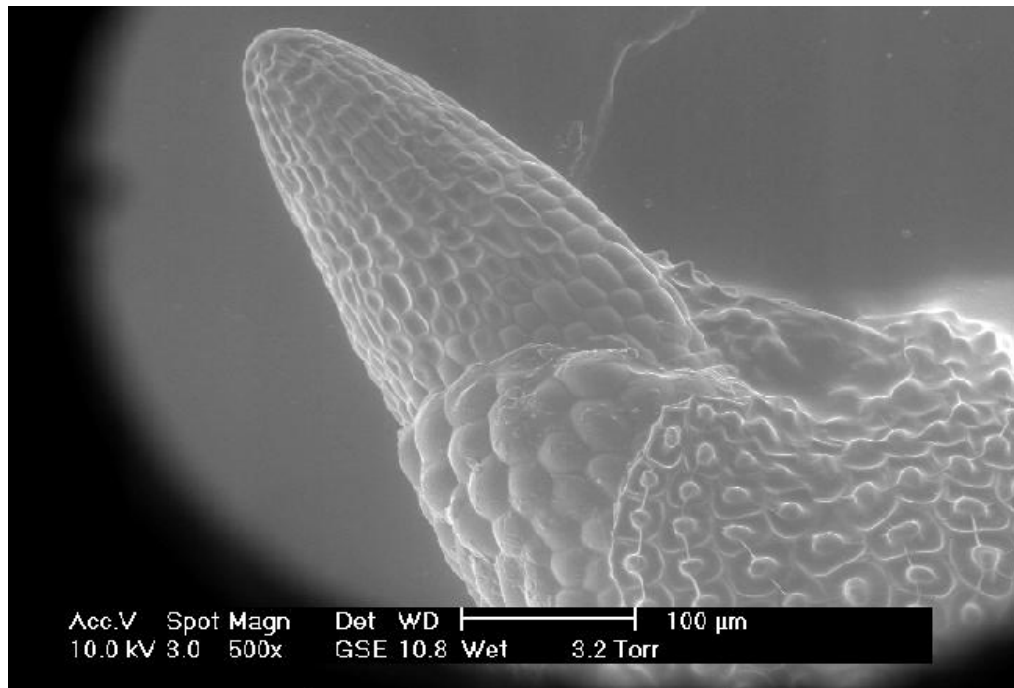


Fig. 5.1: eSEM picture of germinated seed, the radicle is pointing towards the top left of the picture with some of the top most cells beginning to dehydrate. The endosperm can be seen towards the bottom of the centre of the picture and the distinct cells in the bottom right belong to the testa.

each polysaccharide to the germination event with the following discussion regarding the remaining cell wall properties, cell wall extensibility and permeability, following on from Section 4.5.

5.2 *Biological Network*

The homogalacturonan, xyloglucan and arabinan networks considered in section 4 are shown below (Figure 5.2) and broken down through the rest of this section.

These three networks contribute to the cell wall properties, namely extensibility, permeability and cell separation. The degree to which each network contributes and is affected by these properties is unknown but has been discussed in Section 4.5.

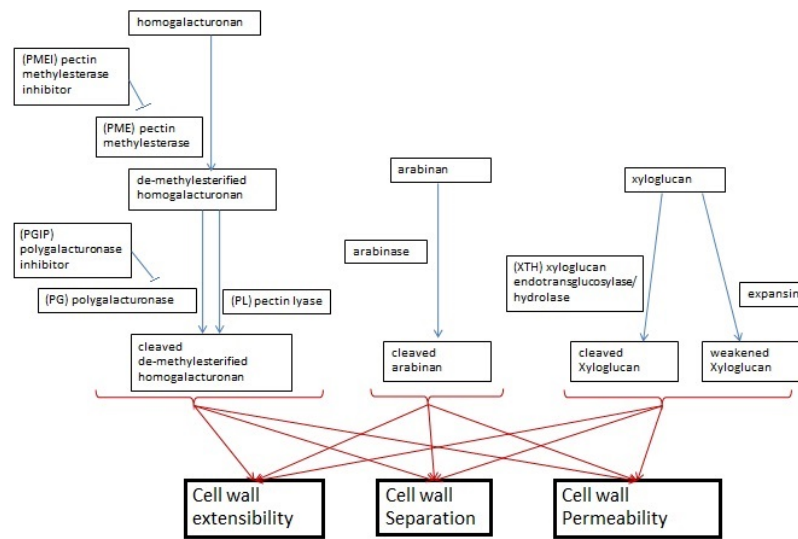


Fig. 5.2: The complete parallel network

With the introduction of a spatial dimension, the plant cell geometry becomes important. This chapter focuses on the endosperm of the seed as introduced in section 1.1.1. The model is set up across two primary cell walls and the junction between these two cell walls, known as the intercellular matrix (illustrated in Figure 5.3) and considers a single spatial dimension horizontally through the centre of the two primary cell walls, along with time. The interior of the two cells is not considered. Plant cell walls vary in thickness significantly, from 5 nm, the lower bound discussed by Gabrielle [26], to the 100 nm cell walls of an onion stated by McCann [49]; due to *Arabidopsis*' small size a cell wall thickness of 10 nm is used for the model. The intercellular matrix is difficult to detect and measure due to its small size even in comparison to the cell walls and as such we will assume that the centre point of the considered domain is the intercellular matrix.

The three areas of this model, namely primary cell wall, intercellular matrix and primary cell wall, are considered to establish the components present within them. The components from the first and third areas were

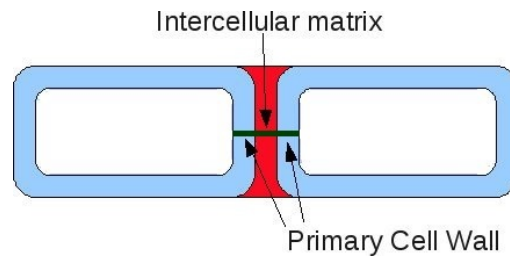


Fig. 5.3: A cartoon representation of two cells with the respective primary cell walls (blue), separated by the intercellular matrix (red). The green line represents the model domain.

considered in the previous ODE models in chapter 4. The intercellular matrix is thought to comprise solely of pectin and so will use the same homogalacturonan and arabinan model as with the two primary cell walls. This model will be symmetric about the centre of the intercellular matrix but since this is the location we are interested in when considering the cell separation event, the model will not be simplified to exploit this symmetry.

Primary Cell Wall	Intercellular matrix	Primary Cell Wall
<ul style="list-style-type: none"> • homogalacturonan • arabinan • xyloglucan 	<ul style="list-style-type: none"> • homogalacturonan • arabinan 	<ul style="list-style-type: none"> • homogalacturonan • arabinan • xyloglucan

Fig. 5.4: Table of the components present within the intercellular model

For the purpose of this model we will consider the polysaccharide elements to be stationary and allow all the cell wall remodelling enzymes and proteins to move freely from the interior of the plant cell. The polysaccharides and proteins are discussed in section 1.2 and the homogalacturonan network in section 5.2.1, the xyloglucan network in section 5.2.2 and the arabinan network in section 5.2.3.

5.2.1 Homogalacturonan network

Homogalacturonan is considered the major component of pectin within the plant cell wall and is described in Section 1.2.1. The full homogalac-

turonan network is constructed and discussed in Section 4.2.

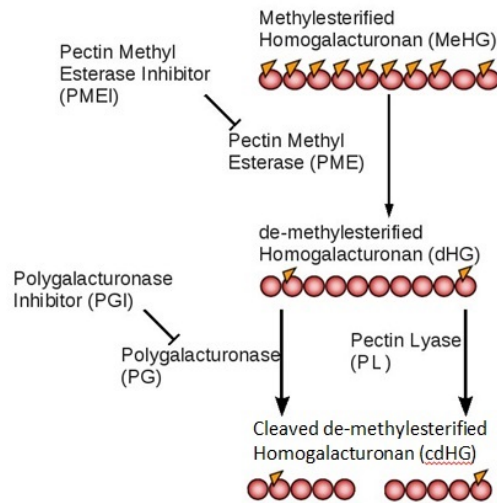


Fig. 5.5: The homogalacturonan network as seen in Section 4.2. Edited from an image provided by Kieran Lee (University of Leeds), unpublished

Polygalacturonase and pectin lyase cannot cleave the homogalacturonan without it first being de-methyl-esterified; this de-methyl-esterification is performed by pectin methylesterase; both polygalacturonase and pectin methylesterase have their own inhibitors which remove the ability of the respective protein to alter the homogalacturonan polysaccharide.

The different states of homogalacturonan are thought to contribute to the mechanical properties of the plant cell wall as discussed in Section 4.5. It is likely that the HG network will be a minor contributor to the extensibility property but a major contributor to the permeability and almost the sole reason for the separation event.

5.2.2 Xyloglucan network

Xyloglucan is altered by one of two proteins, either expansin or XTH with differing resulting cell wall properties. The xyloglucan network is illustrated below in Figure 5.6 and discussed in section 4.4.

The alterations made to the xyloglucan are likely to affect the extensi-

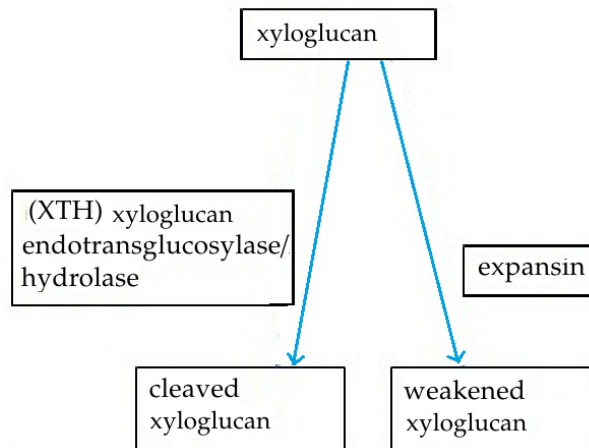


Fig. 5.6: The Xyloglucan network

bility property of the cell wall. Due to the location of the cell separation event, the xyloglucan network is not thought to impact the separation property but is to affect the permeability and extensibility of the cell wall.

5.2.3 Arabinan network

Arabinan is part of the Rhamnogalacturonan I group of pectins and the transcriptomics have highlighted Arabinase activity. The arabinan network is introduced in Section 4.3.

Arabinan is abundant in the cell wall of the endosperm and is one of the major differences between the endosperm's cell walls and the cell walls elsewhere in the plant. Little is known about the activity of arabinases and in this network they are simply assumed to change the state of the arabinan without specifying how the state is changed. It may be logical to assume the change of state is a cleaving in order for the separation event to be enzyme controlled; however, this is not an essential assumption for germination to occur, since the radicle plays a part in the germination process.

The simplicity of the model shows our lack of knowledge regarding arabinan. As part of the pectin it is likely to have a large impact on cell

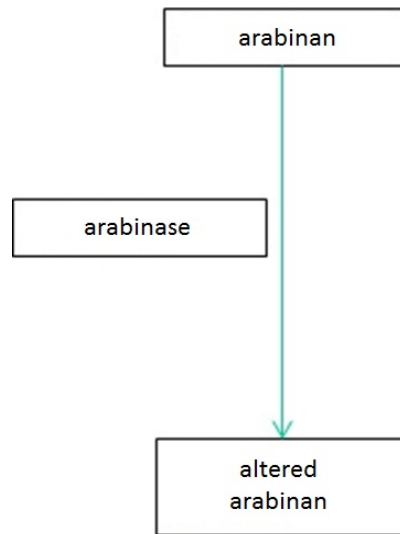


Fig. 5.7: The arabinan network

wall permeability and separation but since it is not the main load bearing structure it may only have a small role in the extensibility property.

5.3 Mathematical Model

This is modelled using partial differential equations since the level of each protein and polysaccharide is of interest across the whole domain considered, namely the two cell walls and the intercellular matrix. A compartmental model may be sufficient, using the two primary cell walls and the intercellular matrix as three separate compartments but will produce no information about the progress of the proteins through each compartment and as such may not capture interesting behaviour.

The complete set of partial differential equations used to describe this model are below; this model is extended from the models constructed in Sections 4.2, 4.3 and 4.4, to include one spatial element, x , the locations along the green line in Figure 5.3 set with the centre of the intercellular matrix as $x = 0$.

$$\frac{\partial[\text{MeHG}]}{\partial t} = -D[\text{PME}][\text{MeHG}], \quad (5.1)$$

$$\frac{\partial[d\text{HG}]}{\partial t} = D[\text{PME}][\text{MeHG}] - (E[\text{PL}] + F[\text{PG}])[d\text{HG}], \quad (5.2)$$

$$\frac{\partial[cd\text{HG}]}{\partial t} = (E[\text{PL}] + F[\text{PG}])[d\text{HG}], \quad (5.3)$$

$$\frac{\partial[\text{PME}]}{\partial t} = \mathcal{D}_{\text{PME}} \frac{\partial^2[\text{PME}]}{\partial x^2} - d[\text{PMEI}][\text{PME}], \quad (5.4)$$

$$\frac{\partial[\text{PMEI}]}{\partial t} = \mathcal{D}_{\text{PMEI}} \frac{\partial^2[\text{PMEI}]}{\partial x^2} - d[\text{PMEI}][\text{PME}], \quad (5.5)$$

$$\frac{\partial[\text{PME} : \text{PMEI}]}{\partial t} = d[\text{PMEI}][\text{PME}], \quad (5.6)$$

$$\frac{\partial[\text{PG}]}{\partial t} = \mathcal{D}_{\text{PG}} \frac{\partial^2[\text{PG}]}{\partial x^2} - c[\text{PGI}][\text{PG}], \quad (5.7)$$

$$\frac{\partial[\text{PGI}]}{\partial t} = \mathcal{D}_{\text{PGI}} \frac{\partial^2[\text{PGI}]}{\partial x^2} - c[\text{PGI}][\text{PG}], \quad (5.8)$$

$$\frac{\partial[\text{PGI} : \text{PG}]}{\partial t} = c[\text{PGI}][\text{PG}], \quad (5.9)$$

$$\frac{\partial[\text{PL}]}{\partial t} = \mathcal{D}_{\text{PL}} \frac{\partial^2[\text{PL}]}{\partial x^2}, \quad (5.10)$$

$$\frac{\partial[\text{Xylo}]}{\partial t} = -(A[\text{Expan}] + B[\text{XTH}])[\text{Xylo}], \quad (5.11)$$

$$\frac{\partial[\text{Expan}]}{\partial t} = \mathcal{D}_{\text{Expan}} \frac{\partial^2[\text{Expan}]}{\partial x^2} - A[\text{Xylo}][\text{Expan}], \quad (5.12)$$

$$\frac{\partial[\text{XTH}]}{\partial t} = \mathcal{D}_{\text{XTH}} \frac{\partial^2[\text{XTH}]}{\partial x^2} - B[\text{Xylo}][\text{XTH}] \quad (5.13)$$

$$\frac{\partial[w\text{Xylo}]}{\partial t} = A[\text{Xylo}][\text{Expan}], \quad (5.14)$$

$$\frac{\partial[c\text{Xylo}]}{\partial t} = B[\text{Xylo}][\text{XTH}], \quad (5.15)$$

$$\frac{\partial[\text{arabinan}]}{\partial t} = -k[\text{arabinan}][\text{arabinase}], \quad (5.16)$$

$$\frac{\partial[\text{arabinase}]}{\partial t} = \mathcal{D}_{\text{arabinase}} \frac{\partial^2[\text{arabinase}]}{\partial x^2}, \quad (5.17)$$

$$\frac{\partial[A\text{arabinan}]}{\partial t} = k[\text{arabinan}][\text{arabinase}], \quad (5.18)$$

As well as the initial conditions, whose value is stated in Section 5.3.4, the Boundary conditions for this model describe a flux of protein into the domain which depends on time, this flux is described by the production terms from the ODE model, Sections 4.2, 4.3 and 4.4 and stated below:

$$\frac{\partial[PME]}{\partial x} = \alpha\beta_{PME}(t) \quad \text{at } x=-1, \quad (5.19)$$

$$\frac{\partial[PME]}{\partial x} = -\alpha\beta_{PME}(t) \quad \text{at } x=1, \quad (5.20)$$

$$\frac{\partial[PMEI]}{\partial x} = \alpha\beta_{PMEI}(t) \quad \text{at } x=-1, \quad (5.21)$$

$$\frac{\partial[PMEI]}{\partial x} = -\alpha\beta_{PMEI}(t) \quad \text{at } x=1, \quad (5.22)$$

$$\frac{\partial[PG]}{\partial x} = \alpha\beta_{PG}(t) \quad \text{at } x=-1, \quad (5.23)$$

$$\frac{\partial[PG]}{\partial x} = -\alpha\beta_{PG}(t) \quad \text{at } x=1, \quad (5.24)$$

$$\frac{\partial[PGI]}{\partial x} = \alpha\beta_{PGI}(t) \quad \text{at } x=-1, \quad (5.25)$$

$$\frac{\partial[PGI]}{\partial x} = -\alpha\beta_{PGI}(t) \quad \text{at } x=1, \quad (5.26)$$

$$\frac{\partial[PL]}{\partial x} = \alpha\beta_{PL}(t) \quad \text{at } x=-1, \quad (5.27)$$

$$\frac{\partial[PL]}{\partial x} = -\alpha\beta_{PL}(t) \quad \text{at } x=1, \quad (5.28)$$

$$\frac{\partial[arabinase]}{\partial x} = \alpha\beta_{arabinase}(t) \quad \text{at } x=-1, \quad (5.29)$$

$$\frac{\partial[arabinase]}{\partial x} = -\alpha\beta_{arabinase}(t) \quad \text{at } x=1, \quad (5.30)$$

with all β variables found using the vSEED data discussed in Section 1.3. It should be noted that the equations explaining polysaccharides contain the same terms as in their ordinary differential equation model; however, the equations used to describe the rate of change for the proteins contain previously unseen diffusion terms (in red), Section 5.3.2, while the production terms are present in the boundary conditions due to the spatial nature of the model, Section 5.3.3, and reaction terms remain the same as discussed previously in the chapter 4.

The parameters within this model are separated into rate constants, diffusion constants and those in the boundary conditions and initial conditions, explained below. Each set of parameters is then divided

or multiplied by an constant for length, \hat{L} , time, \hat{t} , and mass, \hat{M} , in order to remove the dimensional dependencies of each parameter. The length constant is chosen to be the thickness of a cell wall and mass is one milligram. The time factor is one hour in order to easily relate physically observed changes, such as testa rupture, with the curve profiles predicted by the model. In this chapter one parameter of each type is chosen to implement the non-dimensionalisation process explicitly.

5.3.1 Rate constants

These parameters were introduced in the previous ODE models (Sections 4.2, 4.3 and 4.4). Table 5.1 lists all rate constants with their values.

Parameter	D	E	F
Parameter value	$0.3586 \mu\text{m}^3/\text{mg s}$	$0.4 \mu\text{m}^3/\text{mg s}$	$0.4 \mu\text{m}^3/\text{mg s}$
Parameter	d	c	k
Parameter value	$0.8775 \mu\text{m}^3/\text{mg s}$	$0.9 \mu\text{m}^3/\text{mg s}$	$0.4 \mu\text{m}^3/\text{mg s}$
Parameter	A	B	
Parameter value	$0.4 \mu\text{m}^3/\text{mg s}$	$0.4 \mu\text{m}^3/\text{mg s}$	

Tab. 5.1: Rate constants used for complete PDE model

With this larger complex model non-dimensionalisation is performed to simplify the system. This non-dimensionalisation is done by considering the dimensions of a parameter and dividing by a constant value assigned to each dimension. Equation (5.31) considers the rate constant D ,

where \hat{D} is the dimensionless form of D and \hat{t} , \hat{L} and \hat{M} are chosen constants for the dimensions of time, length and mass respectively:

$$D = \frac{\hat{L}^3}{\hat{M}\hat{t}}\hat{D}, \quad (5.31)$$

All the rate constants have the same dimensions and so are found in this way, the complete set of parameters being shown in section 5.4.

5.3.2 *Diffusion constants*

The diffusion terms describe the rate at which a protein travels through the cell wall and are discussed by Young [83]. These constants \mathcal{D}_i are found using the Stokes-Einstein equation; this equation describes the diffusion of spherical particles in a fluid with low Reynolds number; although there is no evidence to suggest that these proteins are spherical, the simplification is a reasonable first approach. The Stokes Einstein equation is:

$$\mathcal{D} = \frac{k_b T}{6\pi\eta r} \quad (5.32)$$

in this equation T is the temperature, assumed to be roughly room temperature, r is the radius of the particle, η is the dynamic viscosity and k_b is the Boltzmann's constant. The Boltzmann's constant relates the energy of a particle to the temperature of the tissue and r denotes the radius of the particle, assuming it is spherical. There is no shape information in available literature for any of the considered proteins and so we approximate a radius by dividing the molecular weight of required protein by the density of amino acids, ρ , and take the cubed root to conserve

dimensions. The table below, Table 5.2, lists the approximations used for radius as well as the other constants used in the Stokes-Einstein equation.

Viscosity is very difficult to measure due to the size of the medium and challenge of producing pectin in vitro. Guimaraifes [32] found the viscosity of 1% pectin in an aqueous solution, in this paper a temperature of 303.1K, this estimate is in the order of 10^{-3} kg/ms, which is a lot smaller than the viscosity estimated range within a paper by Dyson [23], 10^9 - 10^{11} kg/ms Diffusion can be calculated in different ways such as the fluorescence microscopy produced by Schmidt [71]. It is important to note that none of these estimates were done using the distinctive endosperm cell wall but how the differing components of the cell walls affect the viscosity is also unknown.

The diffusion terms, \mathcal{D} , have dimensions length squared over time and so the dimensionless form of diffusion terms, $\hat{\mathcal{D}}$, have the form:

$$\hat{\mathcal{D}} = \frac{\mathcal{D}\hat{t}}{\hat{L}^2}. \quad (5.33)$$

The resulting diffusion constants are listed in Section 5.31.

Assumptions that the proteins are spherical is likely to be incorrect but since this assumption has been used for all the proteins, they will presumably diffuse at appropriate, relative, speeds to one another. The viscosity estimation is an important parameter of the model and its recorded range is large.

5.3.3 *Boundary conditions*

The production terms describe the introduction of enzymes and proteins into the cell wall from the cell itself, expressed mathematically as the boundary conditions.

Parameter	values	Units	Definition
ρ	9.03×10^{11}	$\frac{da}{\mu m^3}$	density of amino acids
mW_{PMEI}	19069.6	Da	molecular weight of PMEI {At5g46950}
mW_{PME}	64255.4	Da	molecular weight of PME {At3g14310}
mW_{PGI}	36688.9	Da	molecular weight of PGIP {At5g06860}
mW_{PG}	43462	Da	molecular weight of PG {At2g43860}
mW_{expan}	27748.7	Da	molecular weight of expansin {At5g05290}
mW_{XTH}	33540.4	Da	molecular weight of XTH {At3g44990}
$mW_{arabinase}$	114260.3	Da	molecular weight of arabinase {At4g16130}
r_{PMEI}	0.001714	μm	approximate radius of PMEI {At5g46950}
r_{PME}	0.00257	μm	approximate radius of PME {At3g14310}
r_{PGI}	0.002132	μm	approximate radius of PGIP {At5g06860}
r_{PG}	0.002256	μm	approximate radius of PG {At2g43860}
r_{expan}	0.001943	μm	approximate radius of expansin {At5g05290}
r_{XTH}	0.00207	μm	approximate radius of XTH {At3g44990}
$r_{arabinase}$	0.003114	μm	approximate radius of arabinase {At4g16130}
k_B	8.3106×10^{15}	$\frac{\mu m^2 da}{s^2 K}$	Boltzmann's constant
T	300	K	Temperature
η	4.64679×10^{18}	$\frac{da}{\mu m s}$	estimated viscosity

Tab. 5.2: Parameters used in the Stokes-Einstein equation, including molecular weights and amino acid density for radius approximation. Molecular weights were found using tair [2] and consider only the most active protein, according to the vSEED trascriptomics data, from each family.

Biologically, the cell wall remodelling proteins will be produced within the cell and will diffuse into the primary cell wall before diffusing through the wall and then the intercellular matrix. This model will assume that the proteins are produced straight into the cell wall and so the boundary conditions for the model will be the production rate of each protein and enzyme. This production will be the same at both boundaries of the line considered. The boundary conditions for each protein are of the form:

$$\frac{\partial[p]}{\partial x} = \alpha\beta_p(t) \quad \text{at } x=-1, \quad \frac{\partial[p]}{\partial x} = -\alpha\beta_p(t) \quad \text{at } x=1, \quad (5.34)$$

with p the considered protein, α a dimensionless constant described in Section 3.2 and $\beta_p(t)$ the time dependant production found using the time course data described in Section 1.3. It is assumed that the level of mRNA is proportional to the protein production, which is true if all the mRNA is active; we also assume that this proportionality is constant between all mRNA. So, a linear fit is found to the mRNA levels, as an approximation of proportional protein production.

The production terms have dimension of volume per time and so denote the dimensional production term as β , as described in Sections 4.2, 4.3 and 4.4. The dimensionless version, $\hat{\beta}$, by using intermediate parameters for length \hat{L} and time \hat{t} .

$$\beta = \frac{\hat{L}^3}{\hat{t}} \hat{\beta} \implies \hat{\beta} = \frac{\hat{t}}{\hat{L}^3} \beta \quad (5.35)$$

The previously discussed α from Chapter 4 is dimensionless and so

requires no alteration.

These parameters are our best informed set of parameters, although it is assumed that all mRNA is active and that entrance into the cell wall once produced is instant and certain, no proteins diffusing away from the cell wall.

5.3.4 *Initial Conditions*

The initial conditions are simply a set of numbers giving the starting time point of the system, $t = 0$ over all values of x . In this model the initial conditions are the levels of each of the polysaccharides and protein considered in the model. It is assumed that there are no cell wall remodelling proteins within the primary cell wall or intercellular matrix initially. There is an even level of methylesterified homogalacturonan across the whole area considered but no other forms of homogalacturonan. The xyloglucan will be uniformly distributed between the two primary cell walls with none present in the intercellular matrix and no modified xyloglucan.

The cell walls are constructed from the polysaccharides considered in this model and it is of course essential that they are present initially. Polysaccharides comprise a chain of monosaccharides and, from a mathematical point of view, they constitute a number of action sites for the proteins of interest. The difficulty is knowing how many action sites are present for each polysaccharide. The initial conditions used in the ODE model in Chapter 4 are used in this section, although due to the spatial dimension the level of each polysaccharide is assumed to be evenly spaced across the cell walls.

When non-dimensionalising, polysaccharide or protein i has dimensional initial condition, i_0 and its dimensionless form can be calculated

as:

$$\hat{i}_0 = \frac{\hat{L}^3 i_0}{\hat{M}}.$$

The full list of initial conditions is listed in Table 5.3. Although these parameters are not known the impact of altering them is clear. When using the assumption that the polysaccharides' activity sites are equally distributed for all the considered polysaccharides, the initial conditions of the polysaccharides could be parametrised to reduce the number of parameters in the model. We use P and the cell wall composition in percentage; Homogalacturonan makes up 40% of the cell wall along with the xyloglucan, while the arabinan is roughly 20% of the cell walls composition, resulting in equations 5.36.

$$[MeHG]_0 = 40P, \quad [arabinan]_0 = 20P, \quad [Xylo]_0 = 40P, \quad (5.36)$$

For this model we use $P = 235$.

5.4 Non-dimensionalised model

The method of non-dimensionalising requires all of the terms of the equations, boundary conditions and initial conditions to be looked at individually. The dimensions of all of these elements are considered and shown in the table below.

First, the constants used to non-dimensionalise are selected, the obvious choice for \hat{L} is the cell wall thickness of 10nm resulting in the considered domain being 2 rather 20 nm. For ease the domain is centred around the origin and so ranges from $x = -1$ to $x = 1$, with $x = 0$ the intercellular matrix.

The mass non-dimensionaliser, \hat{M} will be taken as 1 mg and for \hat{t} , 1 hour is used so that key times in the germination process are still recognisable.

The rest of this chapter will be done with dimensionless parameters although the hats are dropped for convenience.

5.5 Results

In this section, the change of protein and polysaccharide levels across the spatial and temporal domain of interest are shown. Firstly, a general overview of the whole surface representing each variable is shown and then a closer look at testa rupture and endosperm rupture time points are considered. Section 5.6 then considers specific locations to highlight possible impacts on cell wall properties in Section 5.6.

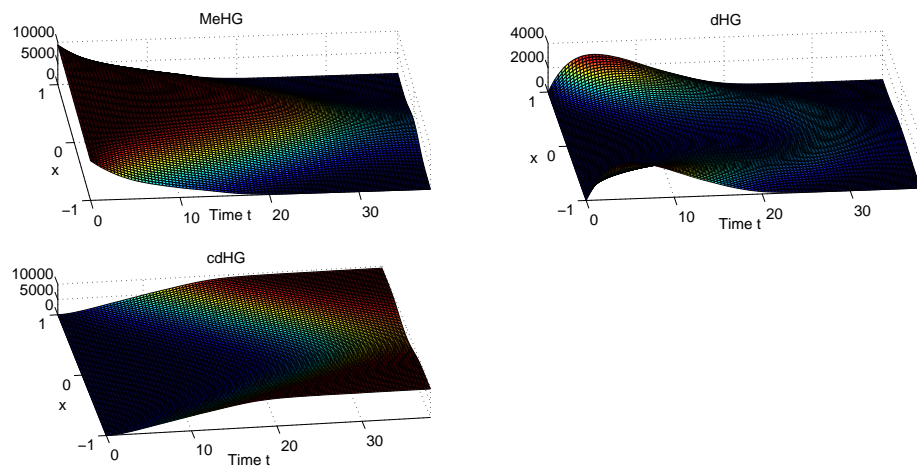


Fig. 5.8: Change of homogalacturonan polysaccharide levels over time across the two primary cell walls and intercellular matrix.

As expected, the MeHG is converted into dHG, beginning with the outer edges of our domain, which simulates inner edge of the cell wall, where the PME enter the cell wall, Figure 5.8. The de-methylesterification of the cell wall's and intercellular matrix's homogalacturonan happens at

Parameter	Dimensionless Value	Definition
D	0.3586	reaction constants (MeHG-PME)
d	0.8775	reaction constants (PMEI-PME)
c	0.9	reaction constants (PGI-PG)
E	0.4	reaction constants (dHG-PL)
F	0.4	reaction constants (dHG-PG)
A	0.4	reaction constants (expansin-Xylo)
B	0.4	reaction constants (XTH-Xylo)
k	0.4	reaction constants (arabinan - arabinase)
\mathcal{D}_{PME}	0.0932	diffusion rate of PME
\mathcal{D}_{PMEI}	0.1398	diffusion rate of PMEI
\mathcal{D}_{PG}	0.1062	diffusion rate of PG
\mathcal{D}_{PGI}	0.1124	diffusion rate of PGI
\mathcal{D}_{PL}	0.1029	diffusion rate of PL
\mathcal{D}_{Expan}	0.1234	diffusion rate of Expan
\mathcal{D}_{XTH}	0.1158	diffusion rate of XTH
$\mathcal{D}_{arabinase}$	0.077	diffusion rate of arabinase
$[MeHG]_0$	9355.335	initial quantity of MeHG
$[dHG]_0$	0.0047	initial quantity of dHG
$[cdHG]_0$	0	initial quantity of cdHG
$[PMEI]_0$	40.207	initial quantity of PMEI
$[PME]_0$	0.0001	initial quantity of PME
$[PMEI : PME]_0$	0.1011	initial quantity of PMEI:PME
$[PGI]_0$	0	initial quantity of PGI
$[PG]_0$	0	initial quantity of PG
$[PL]_0$	0	initial quantity of PL
$[PGIPG]_0$	0	initial quantity of PGI:PG
$[Xylo]_0$	10000	initial quantity of xyloglucan
$[wXylo]_0$	0	initial quantity of wXylo
$[cXylo]_0$	0	initial quantity of cXylo
$[expan]_0$	0	initial quantity of expansin
$[XTH]_0$	0	initial quantity of XTH
$[arabinan]_0$	4700	initial quantity of arabinan
$[arabinase]_0$	0	initial quantity of arabinase
$[Aarabinan]_0$	0	initial quantity of altered arabinan
α	0.003573	scaling constant for production rates

Tab. 5.3: The parameters and their dimensionless values used in the partial differential equation model stated in Section 5.3.

a steady rate, controlled primarily by the diffusion term. de-methylesterified homogalacturonan reaches a peak at $t = 5$, on the inner edge of the

cell wall, this is due to the polygalacturonase and pectin lyase accumulating slower than the pectin methyl esterase for $t < 5$. The homogalacturonan appears solely in its cleaved form at the cell side of the cell wall from twenty one hours and this complete conversion spreads towards the intercellular matrix but the homogalacturonan in the intercellular matrix is not completely cleaved by the germination point, $t = 38$.

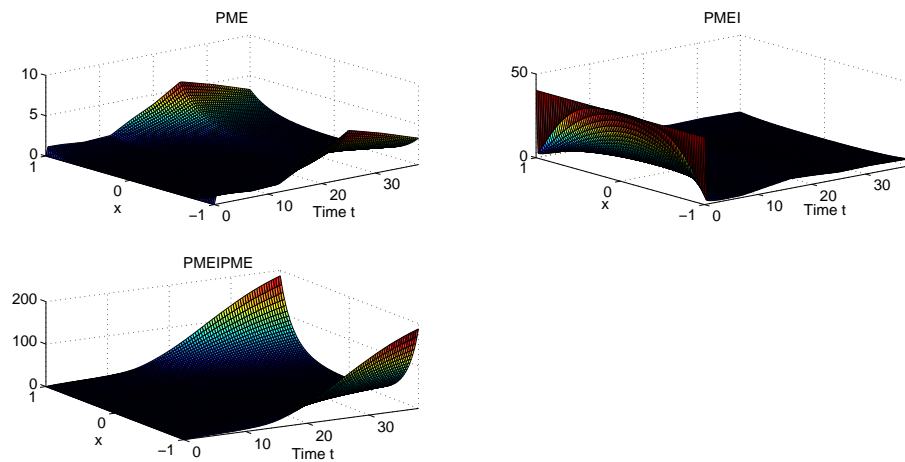


Fig. 5.9: Change of PME, its inhibitor, PMEI, and the complex, PMEIPME, levels over time across the two primary cell walls and intercellular matrix.

From Figure 5.9 it can be seen that the majority of the PME, PMEI complex is created at the cell-ward edge of the cell wall, this is unsurprising since that is where the proteins are introduced to the cell wall. PME is present at low levels throughout the cell walls and intercellular matrix by $t = 20$. The levels of PME are consistently lower than that of its inhibitor, PMEI. PMEI is quick to spread through the the whole domain which is expected when considering the molecular weights and estimated radii in Table 5.2.

The PG and PL proteins moves quickly through the domain, as seen in Figure 5.9, which explains the brief time that homogalacturonan stays in de-methylesterified state before being cleaved. PGI appears to diffuse slowly but this is due to the creation of the complex PGIPG consuming

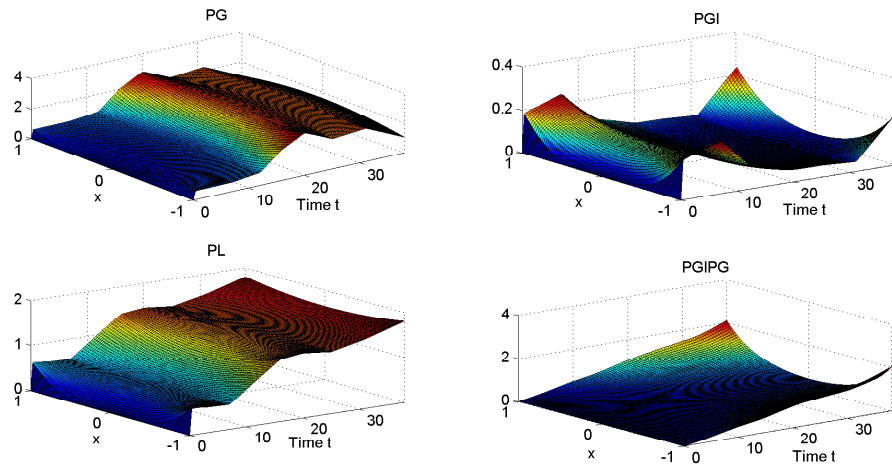


Fig. 5.10: Change of PG, its inhibitor, PGI, and the complex, PGIPG, levels over time across the two primary cell walls and intercellular matrix.

the relatively low levels of PGI, with plenty of PG left to cleave the homogalacturonan. Even though PL has no inhibitor it is produced at levels which mean it does not overwhelm the system and increases over time to a lower level than PG, at its peak; The comparative levels of PL and PG, shown here, can be seen in the previously discussed ODE model, Section 4.2.

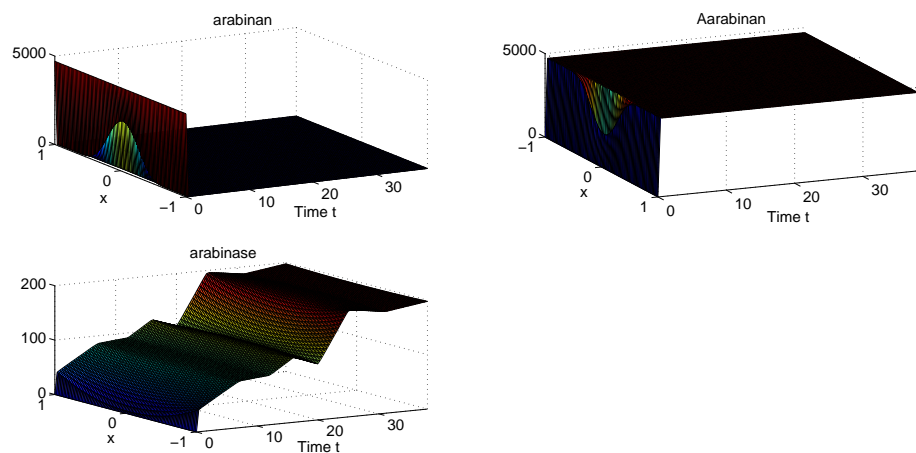


Fig. 5.11: Change in arabinan, and its remodelling protein, arabinase, levels over time across the two primary cell walls and intercellular matrix. Arabinase is not consumed during remodelling as in system described in section 5.3.

Figure 5.11 shows that the arabinan is completely remodelled by $t = 1$, this would fit with data presented by Lee [44]. Arabinase continues to accumulate to high levels when compared to the enzymes used to remodel the homogalacturonan network; the levels predicted by the model are closer to those of XTH protein which is consumed during remodelling; Since the way in which arabinase acts upon arabinan is unknown, the partial differential equation model is used to investigate whether the arabinase activity is likely to be that of a true enzyme, as modelled so far, or a consumed protein. The system of partial differential equations presented in section 5.3 are run again with equation (5.17) replaced by equation (5.37), below.

$$\frac{\partial[\text{arabinase}]}{\partial t} = \mathcal{D}_{\text{arabinase}} \frac{\partial^2[\text{arabinase}]}{\partial x^2} - k[\text{arabinan}][\text{arabinase}], (5.37)$$

This change impacts only the arabinan, arabinase and Aarabinan levels and the results are shown in Figure 5.12.

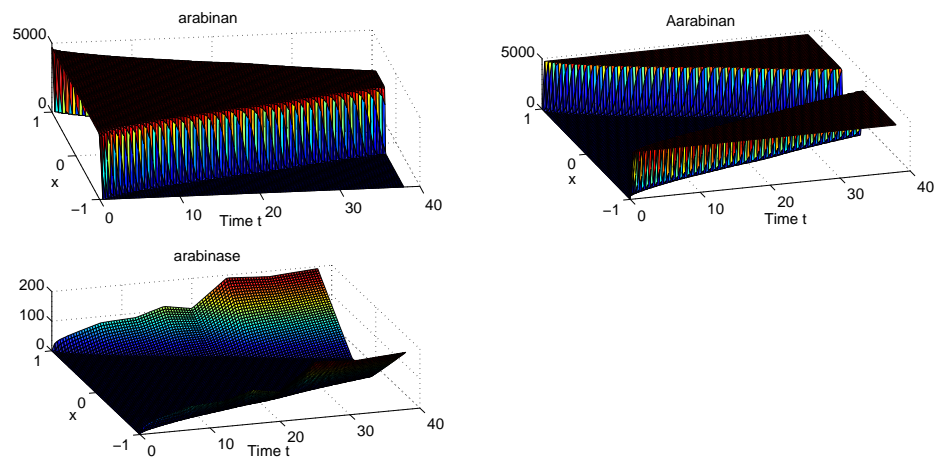


Fig. 5.12: Change in arabinan, and its remodelling protein, arabinase, levels over time across the two primary cell walls and intercellular matrix. Arabinase is consumed during the polysaccharide remodelling.

The arabinan present in this domain is not completely converted to

Aarabinan, Figure 5.12, this is due to the arabinase, which causes this conversion, being consumed during the remodelling process. In this case not all arabinan is altered before germination occurs and so if arabinase is shown to be consumed when altering arabinan, the model would predict that arabinan is altered earlier in the seed's life, possibly during seed maturation.

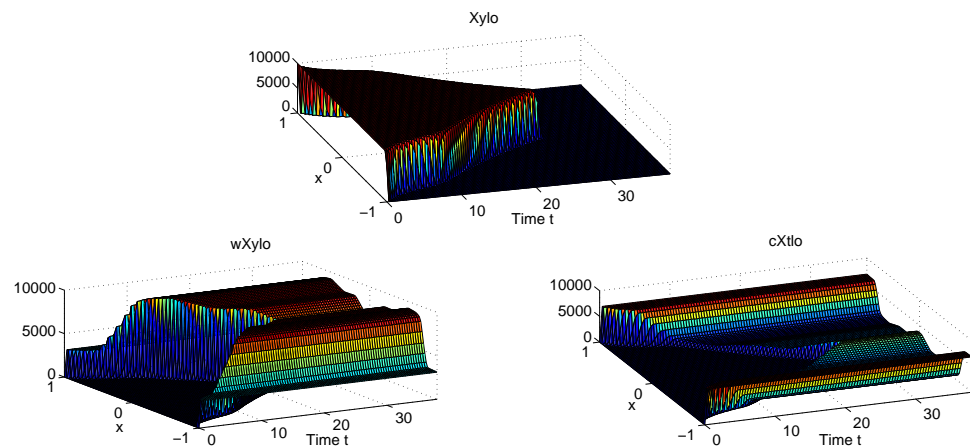


Fig. 5.13: Change in xyloglucan polysaccharide state levels over time across the two primary cell walls and intercellular matrix.

The xyloglucan polysaccharide states are shown in Figure 5.13. All of the xyloglucan has been remodelled by $t = 27$. Testa rupture occurs at around $t = 25$: This testa rupture requires an element of cell expansion from the radicle which would stretch the endosperm, so it is expected that the endosperm cell walls would need to be remodelled to cope with this, consistent with model predictions.

The XTH and expansin proteins compete for the xyloglucan, resulting in different levels of the altered form of xyloglucan at different areas of the cell walls. Figure 5.14 shows the proteins, XTH and expansin, and their levels during germination across the two cell walls and intercellular matrix. With levels of XTH higher than expansin early in the germination process, the inner edge of the cell wall (outer edge of our domain) is

predominately cleaved by XTH activity whereas the middle of the cell wall and edge of the cell wall furthest from the cell is mainly altered by expansin. The change in dominant polysaccharide state through the cell wall is likely to have an impact on the cell wall properties and will be discussed in Section 5.6.

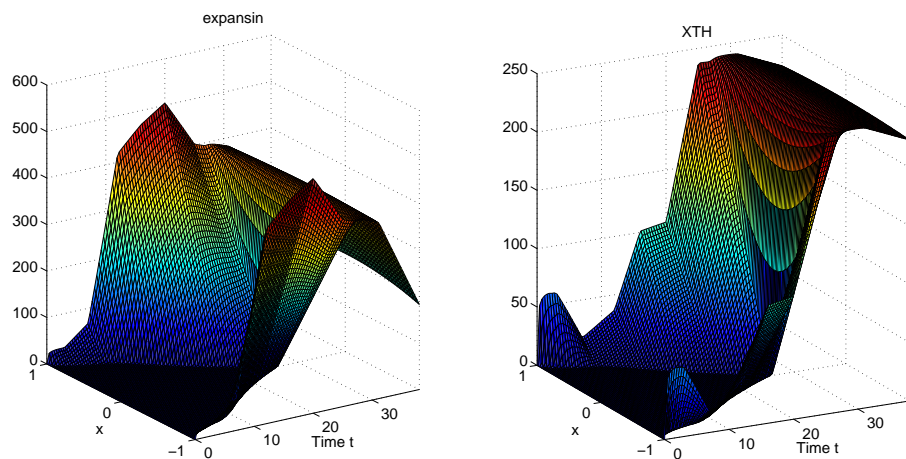


Fig. 5.14: Change in XTH and expansin levels over time across the two primary cell walls and intercellular matrix.

Figures 5.15 and 5.16 show the level of the homogalacturonan and xyloglucan polysaccharide states at early time point, $t = 1$, testa rupture, $t = 25$, and endosperm rupture, $t = 36$, over the two cell walls and intercellular matrix.

As with the earlier figure, Figure 5.8, the level of methylesterified homogalacturonan reduces gradually over time with the outer edges of the considered domain being remodelled first. During testa rupture dHG is the dominant form of homogalacturonan in the cell walls, this may not have any impact of the testa rupture, instead necessary in order for sufficient homogalacturonan to be cleaved in time for germination.

By the time of testa rupture most of the xyloglucan is remodelled, as seen in Figure 5.16. the remodelling proteins, XTH and expansin, are diffusing towards the intercellular matrix clearly at $t = 25$ before

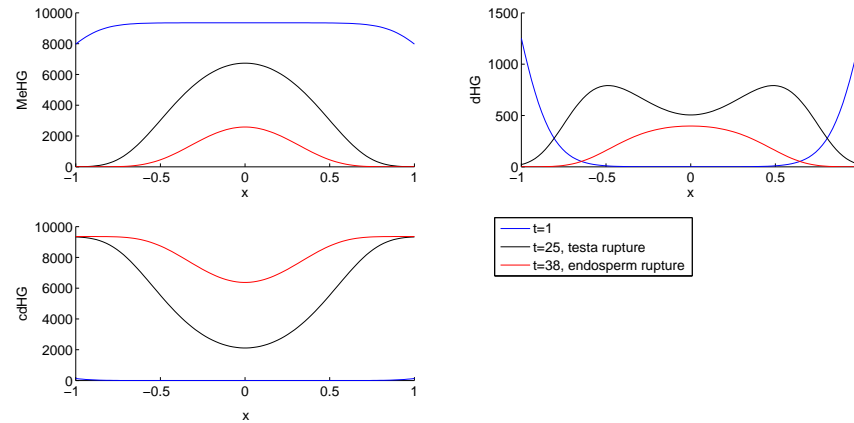


Fig. 5.15: homogalacturonan polysaccharide levels at $t = 1$, testa rupture and endosperm rupture.

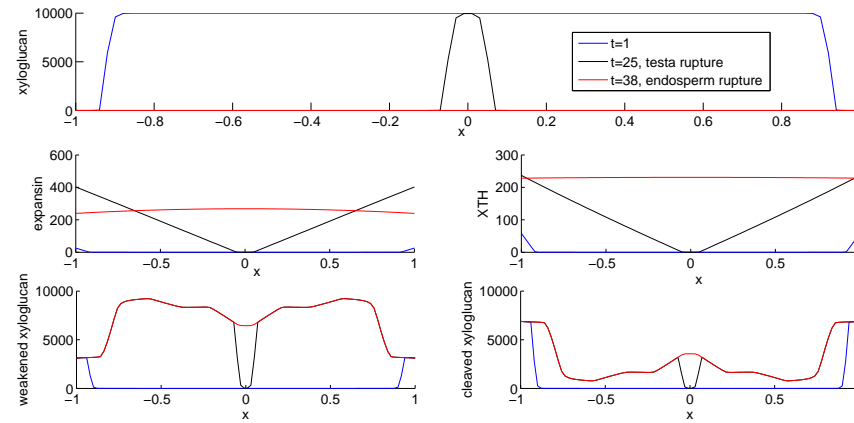


Fig. 5.16: xyloglucan polysaccharide and relevant protein levels at $t = 1$, testa rupture and endosperm rupture.

spreading evenly across the cell walls by the time germination occurs. The remodelled states of xyloglucan, weakened xyloglucan and cleaved xyloglucan, compete for the available xyloglucan, starting at the edge of the cell wall closest to the cell. To begin with XTH is present at higher levels than expansin, converting more of the inner edge of the cell wall to the cleaved form of xyloglucan. The majority of the cell wall is however, remodelled into the weakened form.

5.6 Model Implications on Cell Wall Properties

In this section, the cell wall properties discussed in Section 4.5 are revisited given the partial differential equation model presented earlier in the chapter. Aspects of the surfaces shown in Figures 5.8, 5.9, 5.10, 5.11, 5.13 and 5.14 will be highlighted to focus on elements of the model relevant to cell wall properties.

5.6.1 Cell Separation

The eSEM image in Figure 5.1 appears to show only whole cells in the endosperm and so the cell separation is thought to happen in the intercellular matrix. To investigate this intercellular matrix, all the graphs in this section consider the change of protein and polysaccharide levels between the two cell walls in the constructed domain, $x = 0$.

In Section 4.5.1, evidence was presented showing a clear change in the force required to rupture the endosperm of *Lepidium*, Figure 4.28. The initial force required for endosperm rupture is around 100mN and shortly before testa rupture there begins a transition to a lower rupture force of 30mN. An ordinary differential equation model was used to highlight the variables most likely to cause this reduction in cell wall cohesion and polygalacturonan appeared to be most likely.

Xyloglucan is not present in the intercellular matrix and as such will not be considered as the cause of cell separation.

The data considered in Section 4.5.1 pointed to the cell wall cohesion reducing shortly before testa rupture for a short period of time, in *Lepidium*, between eleven and fourteen hours after imbibition with testa rupture occurring around twelve hours; in *Arabidopsis*, for which our model is constructed, testa rupture is around twenty five hours. So, in

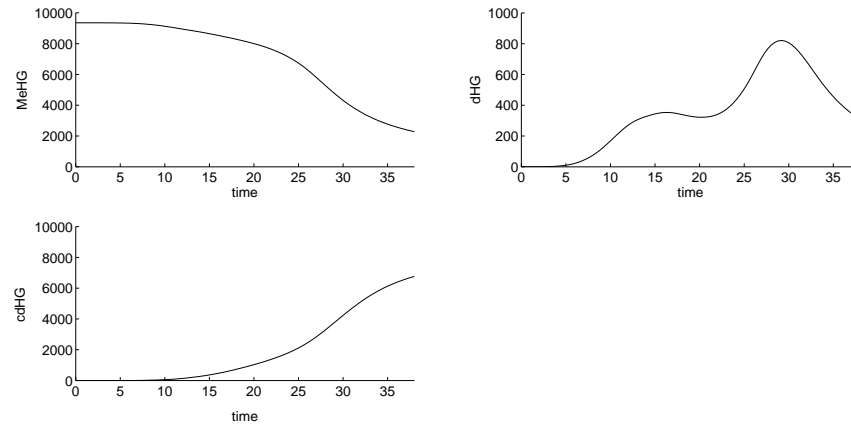


Fig. 5.17: Change in homogalacturonan polysaccharide states, over time, in the intercellular matrix, using *Arabidopsis* transcriptomics data for protein production.

Figure 5.17, the level of cdHG is relatively low at $t = 25$ and continues to increase until germination. Not all homogalacturonan is cleaved by the point of germination but the majority of it has.

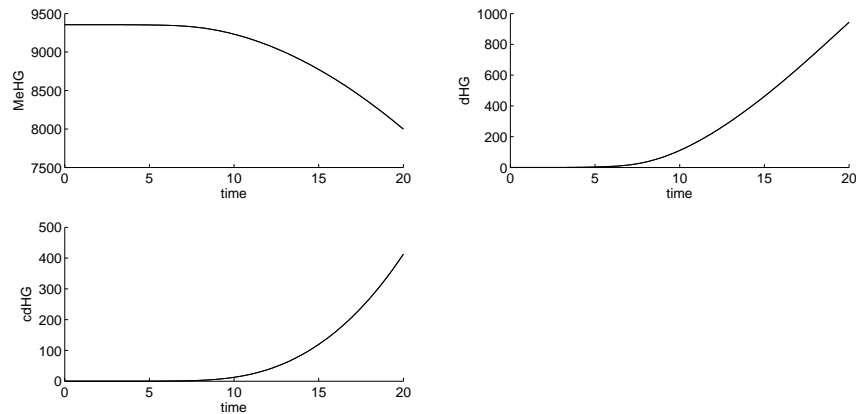


Fig. 5.18: Change in homogalacturonan polysaccharide states, over time, in the intercellular matrix, using *Lepidium* transcriptomics data for protein production.

Figure 5.18 is more directly comparable to the puncture force data, as both consider *Lepidium*. We see that cdHG is present at low levels at $t = 11$, the time at which the puncture force required for endosperm rupture begins to reduce. cdHG continues to increase until germination but does not plateau at $t = 14$, the time at which the required puncture

force stops reducing. Only a small portion of the available homogalacturonan is remodelled and a third of the remodelled homogalacturonan becomes cleaved, this is especially small when compared to the same graphs using *Arabidopsis*. The change between the two species is predominantly the time scale, *Lepidium* germinates faster than *Arabidopsis* giving the proteins, with the same diffusion rate across the same domain, less time to reach the intercellular matrix. The minimal cdHG is unlikely to weaken the endosperm as significantly as shown in Figure 4.28. The PG activity in the intercellular matrix could be due to PG targeting the specific location through some unknown mechanism. Lowering the viscosity of the call wall could also expedite the cleaving but with the assumption that the *Arabidopsis* and *Lepidium* cell walls have the same viscosity, lowering the viscosity in *Arabidopsis* would result in complete cleaving of the available homogalacturonan prior to germination.

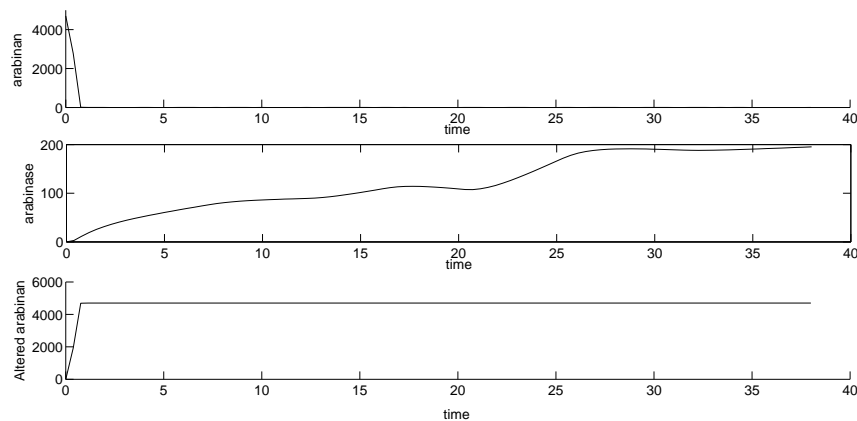


Fig. 5.19: Change in arabinan polysaccharide states and arabinase, over time, in the intercellular matrix.

Arabinan levels, in the intercellular matrix, become negligible by $t = 2$ and so cannot be responsible for any major change in cell wall properties later than two hours after imbibition.

The model, therefore, supports the hypothesis that polygalacturonase

is the major cause of reducing the cell wall cohesion and so responsible for the germination event.

5.6.2 Cell Wall Permeability

In Section 4.5.2 cell wall permeability was discussed and a two element model was proposed.

The first element of this model was a porous cellulose and hemicellulose structure which was controlled by the xyloglucan network. The model constructed in this chapter would be useful for estimating the change in the pore sizes of the porous structure, but without initial sizes pore size, microfibril density and orientation it is difficult to know whether this element of the permeability is relevant. With the exception of PME1, the xyloglucan remodelling proteins are estimated to be the smallest proteins present in the system although not by a very large margin, see Table 5.2. These proteins, XTH and expansin, could reach activity sites and then widen pores which previously were too small for other remodelling proteins.

Within this porous framework, the second element governing the permeability is the viscous pectin. The model constructed in this chapter considers the cell wall viscosity, η , within each diffusion term, Section 5.3.2. Cell wall viscosity has been estimated to be 10^9 - 10^{11} kg/ms [23] for the cell walls of root cells. It is unknown whether this viscosity is valid for the endosperm: the presence of arabinan would suggest a difference between root cells and endosperm cells but not to what degree or which it is, more or less viscous.

The large amount of cell wall remodelling suggests that this viscosity varies over the germination process. However, the current viscosity is not the controlling factor for how fast the proteins travel through the

cell wall, the presence of polysaccharide activity sites and inhibiting proteins slowing the protein movement as seen with the proteins consumed during remodelling, namely XTH and expansin, in Figure 5.14.

5.6.3 Cell Wall extensibility

The cell wall extensibility is discussed in Section 4.5.3, where the xyloglucan network is thought to be the controlling factor of extensibility. Data is introduced which suggests that any change in the cell wall extensibility is insignificant, Figure 4.31.

When the xyloglucan network is considered using *Lepidium* transcriptomics data very little activity occurs in the cell wall as seen in Figure 5.20. By the germination event less than a fifth of the cell wall has been remodelled and as such we may not expect a noticeable change in extensibility.

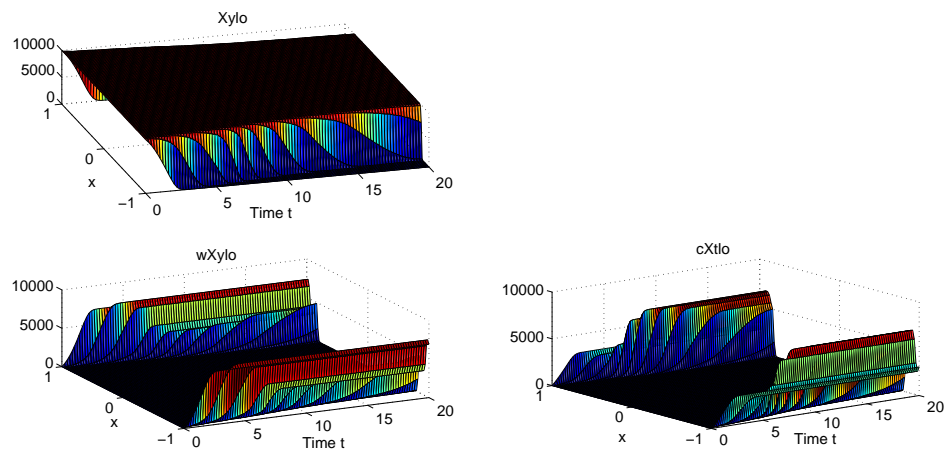


Fig. 5.20: Change in xyloglucan polysaccharide states, over time, using *Lepidium* transcriptomics.

There is a more significant change in the *Arabidopsis* model as shown in Figure 5.13 but, due to the size of *Arabidopsis* seeds, the elasticity experiment performed on *Lepidium*, described in Section 4.5.3, is currently not possible.

5.7 Conclusion

This chapter generalised the ordinary differential equation model constructed in Section 4 to include a spatial dimension. The reactions are still assumed to be irreversible.

Out of the proteins considered in this model, polygalacturonase is the most likely to control the germination event or cell separation event. This agrees with the initial hypothesis, informed by Chisari [14] and Roberts [69].

The permeability of cell walls seems to vary considerably amongst the literature, [23], [32] and the model suggests that the viscosity of *Arabidopsis* and *Lepidium* are significantly different if the two species undergo the same changes at respective times.

This model can be further expanded to consider the central parts of the cell, allowing for protein diffusion to the cell wall. This would allow for the consideration of a complete endosperm and consideration of protein control from the radicle, including the upstream hormone activity controlling the cell wall remodification. The pH levels have not been considered due to the limited information available regarding the pH of cell walls.

6. CONCLUSIONS AND FURTHER WORK

6.1 *Cell Shape Analysis*

The cell shape analysis in Chapter 2 considers a section of an *Arabidopsis* radicle, from an early stage in the germination process. A systematic method for analysing cells within a seed's axis is developed to try to differentiate the cell types which form this radicle. The constructed method found no difference between the cells investigated, this may be the case for the radicle analysed, alternatively the method used may not be accurate enough in simplifying the cells and so failed to distinguish between the two tissues investigated. This method may prove to be more successful at differentiating the tissues of the radicle further through the germination process, when cells in different areas of the axis may change shape. Until the method is tested on a later seed, and thus determined whether the constructed method is sufficient, complicating the method is unnecessary. The accuracy of the shape simplification can be improved by using a weighted vertex system, removing the assumption that the vertices are evenly spaced throughout the vertex-vertex mesh.

The parametrised (Bézier) curve enables easy comparison between radicles of different ages, and different species. With similar vertex-vertex meshes for different radicles, no change would be needed for the method constructed, potentially making it a powerful tool for comparing radicles and pin-pointing areas of interest during the germination process.

6.2 *Plant Cell walls*

All plant cell wall polysaccharides can be broken down into cellulose, hemicellulose and pectin but not all walls have the same types of each polysaccharide or the same proportions of each group of polysaccharide. This thesis focuses on the cell walls of a germinating endosperm, although xyloglucan and homogalacturonan are the major components of the majority of plant cell walls, making the respective networks easily alterable to represent most plant cell walls. The arabinan polysaccharide is a minor component in most cell walls and so its considerable presence in the endosperm differentiates this tissue from other tissues in the seed and even the plant.

Chapter 3 considers pectin methylesterase, its inhibitor and a family of proteins which contain the domains required to perform PME activity and PME inhibition. These so called group II PMEs, are suggested to be self controlling proteins, used for smaller changes to the cell wall. This self controlling activity could be simulated by assuming that group II PMEs inhibit themselves immediately after performing a PME action, instead of the rate constant used in Chapter 3. The simplified model constructed within this chapter is fitted to available data and the rate constants found informed the later discussed reactions.

The PME network is expanded in Chapter 4, as well as the introduction of arabinan and xyloglucan as components of the endosperm cell wall. These ordinary differential equation models are used to discuss changing cell wall properties and likely candidates for such changes.

The three networks, homogalacturonan, arabinan and xyloglucan, are considered with a spatial element in Chapter 5. The arabinan network highlighted two possible hypothesis with regard to arabinase: either

arabinan remodelling occurs at an earlier stage in seed development or arabinase acts as a true enzyme and is not consumed while remodelling arabinan. One of these hypotheses does not preclude the other.

Viscosity is highlighted as a key parameter for the partial differential equation model, and with large range suggested in available literature, an accurate measure for the endosperm would greatly improve the accuracy of the model. Further improvements can be made to the modelled cell wall permeability by considering the suggested porous framework provided by the hemicellulose and cellulose within the cell wall. This increased complexity would require greater understanding of hemicellulose distribution and binding than is currently available in literature.

Polygalacturonase and, to a lesser extent, pectin lyase are the only considered proteins able to be responsible for the cell separation event under the modelled conditions. The puncture force data discussed in Section 4.5.1 points to the polygalacturonase and pectin lyase remodelling to have the greatest impact on cell wall cohesion.

The change in cell wall extensibility is not significant, according data discussed in section 4.5.3, in spite of the changes to the properties of the xyloglucan. This can be explained in that the experimental work which provided the extensibility data was performed on *Lepidium* endosperms; when a *Lepidium* endosperm is considered, the xyloglucan network is not remodelled to an extent that would suggest a large change in cell wall extensibility. Therefore, the models suggest that the *Arabidopsis* endosperm would increase its extensibility over the germination process, but the size of the *Arabidopsis* seed prevents experimental validation with current equipment.

An article by Lee et al [44], points to *Nicotiana tabacum*, tobacco, seeds as a practice species to model germination. The models presented in

this Thesis could be extended to describe tobacco, with the addition of a endo- β -mannanase network. The advantages of tobacco lie in its structural symmetry and predictable cell separation point, it is also large enough for physical experiments.

Cell wall pH is important for estimating protein activity, since all the considered proteins have a preferred pH level. Modelling pH levels within a cell wall would require greater knowledge of so called pH micropockets. pH may be the controlling factor in the competition between expansin and XTH for xyloglucan, since both proteins work very different pH levels. A pH model for the cell wall would allow an investigation into the suggested dual purpose (inhibition and activation) of PGI proteins suggested by Kemp [38]

The next step for the constructed cell wall model would be to include the upstream hormones, gibberellin, GA, and abscisic acid, ABA. Gibberellin is known to promote germination and a GA network has been modelled by Middleton et al [50]. Abscisic acid promotes seed dormancy and a possible signalling network is described by Cutler [19] and Umezawa [79]. Since these hormones control germination they will have downstream interaction with the cell wall remodelling proteins discussed here and the inclusion of ABA and GA will go a long way to more comprehensively modelling the biochemistry of seed germination.

BIBLIOGRAPHY

- [1] *Plant Cell Walls*.
<http://www.ccrcc.uga.edu/~mao/cellwall/main.htm>,
Last accessed: 4th March 2010.
- [2] *The Arabidopsis Information Resource*.
<http://http://www.arabidopsis.org/>,
Last accessed: 8th September 2013.
- [3] Christophe Belin, Christian Megies, Eva Hauserova, and Luis Lopez-Molina. Abscisic acid represses growth of the arabidopsis embryonic axis after germination by enhancing auxin signaling. *The Plant Cell*, 21:2253–2268, 2009.
- [4] J. Bewley and Michael Black. *Seeds Physiology of Germination*. Plenum Press, 1994.
- [5] J. Derek Bewley. Breaking down the walls ? a role for endo-?-mannanase in release from seed dormancy? *Trends in Plant Science*, 2(12):464 – 469, 1997.
- [6] J.D. Bewley. Seed germination and dormancy. *Plant Cell*, 7:1055–1066, 1997.
- [7] E. Bonnin, A. Le Goff, R. Krner, G. J. W. M. Van Alebeek, T. M. I. E. Christensen, A. G. J. Voragen, P. Roepstorff, C. Caprari, and J. F. Thibault. Study of the mode of action of endopolygalacturonase

- from fusarium moniliforme. *Biochimica et Biophysica Acta (BBA) - General Subjects*, 1526(3):301 – 309, 2001.
- [8] J. W. Bradbeer. *Seed Dormancy and Germination*. Chapman and Hall, 1992.
- [9] R. C. Brown, Betty E. Lemmon, Hong Nguyen, and Odd-Arne Olsen. Development of endosperm in *Arabidopsis thaliana*. *Sexual Plant Reproduction*, 12:32–42, 1999. 10.1007/s004970050169.
- [10] Maxwell S. Bush, Mazz Marry, I. Max Huxham, Michael C. Jarvis, and Maureen C. McCann. Developmental regulation of pectic epitopes during potato tuberisation. *Planta*, 213:869–880, 2001.
- [11] KH Caffall and D Mohnen. The structure, function, and biosynthesis of plant cell wall pectic polysaccharides. *Carbohydrate Research*, 344(14):1879–1900, 2009.
- [12] Paul Campbell and Janet Braam. Xyloglucan endotransglycosylases: diversity of genes, enzymes and potential wall-modifying functions. *Trends in Plant Science*, 4(9):361 – 366, 1999.
- [13] Nick Carpita, Mary Tierney, and Malcolm Campbell. Molecular biology of the plant cell wall: searching for the genes that define structure, architecture and dynamics. *Plant Molecular Biology*, 47:1–5, 2001. 10.1023/A:1010603527077.
- [14] Marco Chisari, Ana C. Silveira, Riccardo N. Barbagallo, Giovanni Spagna, and Francisco Arts. Ripening stage influenced the expression of polyphenol oxidase, peroxidase, pectin methylesterase and

- polygalacturonase in two melon cultivars. *International Journal of Food Science & Technology*, 44(5):940–946, 2009.
- [15] Peter Cloetens, Regis Mache, Michel Schlenker, and Silva Lerbs-Mache. Quantitative phase tomography of arabidopsis seeds reveals intercellular void network. *PNAS*, 103:14626–14630, 2006.
- [16] Daniel J. Cosgrove. Wall structure and wall loosening. a look backwards and forwards. *Plant Physiology*, 125:131–134, 2001.
- [17] Daniel J. Cosgrove. Growth of the plant cell wall. *Nature Reviews Molecular Cell Biology*, 6:850–861, 2005.
- [18] Daniel J. Cosgrove, Lian Chao Li, Hyung-Taeg Cho, Susanne Hoffmann-Benning, Richard C. Moore, and Douglas Blecker. The growing world of expansins. *Plant and Cell Physiology*, 43(12):1436–1444, 2002.
- [19] Sean R. Cutler, Pedro L. Rodriguez, Ruth R. Finkelstein, and Suzanne R. Abrams. Abscisic acid: Emergence of a core signaling network. *Annual Review of Plant Biology*, 61:651–679, 2010.
- [20] Isabelle Debeaujon, Karen M. Lon-Kloosterziel, and Maarten Koornneef. Influence of the testa on seed dormancy, germination, and longevity in arabidopsis. *Plant Physiology*, 122(2):403–414, 2000.
- [21] Bas J.W. Dekkers, Simon Pearce, R.P. (Marieke) van Bolderen-Veldkamp, Alex Marshall, Paweł Widera, James Gilbert, Hajk-Georg Drost, George W. Bassel, Kerstin Müller, John R. King, Andrew T.A. Wood, Ivo Grosse, Marcel Quint, Natalio Krasnogor, Gerhard Leubner-Metzger, Michael J. Holdsworth, and Lenie Bentsink. Transcriptional dynamics of two seed compartments with opposing

-
- roles in arabidopsis seed germination. *Plant Physiology*, 163:205–210, 2013.
- [22] Paul Derbyshire, Maureen McCann, and Keith Roberts. Restricted cell elongation in arabidopsis hypocotyls is associated with a reduced average pectin esterification level. *BMC Plant Biology*, 7(1):31, 2007.
- [23] R. J. Dyson and O. E. Jensen. A fibre-reinforced fluid model of anisotropic plant cell growth. *Journal of Fluid Mechanics*, 655:472–503, 2010.
- [24] R.J. Dyson, L.R. Band, and O.E. Jensen. A model of crosslink kinetics in the expanding plant cell wall: Yield stress and enzyme action. *Journal of theoretical Biology*, 307:125–136, 2012.
- [25] William E. Finch-Savage and Gerhard Leubner-Metzger. Seed dormancy and the control of germination. *New Phytologist*, 171(3):501–523, 2006.
- [26] Edwards I. Gabrielle. *Biology The Easy Way*. New York: Barron's Educational Series, Inc., 1990.
- [27] Karine Gallardo, Claudette Job, Steven P.C. Groot, Magda Puype, Hans Demol, Jol Vandekerckhove, and Dominique Job. Proteomics of arabidopsis seed germination. a comparative study of wild-type and gibberellin-deficient seeds. *Plant Physiology*, 129(2):823–837, 2002.
- [28] A. Ghiani, E. Onelli, R. Aina, M. Cocucci, and S. Citterio. A comparative study of melting and non-melting flesh peach cultivars

- reveals that during fruit ripening endo-polygalacturonase (endo-pg) is mainly involved in pericarp textural changes, not in firmness reduction. *Journal of Experimental Botany*, 62(11):4043–4054, 2011.
- [29] Danica E. Goggin, Stephen B. Powles, Peter E. Toorop, and Kathryn J. Steadman. Dark-mediated dormancy release in stratified *lolium rigidum* seeds is associated with higher activities of cell wall-modifying enzymes and an apparent increase in gibberellin sensitivity. *Journal of Plant Physiology*, 168(6):527 – 533, 2011.
- [30] Kai Graeber, Ada Linkies, Andrew T.A. Wood, and Gerhard Leubner-Metzger. A guideline to family-wide comparative state-of-the-art quantitative rt-pcr analysis exemplified with a brassicaceae cross-species seed germination case study. *The Plant Cell Online*, 23(6):2045–2063, 2011.
- [31] P.J. Green and B.W Silverman. *Nonparametric regression and generalized linear models: A roughness penalty approach*. Chapman & Hall/CRC, 1993.
- [32] Guilherme C. Guimaraes, Marcos C. Coelho Junior, and Edwin E. Garcia Rojas. Density and kinematic viscosity of pectin aqueous solution. *Journal of Chemical & Engineering Data*, 54(2):662–667, 2009.
- [33] Sathyanarayana N. Gummadi and T. Panda. Purification and biochemical properties of microbial pectinases??a review. *Process Biochemistry*, 38(7):987 – 996, 2003.
- [34] George Haughn and Tamara Western. Arabidopsis seed coat mucilage is a specialized cell wall that can be used as a model for genetic analysis of plant cell wall structure and function. *Frontiers in plant science*, 3:64, April 2012.

-
- [35] Michael J. Holdsworth, Lenie Bentsink, and Wim J. J. Soppe. Molecular networks regulating arabidopsis seed maturation, after-ripening, dormancy and germination. *New Phytologist*, 179(1):33–54, 2008.
- [36] Louise Jones, Jennifer L. Milne, David Ashford, and McQueen-Mason Simon J. Cell wall arabinan is essential for guard cell function. *Proceedings of the National Academy of Science of the United States of America*, 100(20):11783–11788, 2003.
- [37] Peter E. Jupp and John T. Kent. Fitting smooth paths to spherical data. *Journal of the Royal Statistical Society. Series C (Applied Statistics)*, 36(1):pp. 34–46, 1987.
- [38] G. Kemp, L. Stanton, C.W. Bergmann, R.P. Clay, P. Albersheim, and A. Darvill. Polygalacturonase-inhibiting proteins can function as activators of polygalacturonase. *Mol. Plant Microbe. Interact*, 17:888–894, 2004.
- [39] Daniel Kierzkowski, Naomi Nakayama, Anne-Lise Routier-Kierzkowska, Alain Weber, Emmanuelle Bayer, Martine Schorderet, Didier Reinhardt, Cris Kuhlemeier, and Richard S. Smith. Elastic domains regulate growth and organogenesis in the plant shoot apical meristem. *Science*, 335(6072):1096–1099, 2012.
- [40] Frans M Klis, Pieterella Mol, Klaas Hellingwerf, and Stanley Brul. Dynamics of cell wall structure in *saccharomyces cerevisiae*. *FEMS Microbiology Reviews*, 26(3):239–256, 2002.
- [41] Birgit Kucera, Marc Alan Cohn, and Gerhard Leubner-Metzger. Plant hormone interactions during seed dormancy release and germination. *Seed Science Research*, 15(04):281–307, 2005.

-
- [42] Keun Pyo Lee, Urszula Piskurewicz, Veronika Tureckov, Miroslav Strnad, and Luis Lopez-Molina. A seed coat bedding assay shows that rgl2-dependent release of abscisic acid by the endosperm controls embryo growth in arabidopsis dormant seeds. *PNAS*, 107:19108–19113, 2010.
- [43] Kieran J. D. Lee, Valérie Cornuault, Iain W. Manfield, Marie-Christine Ralet, and J. Paul Knox. Multi-scale spatial heterogeneity of pectic rhamnogalacturonan i (rg?i) structural features in tobacco seed endosperm cell walls. *The Plant Journal*, 75:1018–1027, 2013.
- [44] Kieran J.D. Lee, Bas J.W. Dekkers, Tina Steinbrecher, Cherie T. Walsh, Tony Bacic, Leonie Bentsink, Gerhard Leubner-Metzger, and J. Paul Knox. Distinct cell wall architectures in seed endosperms in representatives of the brassicaceae and solanaceae. *Plant Physiology*, 160:1551–1568, 2012.
- [45] Kieran J.D. Lee, Susan E. Marcus, and J. Paul Knox. Cell wall biology: Perspectives from cell wall imaging. *Molecular Plant*, 4:212–219, 2011.
- [46] A. Maller, T. M. da Silva, A. R. L. Damsio, V. R. A. Reis, J. A. Jorge, and M. L. T. M. Polizeli. Production of pectin lyase by aspergillus niveus under submerged and solid state fermentations using agro-industrial residues as carbon sources. *International Research Journal of Microbiology*, 3:29–35, 2012.
- [47] Susan E. Marcus, Anthony W. Blake, Thomas A. S. Benians, Kieran J. D. Lee, Callum Poyser, Lloyd Donaldson, Olivier Leroux, Artur Rogowski, Henriette L. Petersen, Alisdair Boraston, Harry J. Gilbert, William G. T. Willats, and J. Paul Knox. Restricted access of proteins

- to mannan polysaccharides in intact plant cell walls. *The Plant Journal*, 64(2):191–203, 2010.
- [48] M. Celia Marn-Rodríguez, John Orchard, and Graham B. Seymour. Pectate lyases, cell wall degradation and fruit softening. *Journal of Experimental Botany*, 53(377):2115–2119, 2002.
- [49] M. C. McCann, B. Wells, and K. Roberts. Direct visualization of cross-links in the primary plant cell wall. *Journal of Cell Science*, 96(2):323–334, 1990.
- [50] AM Middleton, S beda Toms, J Griffiths, T Holman, P Hedden, SG Thomas, AL Phillips, MJ Holdsworth, MJ Bennett, JR King, and MR Owen. Mathematical modeling elucidates the role of transcriptional feedback in gibberellin signaling. *PNAS*, 109:7571–7576, 2012.
- [51] Zoran Minic, Cao-Trung Do, Christophe Rihouey, Halima Morin, Patrice Lerouge, and Lise Jouanin. Purification, functional characterization, cloning, and identification of mutants of a seed-specific arabinan hydrolase in arabidopsis. *Journal of Experimental Botany*, 57(10):2339–2351, 2006.
- [52] Hatem Ben Mohamed, Ahmedou M. Vadel, Jan M.C. Geuns, and Habib Khemira. Carbohydrate changes during dormancy release in superior seedless grapevine cuttings following hydrogen cyanamide treatment. *Scientia Horticulturae*, 140(0):19 – 25, 2012.
- [53] Debra Mohnen. Pectin structure and biosynthesis. *Current Opinion in Plant Biology*, 11(3):266 – 277, 2008.
- [54] Koshik Mondal, Sarla Malhotra, Veena Jain, and R. Singh. Partial purification and characterization of pectinmethylesterase from

- ripening guava (<i>psidium guajava</i> l.) fruits. *Acta Physiologiae Plantarum*, 31:81–87, 2009. 10.1007/s11738-008-0203-1.
- [55] Grgory Mouille, Marie-Christine Ralet, Cline Cavelier, Cathlene Eland, Delphine Effroy, Kian Hmaty, Lesley McCartney, Hoai Nam Truong, Virginie Gaudon, Jean-Franois Thibault, Alan Marchant, and Herman Hfte. Homogalacturonan synthesis in arabidopsis thaliana requires a golgi-localized protein with a putative methyltransferase domain. *The Plant Journal*, 50(4):605–614, 2007.
- [56] Kerstin Muller, Stefanie Tintelnot, and Gerhard Leubner-Metzger. Endosperm-limited brassicaceae seed germination: Abscisic acid inhibits embryo-induced endosperm weakening of lepidium sativum (cress) and endosperm rupture of cress and arabidopsis thaliana. *Plant and Cell Physiology*, 47:864–877, 2006.
- [57] J.D. Murray. *Mathematical Biology: I. An Introduction*. Springer, 2007.
- [58] Eiji Nambara, Satoshi Naito, and Peter McCourt. A mutant of arabidopsis which is defective in seed development and storage protein accumulation is a new abi3 allele. *The Plant Journal*, 2(4):435–441, 1992.
- [59] Doungla E. Ngoumazong, Forkwa F. Tengweh, Ilse Fraeye, Thomas Duvetter, Ruth Cardinaels, Ann Van Loey, Paula Moldenaers, and Marc Hendrickx. Effect of de-methylesterification on network development and nature of ca²⁺-pectin gels: Towards understanding structure?function relations of pectin. *Food Hydrocolloids*, 26(1):89 – 98, 2012.
- [60] Anand Nighojkar, Sadhana Srivastava, and Anil Kumar. Pectin

- methylesterase from germinating vigna sinensis seeds. *Plant Science*, 103(2):115 – 120, 1994.
- [61] Hiroyuki Nonogaki, George W. Bassel, and J. Derek Bewley. Germination—still a mystery. *Plant Science*, 179(6):574 – 581, 2010. Translational Seed Biology: From Model Systems to Crop Improvement.
- [62] Nir Ohad, Linda Margossian, Dyung-Chao Hsu, Chad Williams, Peter Repetti, and Robert L Fischer. A mutation that allows endosperm development without fertilization. *PNAS*, 93:5319–5324, 1996.
- [63] Natividad Ortega, Silvia De Diego, Jos M. Rodriguez-Nogales, Manuel Perez-Mateos, and Mara D. Busto. Kinetic behaviour and thermal inactivation of pectinlyase used in food processing. *International Journal of Food Science & Technology*, 39(6):631–639, 2004.
- [64] Yong Bum Park and Daniel J. Cosgrove. Changes in cell wall biomechanical properties in the xyloglucan-deficient xxt1/xt2 mutant of arabidopsis. *Plant Physiology*, 158(1):465–475, 2012.
- [65] Alexis Peaucelle, Siobhan A. Braybrook, Laurent LeGuillou, Emeric Bron, Cris Kuhlemeier, and Herman Hfte. Pectin-induced changes in cell wall mechanics underlie organ initiation in arabidopsis. *Current Biology*, 21(20):1720 – 1726, 2011.
- [66] M. Protsenko, N. Buza, A. Krinitsyna, E. Bulantseva, and N. Korobleva. Polygalacturonase-inhibiting protein is a structural component of plant cell wall. *Biochemistry (Moscow)*, 73:1053–1062, 2008. 10.1134/S0006297908100015.

-
- [67] Marie-Christine Ralet, Martin A. K. Williams, Abrisham Tanhatan-Nasseri, David Ropartz, Bernard Qumner, and Estelle Bonnin. Innovative enzymatic approach to resolve homogalacturonans based on their methylesterification pattern. *Biomacromolecules*, 13(5):1615–1624, 2012.
- [68] Wolf-Dieter Reiter, Clint Chapple, and Chris R. Somerville. Mutants of *arabidopsis thaliana* with altered cell wall polysaccharide composition. *The Plant Journal*, 12:335–345, 1997.
- [69] Jeremy A. Roberts and Zinnia H. Gonzalez-Carranza. Pectinase functions in abscission. *Stewart Postharvest Review*, 5(1):1–4, 2009.
- [70] Jocelyn K. C. Rose. *The Plant Cell Wall*. Blackwell Publishing, 2003.
- [71] T Schmidt, G J Schtz, W Baumgartner, H J Gruber, and H Schindler. Imaging of single molecule diffusion. *Proceedings of the National Academy of Sciences*, 93(7):2926–2929, 1996.
- [72] Peter Schopfer. Biomechanics of plant growth. *Am. J. Bot.*, 93(10):1415–1425, 2006.
- [73] Allan M. Showalter. Structure and function of plant cell wall proteins. *The Plant Cell*, 5:9–23, 1993.
- [74] Allan M. Showalter. Introduction: plant cell wall proteins. *Cellular and Molecular Life Sciences*, 58:1361–1362, 2001.
- [75] Matteo Spagnuolo, Carmine Crecchio, Maria D. R. Pizzigallo, and Pacifico Ruggiero. Fractionation of sugar beet pulp into pectin, cellulose, and arabinose by arabinases combined with ultrafiltration. *Biotechnology and Bioengineering*, 64(6):685–691, 1999.

-
- [76] Mariam B. Sticklen. Plant genetic engineering for biofuel production: towards affordable cellulosic ethanol. *Nature Reviews Genetics*, 9:433–443, 2008.
- [77] Eiichi Tanimoto, Shuhei Fujii, Ryoichi Yamamoto, and Shinobu Inanaga. Measurement of viscoelastic properties of root cell walls affected by low pH in lateral roots of *Pisum sativum* L. *Plant and Soil*, 226(1):21–28, 2000.
- [78] D.S. Thompson. Extensiometric determination of the rheological properties of the epidermis of growing tomato fruit. *Journal of Experimental Botany*, 52(359):1291–1301, 2001.
- [79] Taishi Umezawa, Kazuo Nakashima, Takuya Miyakawa, Takashi Kuromori, Masaru Tanokura, Kazuo Shinozaki, and Kazuko Yamaguchi-Shinozaki. Molecular basis of the core regulatory network in abscisic acid responses: Sensing, signaling and transport. *Plant Cell Physiol*, 51:1821–1839, 2010.
- [80] Tamara Western, D. J Skinner, and George Haughn. Differentiation of mucilage secretory cells of the Arabidopsis seed coat. *Plant Physiology*, 122(2):345–356, Feb 2000.
- [81] J G White, W B Amos, and M Fordham. An evaluation of confocal versus conventional imaging of biological structures by fluorescence light microscopy. *The Journal of Cell Biology*, 105(1):41–48, 1987.
- [82] Fujio Yamaguchi and Fujio Yamaguchi. *Curves and surfaces in computer aided geometric design*. Springer-Verlag Berlin, 1988.
- [83] M. E. Young, P. A. Carroad, and R. L. Bell. Estimation of diffusion

coefficients of proteins. *Biotechnology and Bioengineering*, 22(5):947–955, 1980.

- [84] Joshua Yuan, Xiaohan Yang, Jingru Lai, Hong Lin, Zong-Ming Cheng, Hiroyuki Nonogaki, and Feng Chen. The endo- β -mannanase gene families in arabidopsis, rice, and poplar. *Functional and Integrative Genomics*, 7:1–16, 2007.
- [85] Linghui Zhao, Jingqing Jiang, Chuyi Song, Lanying Bao, and Jingying Gao. Parameter optimization for bezier curve fitting based on genetic algorithm. *ICSI*, 7928:451–458, 2013.